Summer 2008

Textural analysis of a rhyolite dike of the southern Oklahoma aulacogen at Medicine Park, Oklahoma

Sean Patrick O'Donnell

Department:

TEXTURAL ANALYSIS OF A RHYOLITE DIKE OF THE SOUTHERN OKLAHOMA AULACOGEN AT MEDICINE PARK, OKLAHOMA

by

SEAN PATRICK O'DONNELL

A THESIS

Presented to the Faculty of the Graduate School of the

MISSOURI UNIVERSITY OF SCIENCE AND TECHNOLOGY

In Partial Fulfillment of the Requirements for the Degree

MASTER OF SCIENCE IN GEOLOGY AND GEOPHYSICS

2008

Approved by

John P. Hogan, Advisor
Mohamed Abdelsalam
Jeffrey D. Smith

PUBLICATION THESIS OPTION

This thesis consists of the following article that has been submitted for publication as follows:

Pages 1-64 are intended for submission to the JOURNAL OF PETROLOGY.

ABSTRACT

Detailed analysis of the modal abundance and crystal size distribution (CSD) of glomerocrystic quartz and alkali feldspar phenocrysts in a porphyritic "rhyolite" dike at Medicine Park, Oklahoma were integrated with known phase relationships in the system SiO_2-$NaAlSi_3O_8$-$KAlSi_3O_8$-H_2O to constrain the history of this intrusion. Crystallization began at a pressure of ~225 MPa or ~8.6 km depth followed by emplacement at ~50 MPa or ~1.9 km depth. Size and shape of crystals were determined from tracings of phenocryst outlines using sawed slabs and a thin section after deconstructing glomerocrysts into individual crystals (n_{Qtz}=695; n_{Ksp}=398) and converting two dimensional data into three dimensional sizes using *CSD Corrections 1.36*. The crystal nucleation density (intercept) and the product of the crystal growth rate and residence time in the magma (slope) were determined from linear regression of crystal populations in natural log of the population density vs crystal size space. Alkali feldspar preserve highly linear CSDs with a slope = -0.686 and intercept = 0.72 (r^2 = 0.94) indicating constant nucleation and growth preceded glomerocryst formation. Quartz crystals yield complex CSDs with a slope = 1.31 and an intercept = -1.91 (r^2 = 0.0019). Low correlations reflect a mixed population with larger crystals preserving linear relationships and smaller crystals defining a concave down curve - the result of preferential removal of small crystals by resorption during magma ascent. The complex shape of the quartz CSD indicates resorption preceded glomerocryst formation. An estimation of the magma ascent rate is calculated to be 0.0027 m/s using the amount of resorbed quartz, the dissolution rate of quartz, and the distance the magma traveled. Based on this calculation, the rhyolite magma crystallized quartz and alkali feldspar phenocrysts, formed glomerocrysts, and traverse 6.7 km of crust, within 56 days.

ACKNOWLEDGMENTS

I thank my advisor, John Hogan, for his insights and guidance throughout the development and conclusion of this thesis. I also acknowledge and thank my committee members, Mohamed Abdelsalam and Jeff Smith, for their comments and patience.

My fellow graduate students…it would have been an even rougher road without the conversations and shenanigans that necessarily provided me with help and distractions. My office mates at UMR (Dan) and at Wash. U. have both let me bounce ideas, however crazy or improbable, off them and help put me back into perspective of reality.

I also want to thank the Geology Department of UMR (MST) in being patient with me in finishing this thesis. As an undergraduate and graduate here, I had same great experiences, especially with Field Camp and the spring field trips, and learned an incredible amount that has helped and prepared me for further experiences of graduate school.

I, of course, must recognize my parents and my sister in their support and encouragement throughout this long and crazy conclusion. Also, by brother-in-law, Paul, whose example I try to imitate. I owe much of fun and good times I have experienced the past few years to Leah who keeps me on my toes and understands me more than anyone.

TABLE OF CONTENTS

LIST OF ILLUSTRATIONS

LIST OF TABLES

PAPER

Textural Analysis of a Rhyolite Dike of the Southern Oklahoma Aulacogen at Medicine Park, Oklahoma

Sean P. O'Donnell and John P. Hogan
Department of Geological Sciences and Engineering
University of Missouri – Rolla, Missouri, U.S.A 65401
Email: **odonnell@umr.edu**, **jhogan@umr.edu**

ABSTRACT

Detailed analysis of the modal abundance and Crystal Size Distribution (CSDs) of glomerocrystic quartz and alkali feldspar phenocrysts in a porphyritic "rhyolite" dike at Medicine Park, Oklahoma were integrated with known phase relationships in the system SiO_2-$NaAlSi_3O_8$-$KAlSi_3O_8$-H_2O to constrain the history of this intrusion. Crystallization began at ~225 MPa or ~8.6 km depth followed by emplacement at ~50 MPa or ~1.9 km depth. Size and shape of crystals were determined from tracings of phenocryst outlines using sawed slabs and a thin section after deconstructing glomerocrysts into individual crystals (n_{Qtz}=695; n_{Ksp}=398) and converting two dimensional data into three dimensional sizes using *CSD Corrections 1.36*. The crystal nucleation density (intercept) and the product of the crystal growth rate and residence time in the magma (slope) were determined from linear regression of crystal populations in ln of the population density vs crystal size space. Alkali feldspar preserve highly linear CSDs with a slope = -0.686 and intercept = 0.72 (r^2 = 0.94) indicating constant nucleation and growth preceded glomerocryst formation. Quartz crystals yield complex CSDs with a slope = 1.31 and an intercept = -1.91 (r^2 = 0.0019). Low correlations reflect a mixed population with larger crystals preserving linear relationships and smaller crystals defining a concave down curve - the result of preferential removal of small crystals by resorption during magma

ascent. The complex shape of the quartz CSD indicates resorption preceded glomerocryst formation. An estimation of the magma ascent rate is calculated to be 0.0027 m/s using the amount of resorbed quartz, the dissolution rate of quartz, and the distance the magma traveled. Based on this calculation, the rhyolite magma crystallized quartz and alkali feldspar phenocrysts, formed glomerocrysts, and traverse 6.7 km of crust, within 56 days.

***Keywords*:** crystal size distribution (CSD); dike; glomerocryst; resorption; rhyolite

INTRODUCTION

Essential to unraveling the petrogenesis of any rock begins with understanding the origin of the textures they display. Plutonic rocks are favored for decorative stone because of their durability, aesthetically pleasing appearances and deceptively homogeneous textures. The texture of plutonic rocks are typically the integrated result of multiple processes, such as nucleation, growth, resorption, flow sorting, settling, and recrystallization that operate either concurrently or sequentially over the course of crystallization, cooling, and uplift prior to exposure. For some minerals, the earlier stages of crystal growth may be either poorly recorded or not recorded at all in the final plutonic rock due to overprinting by processes (e.g., peritectic reactions, subsolidus recrystallization) operating later in the crystallization history (Higgins, 1998; Schaeben *et al.*, 2002). Petrologists have attempted to overcome the difficulties associated with interpreting plutonic rock textures through studies of volcanic rocks, as these rocks potentially provide a "window" into these early stages of the crystallization history of plutonic rocks (Durand & Sen, 2004; Paulick & Breitkreuz, 2005; Tomiya & Takahashi, 2005). In addition, experimental petrologic studies have been used extensively to examine the crystallization of igneous rocks and the evolution of early forming crystal

textures and processes that directly influence the final textures through the synthesis of rock textures (Swanson, 1977; Petersen & Lofgren, 1986; Acosta-Vigil *et al.*, 2003). However, direct comparison of the results from these experimental approaches to the interpretation of natural plutonic rock textures must be viewed with some caution. Processes specific to volcanism, such as fragmentation of crystals during volcanic eruption (Best & Christiansen, 1997), can alter the original sizes and shapes of crystals produced during magmatic crystallization, thus obscuring comparison with the sizes and shapes of similar crystals in plutonic rocks. Similarly, comparison between experimental studies, which are, typically, compositionally simple systems that operate under static conditions over comparatively short run durations, and natural systems may prove difficult due to the differences in scale and complexity.

"Rhyolite" dikes are hypabyssal felsic igneous rocks that are demonstrably plutonic (e.g., exhibit intrusive contacts) but are very similar in appearance to their extrusive counterparts: rhyolite (e.g., typically porphyritic with phenocrysts set in a fine grained to glassy matrix). The porphyritic texture reflects a rapid increase in the cooling rate of the magma – a "quenching" – during crystallization that can be attributed to intrusion of the partially crystallized magma into relatively cold country rocks presumably at shallow levels in the crust. Conceptually, rhyolite dikes can be regarded as the natural analog of quenched experimental capsules and are appropriate to investigate using well established phase equilibria. Thus, rhyolite dikes afford a unique opportunity to investigate the early to intermediate stages of crystallization and textural development of felsic magmas that, if crystallization had continued uninterrupted, would have presumably evolved to have formed a rock with the appearance of granite.

This study presents the results of a petrologic investigation of a rhyolite dike from the Wichita Mountains of Oklahoma (Ham *et al.*, 1964; Gilbert & Powell, 1988) using quantitative textural analysis through the crystal size distribution (CSD) of the phenocryst populations present in the dike (See Higgins, 2006 for a review) and direct comparison of the reconstructed topological phase relationships preserved by phase assemblages present in the rhyolite dike with experimentally determined equilibrium assemblages in the haplo-granite system SiO_2-$NaAlSi_3O_8$-$KAlSi_3O_8$-H_2O (Johannes & Holtz, 1996). This combined approach, in addition to providing information on the nucleation density and growth rates of quartz and alkali feldspar from felsic magmas, serves to constrain the petrologic significance of CSD relationships that deviate from linearity (constant nucleation and growth) in natural logarithm of the population density (mm^{-4}) vs size (mm) space, the source and emplacement depth of the magma, the rate of ascent of the magma from the source region to the emplacement depth, and insight into the initial stages of development of "granitic" textures.

Geologic Setting

The Southern Oklahoma Aulacogen (SOA) is one of a number of aulacogens formed during the Late Proterozoic to Cambrian rifting of the southern margin of the Laurentian Supercontinent. Igneous rocks associated with this rifting event crop out in the Arbuckle Mountains and in the Wichita Mountains in southern and southwestern Oklahoma, respectively (Fig. 1). The following description of the geology of the Wichita Mountains and its Cambrian igneous components is largely summarized from previous studies (Ham *et al.*, 1964; Lambert *et al.*, 1988; Hogan *et al.*, 1995; Deggeller *et al.*, 1996; Wright & Hogan, 1996; Hogan & Gilbert, 1997; Hogan & Gilbert, 1998). Associated with

formation of the aulacogen are two successive major magmatic episodes resulting in a bimodal suite of igneous rocks (Fig. 2). The earliest igneous rocks associated with rifting are the extensive Glen Mountains Layered Complex (GMLC) of the Raggedy Mountains Gabbro Group (RMGG). The GMLC is a layered anorthositic gabbro with rhythmic cumulate stratigraphy similar to other layered complexes (e.g., Stillwater Complex, Bushveld Complex) covering an area of at least 2,000 km^2. The crystallization age of the GMLC has been constrained to 528 ± 29 Ma using a Sm-Nd whole-rock mineral isochron (Lambert *et al.*, 1988). The GMLC is intruded by isolated plutons (less than 20 km^2) and dikes of biotite-bearing gabbro of the Roosevelt Gabbro Group (RGG). $^{40}Ar/^{39}Ar$ studies of magmatic hornblende and biotite from the Mount Sheridan Gabbro (a pluton of the RGG) yielded dates of 535 ± 8 Ma (late hornblende), 533 ± 2 Ma (hornblende), and 533

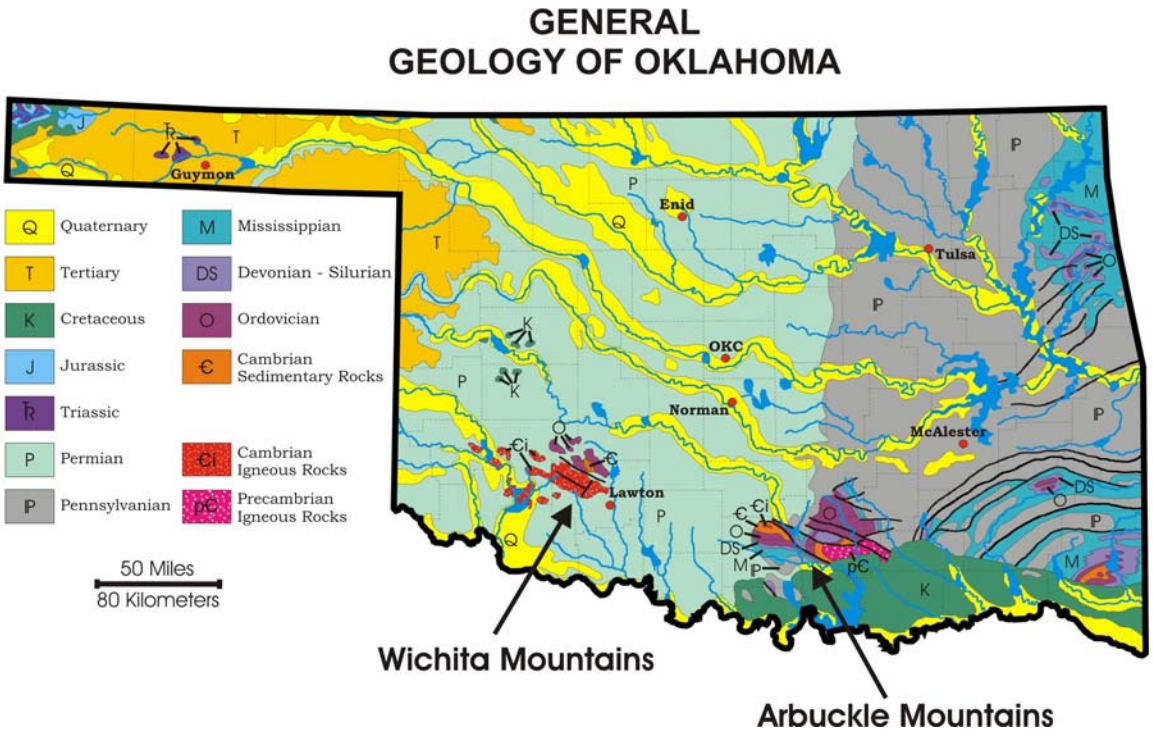

Fig. 1. General geology of Oklahoma. The Southern Oklahoma Aulacogen consists of the Wichita Mountains and the Arbuckle Mountains. (Modified from "General Geology of Oklahoma")

± 4 Ma (biotite) which are interpreted to represent the crystallization age of this gabbro (Hogan *et al.*, 1995).

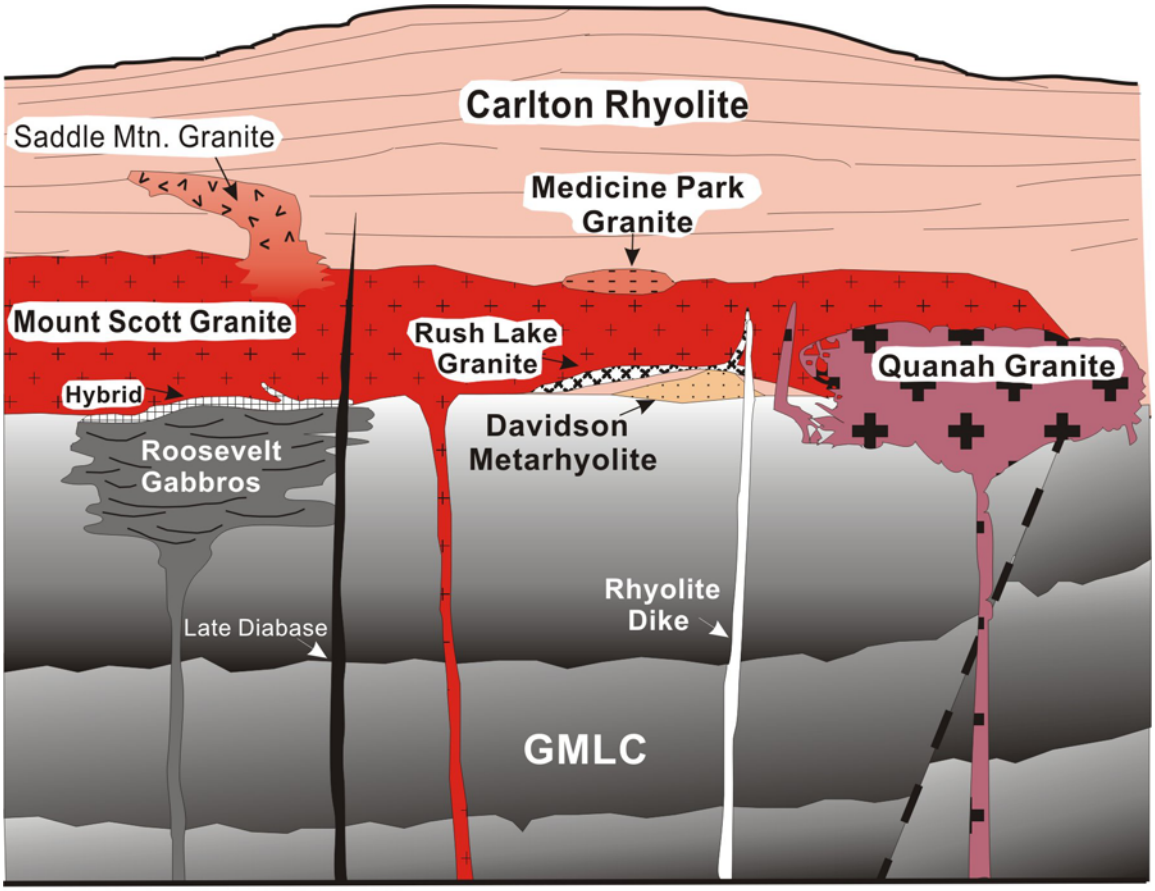

Fig. 2. Schematic cross section of the Southern Oklahoma Aulacogen (SOA). The SOA is a bimodal suite of igneous rocks with the mafic rocks (e.g. the GMLC and Roosevelt Gabbros) being the oldest rocks followed by the Carlton Rhyolite and then the granites (e.g. Mount Scott Granite and Quanah Granite). An example of possible relationships of the Rhyolite Dike at Medicine Park with the SOA is shown. Modified from Price, 1998.

Later stages of the SOA rifting event sequentially produced extensive high-silica, A-type rhyolites in the form of the Carlton Rhyolite Group (CRG) and a group of granitic intrusions, the Wichita Granite Group (WGG), into the rhyolite. The CRG extruded 44,000 km^2 of material that is locally up to 1.4 km thick and is interpreted to unconformably overly marine basalts and spilites of the Navajoe Mountains Group and gabbros of the RMGG. This unconformable relationship can be interpreted as an

erosional event that removed 1 - 3 km of overburden and the upper levels of the GMLC to locally expose the underlying gabbro of the RMGG prior to eruption of the rhyolite and intrusion of the granites. The rhyolites of the CRG consist of thick subaerial flows, minor ignimbrites, non-marine air-fall tuffs, and rare basalt flows. Zircons extracted from a rhyolite xenolith within the Reformatory Granite, a member of the WGG, yielded an U-Pb date of 533 ± 1 Ma and zircons extracted from the Reformatory Granite proper yielded an U-Pb date of 530 ± 1 Ma indicating a close temporal association between these to events (Hogan *et al.*, 1995).

Members of the Wichita Granite Group (WGG) intrude the CRG, typically along the contact between the GMLC and the CRG, as thin sheets of alkali feldspar leucogranites with A-type granite characteristics. The largest of these granites is the Mount Scott Granite which extends up to 55 km in length with a thickness of approximately 0.5 km. The WGG has been subdivided into "fine grained" granites (<1 cm crystals) and "coarse grained" granites (> 1 cm crystals). Through contact relationships, it is determined that the fine grained granites (Mount Scott, Cache, Lugert, and Headquarters) were the first to intrude into the Carlton Rhyolite followed by their coarser grained contemporaries (Reformatory and Quanah granites), denoting at least two distinct episodes of felsic magma production and intrusion. The crystallization age of 535 ± 3 Ma was determined for the fine-grained Mount Scott Granite from U-Pb studies of zircon, which is older than the crystallization age of the coarser-grained Reformatory Granite (Hogan *et al.*, 1995).

The last stages of magmatism attributed to rifting consist of intrusion of rhyolite- and diabase-dikes that indicate magmatism was still occurring after the emplacement of

the granites. The rhyolite dikes are rare in occurrence and are only found to crosscut the WGG, while mafic dikes are more prevalent and crosscut all units of the aulacogen. The rhyolite dikes exhibit an "extrusive" texture indicating a shallow, hypabyssal emplacement level. This requires uplift and erosion of the overlying CRG and WGG units prior to intrusion of the rhyolite dikes and signifies ongoing tectonism associated with the SOA continued after the intrusion of the granites.

Rhyolite Dike at Medicine Park

Field Relationships

The rhyolite dike in this study is one of three significant SOA rhyolite dikes known to intrude the WGG (Gilbert & Myers, 1986; Hogan & Gilbert, 1997). The rhyolite dike is exposed in a road cut along US Hwy. 49 immediately north of the Medicine Park State Fish Hatchery (Fig. 3; UTM Coordinates: 546,443 E 3,842,456 N). Ham *et al*. (1964) first documented the rhyolite dike as a late stage dike of the SOA and used it to illustrate the contemporaneous nature of the WGG and the Carlton Rhyolite. Gilbert and Myers (1986) and later Gilbert and Powell (1988) recognized the tectonic significance of the dike's emplacement in that it, texturally, resembles an extrusive rock that intruded a penecontemporaneous granitic (plutonic) rock. This extrusive texture in an intrusive rock indicates that tectonic uplift and erosion of the SOA preceded the intrusion of the rhyolite dike causing the removal of significant overburden.

The rhyolite dike at Medicine Park exhibits clear intrusive contact relationships with the Rush Lake Granite, a member of the WGG that is texturally similar to the Mount Scott Granite, further north (Price, 1998), and is overlain, in places, by the Permian Post Oak Conglomerate and to the north by talus (Fig. 3). The eastern contact of the rhyolite

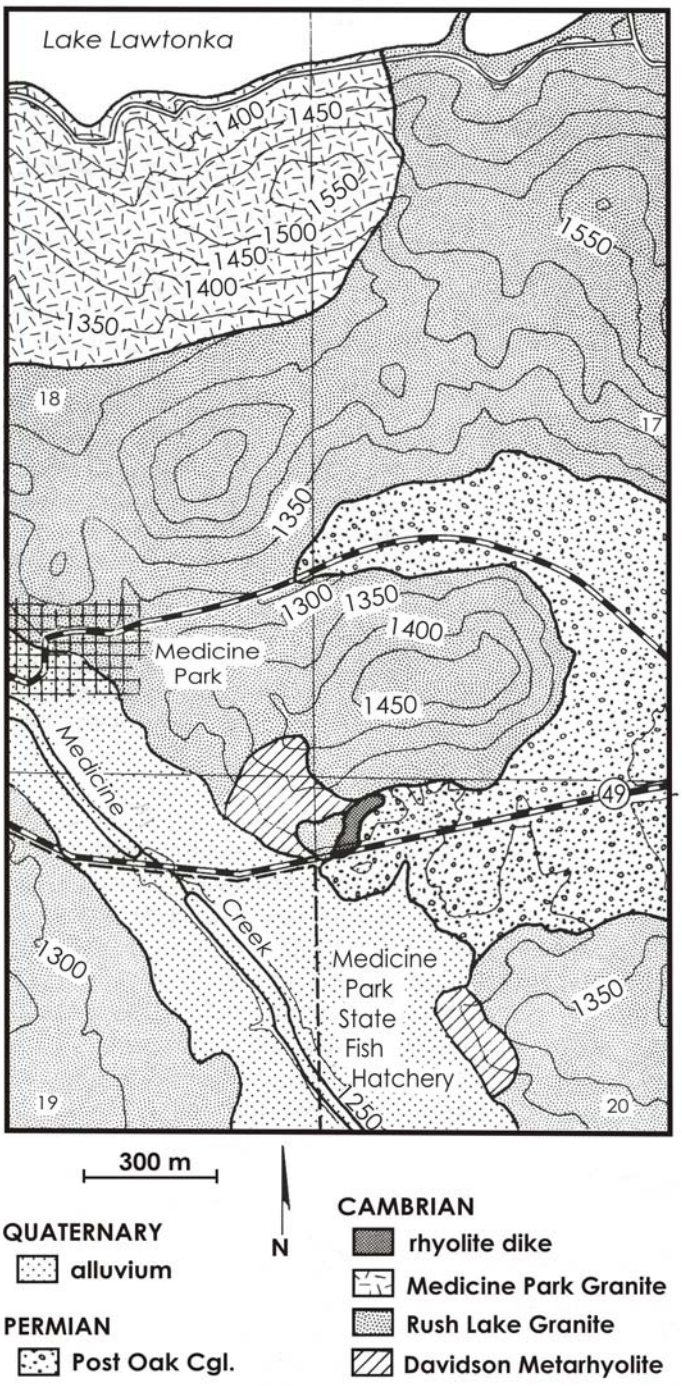

Fig. 3. Geologic map of the Rhyolite Dike at Medicine Park (center, densely stippled) and surrounding area. Exposed contacts of the rhyolite dike are along the eastern and western contacts with the Rush Lake Granite. In places, the Post Oak Conglomerate unconformably overlies the rhyolite dike. Modified from Gilbert & Powell, 1988.

dike displays digitated fingering into the Rush Lake Granite with evidence of a very weak alignment of the alkali feldspar phenocrysts and a marked reduction in phenocryst abundance in a very narrow zone (< 1cm) adjacent to the contact. The western edge of the dike displays a sharp, irregular intrusive contact with the Rush Lake Granite (Gilbert and Powell, 1988; Fig. 4a).

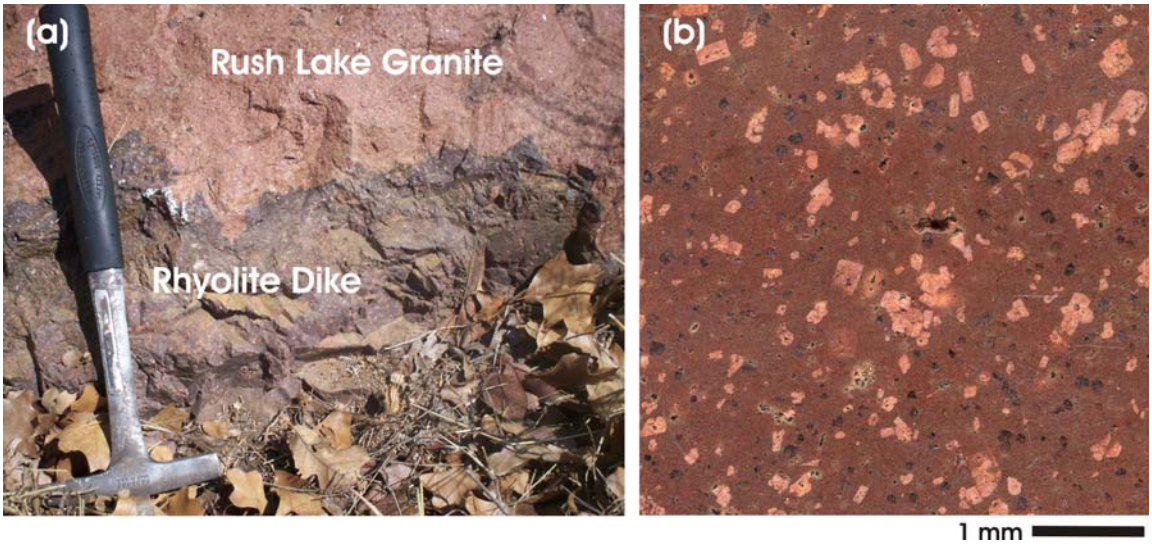

Fig. 4. Macroscopic views of the Medicine Park rhyolite dike. (a) Contact showing the rhyolite dike (dark grey) intruding into the Rush Lake Granite (salmon red; rock hammer for scale. (b) Rock slab showing the porphyritic texture of the rhyolite dike. Individual phenocrysts of alkali feldspar (tabular and light red) and quartz (square to rounded and dark grey) are set in a very fine grained matrix of alkali feldspar and quartz (red). Also readily visible are glomerocrysts of alkali feldspar and a miraolitic cavity (center).

Field Observations

The following rock descriptions assign color values following the Munsell classification (The Rock Color Chart Committee, 1964) using color palettes from a rock color classification chart where the first number and letter represents hue (e.g. 10 R), the second number represents the value (lightness) and the last number represents chroma (degree of saturation). Grays do not have hue or chroma but only a value (lightness). Broken, unweathered surfaces of the rhyolite dike display phenocrysts of orange pink (10 R 6/4) alkali feldspar and medium dark gray (N 4) quartz in a red-brown (10 R 4/3)

matrix. Polished, unweathered surfaces display moderate red-orange (10 R 6/6) alkali feldspar and medium dark gray (N 4) quartz in a dark red-brown (10 R 3/4) matrix. Weathered surfaces are typically a dark yellow-orange (10 YR 6/6) color where the alkali feldspar and quartz cannot be readily discerned.

Glomerocrysts and individual phenocrysts of both alkali feldspar and quartz are easily seen in unweathered portions of the outcrop and have a maximum length of 11 mm for alkali feldspar and 2 mm for quartz (lower size limits are measured in thin section). The "typical" texture of the rhyolite dike away from the contacts appears massive; however, a very weak fabric is locally evident. This fabric is also evident in slabs where both the alkali feldspar and quartz phenocrysts are locally segregated into domains of higher phenocryst abundances (Fig. 4b). Vesicles, or miarolitic cavities, with a maximum length of 3 mm are ellipsoidal in nature, which may reflect distortion due to flow. Sparse ovoid to hexagonal reduction spots where the matrix is "bleached" a light red-orange (10 R 7/6) color is also present.

ANALYTICAL METHODS

Data Acquisition

Modal abundances were calculated using quantitative 2-dimensional (2D) analysis of a 50 mm x 75 mm thin section that is representative of the rhyolite dike. The alkali feldspar and quartz phenocrysts, as well as the whole sample, were outlined and color filled in CorelDRAW (an image editing program) and exported to their own JPEG image. Each image was then imported into ImageJ to calculate the area that each phenocryst occupied, the total phenocryst area, and the total area of the sample.

Previous analysis of whole rock chemistry of the rhyolite dike (Hogan, unpublished data) was obtained using X-ray fluorescence using a Rigaku SMAX 3080 spectrometer at the School of Geology and Geophysics, University of Oklahoma (OU) following the procedure outlined in Weaver *et al*. (1996). Quantitative analyses of alkali feldspar phenocrysts were analyzed using a Cameca SX50 electron microprobe (EMP) at OU. Operating conditions were an accelerating voltage of 20 kV, a beam current of 10 nA and a beam size 3 μm. Alkali feldspar chemical composition was analyzed by measuring the orthoclase domains and the exsolved albite domains separately. Seven random alkali feldspar phenocrysts were chosen to reintegrate the total feldspar composition. Each phenocryst was captured as a backscattered electron (BSE) digital image using the EMP and converted into binary images to distinguish between the dark grey albite phase (perthite) and the light grey orthoclase phase (Fig. 5). The phase proportions of each alkali feldspar grain are calculated using ImageJ (an image analysis program), which calculates the area percent of each phase based on color values. The area percent is converted to weight percent by multiplying the density of albite and orthoclase to the area percent of each respective phase. The weight percents are used as factors for modal recombination, which calculates the total alkali feldspar composition. Microprobe analysis of the matrix was collected in three different phenocryst free regions using a wide beam (25-30 micrometer spot size) for 100 points (10 point x 10 point grid). The matrix composition is used as a proxy for the rhyolite dike melt composition at the time of quenching.

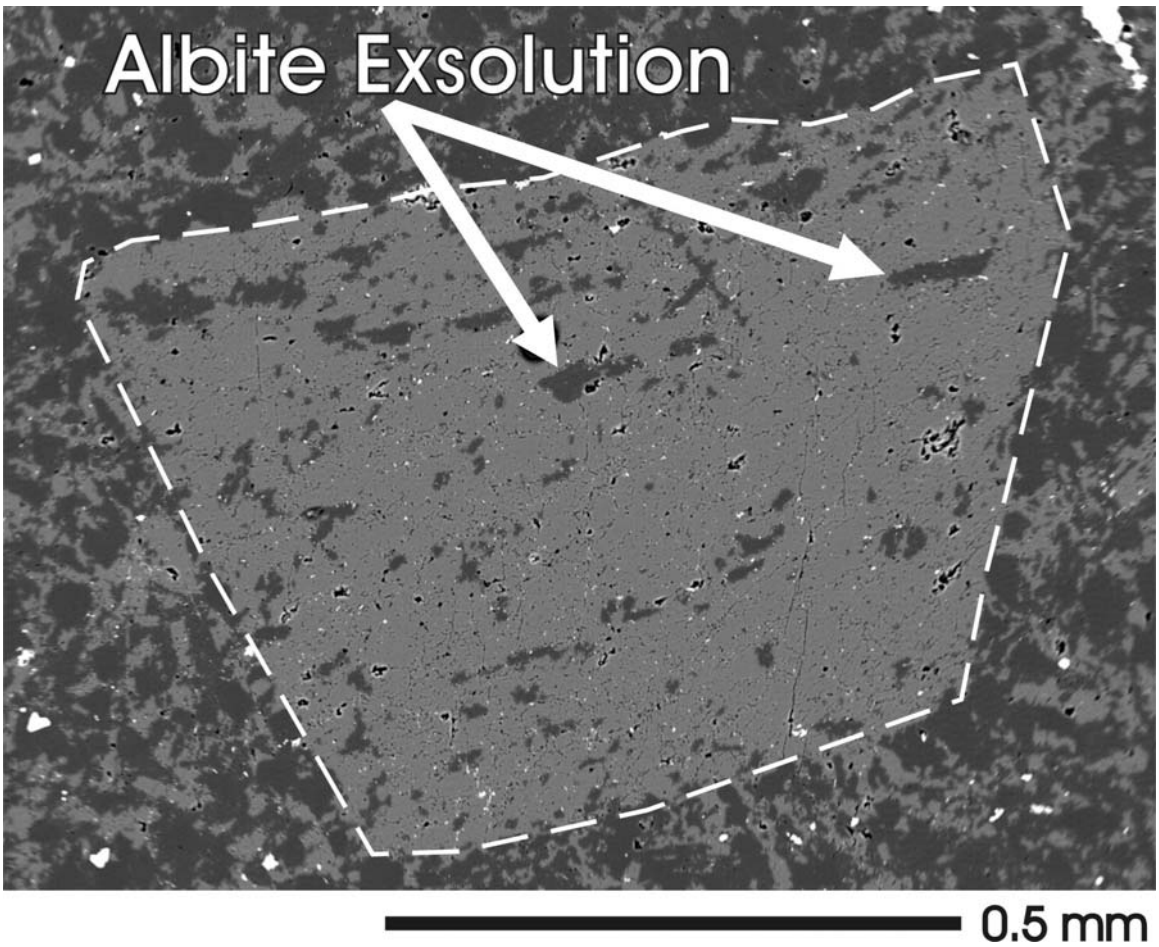

Fig. 5. Cross-polarized micrograph of a typical perthitic alkali feldspar phenocryst. The light grey phase is the orthoclase host and the dark grey phase (arrows) is the exsolved albite lamellae.

Petrography

Phenocrysts

Phenocrysts constitute 18% of the rhyolite dike set in a fine grained matrix. The phenocrysts (Table 1) consist of 60 % alkali feldspar, 40% quartz, and a completely altered mineral (<<1%). Table 1 shows the phenocryst percentages from two rock slabs as well as a thin section. Due to the low contrast of the quartz with the matrix in the slab samples, the smaller sizes of the quartz phenocrysts are not readily discernable (Fig. 4b). However, the quartz phenocrysts can be easily identified in thin section and so the thin section sample (JH-2-04D) should be considered the most accurate measurement for

Table 1. Phenocryst proportions measured from the rhyolite dike.

	Sample Area (mm^2)	Phenocryst Area (mm^2)		% Individual Phenocrysts		% Matrix
		Feldspar	Quartz	Feldspar	Quartz	
S SO 1	900	131.0	39.6	76.8%	23.2%	81.0%
S SO 2	900	99.3	48.4	67.2%	32.8%	83.6%
JH-2-04D	1824	196.5	133.5	59.5%	40.5%	81.9%

S SO 1 and S SO 2 are the slab samples. JH-2-04D is the thin section sample.

phase proportions for the rhyolite dike at Medicine Park. Both alkali feldspar and quartz occur as single crystals and as monomineralic glomerocrysts (clusters of phenocrysts comprised of more than one alkali feldspar crystal or quartz crystal, but not a mixture of both mineral types; Fig. 6 and Fig. 7). Alkali feldspar phenocrysts are tabular and euhedral to subhedral (Fig. 6a to Fig. 6e) with rare resorbed, anhedral crystals (Fig. 6f). The alkali feldspar phenocrysts display perthitic textures (Fig. 5) and Carlsbad twinning is common. Individual alkali feldspar crystals within the glomerocrysts exhibit euhedral to subhedral contacts (Fig. 6a) and mutually corroded, interlocking contacts (Fig. 6b and Fig. 6c). No apparent critical crystal size to be apart of the glomerocrysts is seen for individual alkali feldspar crystals. Individual alkali feldspar crystal sizes are 0.08 mm to 5.5 mm while glomerocrysts sizes range from 0.10 mm to 12 mm. Quartz phenocrysts typically occur as subhedral to anhedral crystals (Fig. 7a to Fig. 7c) exhibiting one or two good crystal faces, while the other faces are irregular to embayed, presumably a result of resorption. Anhedral, embayed crystals (Fig. 7d and Fig. 7e) typically have a corona around the crystal consisting of high concentration of small quartz crystals. Hexagonal, euhedral crystals do occur (Fig. 7f), but are very uncommon. Individual quartz sizes range from 0.08 mm to 1.7 mm while the size range of glomerocrysts is 0.08 mm to 3.25

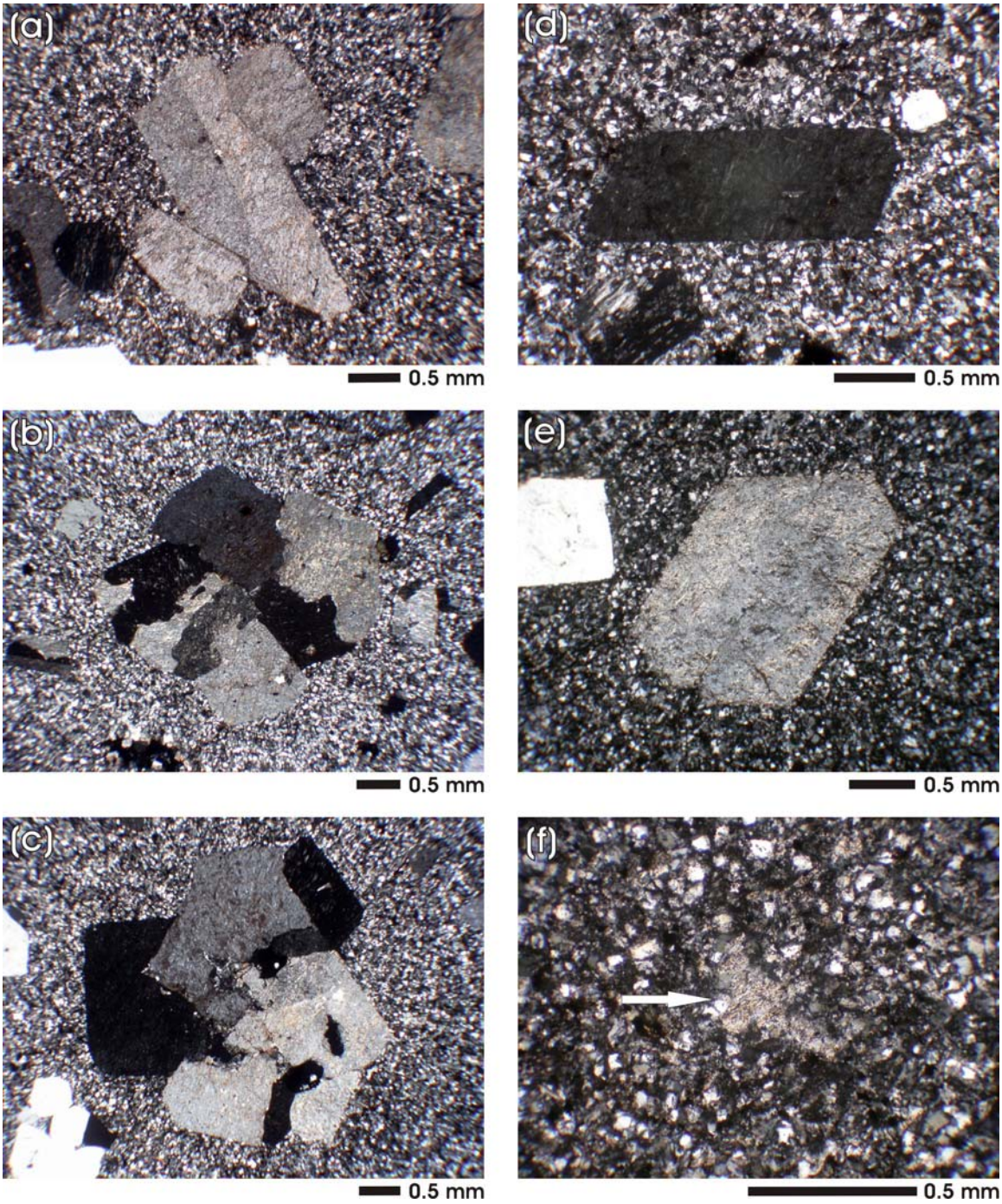

Fig. 6. Cross-polarized micrographs of alkali feldspar phenocrysts of both glomerocrysts and individual crystals. (a) Alkali feldspar glomerocrysts with the center alkali feldspar crystal overgrowing the two smaller crystals. (c – d) Alkali feldspar glomerocrysts with mutually corroded internal contacts. (d - e) Typical single euhedral alkali feldspar phenocryst. (f) Rare resorbed alkali feldspar phenocryst.

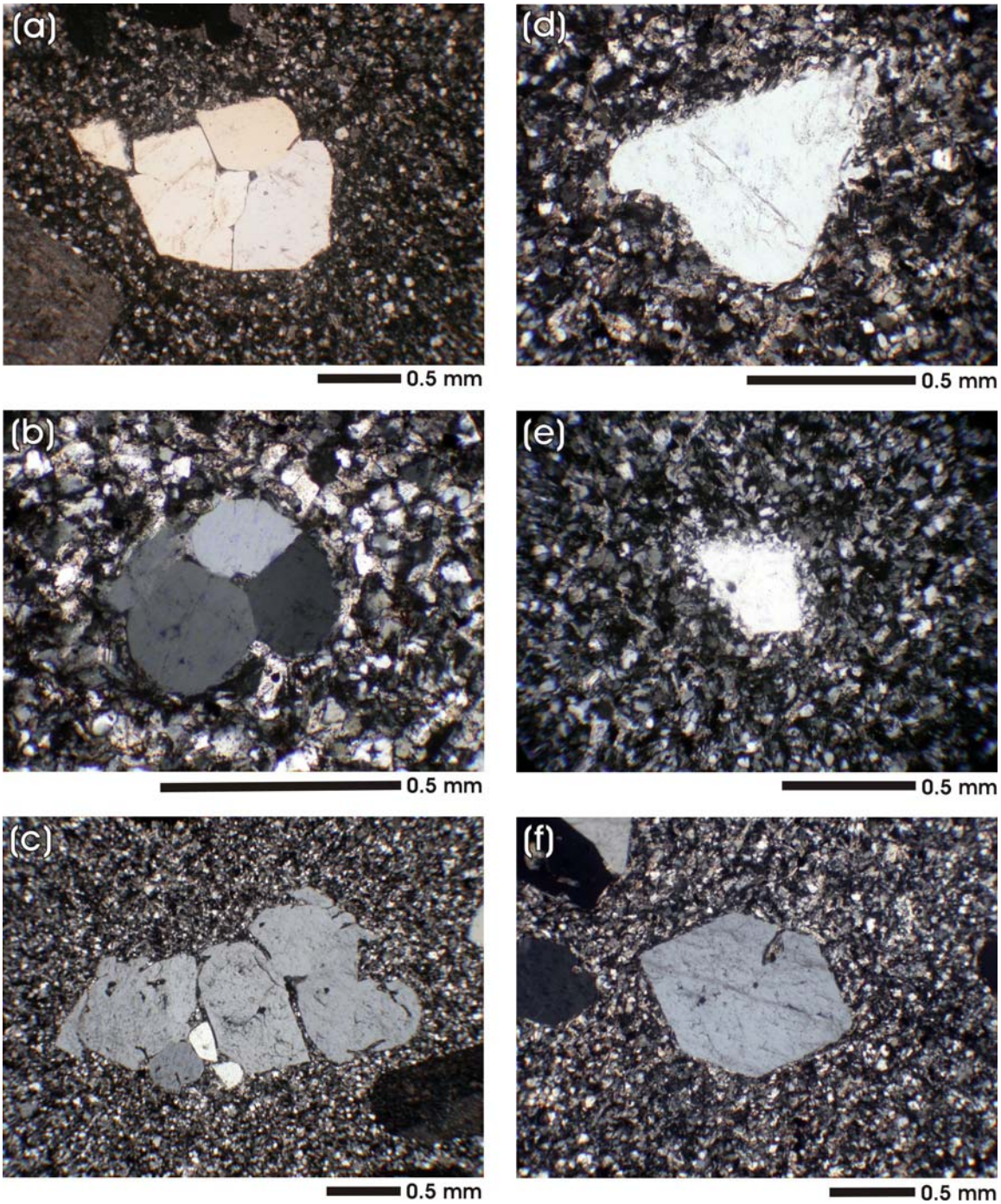

Fig. 7. Cross-polarized micrographs of quartz phenocrysts of both glomerocrysts and individual crystals. (a - b) Anhedral to subhedral quartz glomerocrysts with the borders of tightly clustered individual crystals clearly defined. (c) Loosely clustered, anhedral quartz glomerocryst with corroded edges (evidence of resorption) and the interstitial material between the individual crystals is readily apparent. (d - e) Typical resorbed quartz phenocrysts. Notice the halo of resorbed quartz material that was in the process of going back into the melt at the time of quenching of the rhyolite dike. (f) Rare euhedral quartz phenocryst with no evidence of resorption.

mm. Quartz glomerocrysts consist of crystals that range in size similar to individual phenocrysts sizes, but smaller crystals (i.e., 0.15 mm to 0.55 mm) are more common.

Matrix

The matrix consists of very fine grained (<0.08) granular anhedral crystals of alkali feldspar, quartz and an opaque oxide that is most likely magnetite. Pore spaces in the form of vesicles represent approximately 2% of the rhyolite dike. The opaque crystals occur as a minor constituent of the matrix and as a late stage mineralization in the vesicles. Vesicles vary in texture, but, typically, are rimmed by a concentric ring of opaque minerals (Fig. 8) which, in some cases, can be subsequently rimmed by an outer

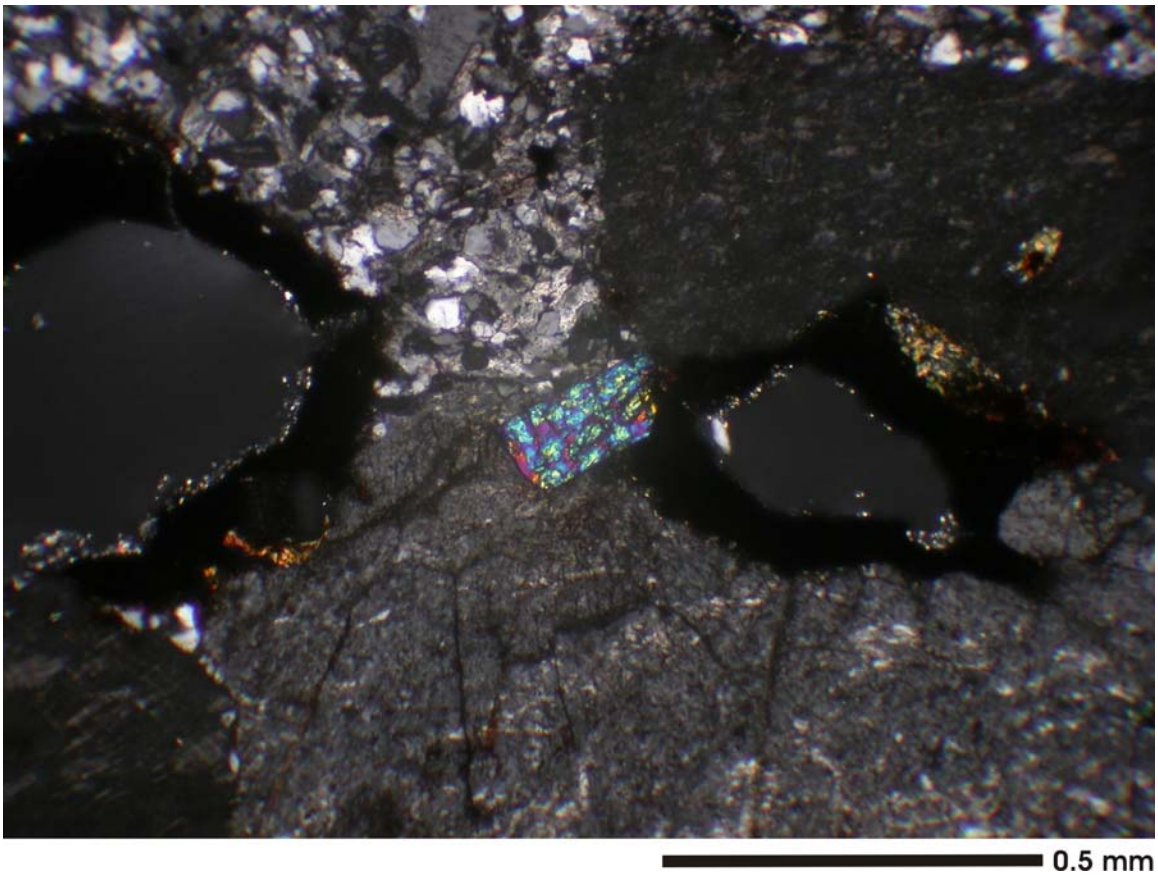

Fig. 8. Cross-polarized micrograph of two vesicles rimmed by opaque minerals. The center mineral with high birefringence is zircon which is in contact with the opaque minerals rimming the vesicle. The large phenocrysts (top and bottom) are alkali feldspar.

ring of matrix minerals that are slightly larger than the typical matrix crystals (<0.08 mm) and are oriented perpendicular to the ring. Zircon is also present is small amounts (<1) and commonly occurs within, or in contact with, the inner opaque ring that rims the vesicles.

Analysis of the Rhyolite Dike at Medicine Park

In this study, crystal size distribution (CSD) is used to model the effects of clustering and resorption of crystals from the rhyolite dike at Medicine Park from the Southern Oklahoma Aulacogen (SOA). Both slab and thin section (TS) samples are used to compare CSDs to exemplify the disadvantages and benefits of both techniques. The rhyolite dike is tested to find its place within the SOA granite model using estimation of pressure from the SiO_2-$NaAlSi_3O_8$-$KAlSi_3O_8$-H_2O diagram to find the depth of crystallization. Using CSD curves the amount of quartz material resorbed may lead to the rate of resorption, the time it took for the rhyolite dike magma to ascend through the crust, and the ascent rate of the magma.

Two different methods were used to obtain data for this study and were modeled after other 2-dimensional image analysis techniques (Higgins, 2000; Castro *et al.*, 2003) to produce CSDs. First, using a flatbed scanner, high resolution digital images (1200 dpi) were acquired of 2 randomly oriented 30 mm x 30 mm from a texturally typical part of 2 rhyolite dike rock slabs. The digital images were then imported into a graphics editing program, CorelDRAW, where the boundaries of all phenocrysts and glomerocrysts present in the scanned image were outlined (Squares S1 and S2 of Fig. 9). The glomerocryst boundaries were outlined, first, as a coherent unit (Fig. 9 and Fig. 10a) as well as the individual crystal phenocrysts. On a separate drawing layer, the boundaries of

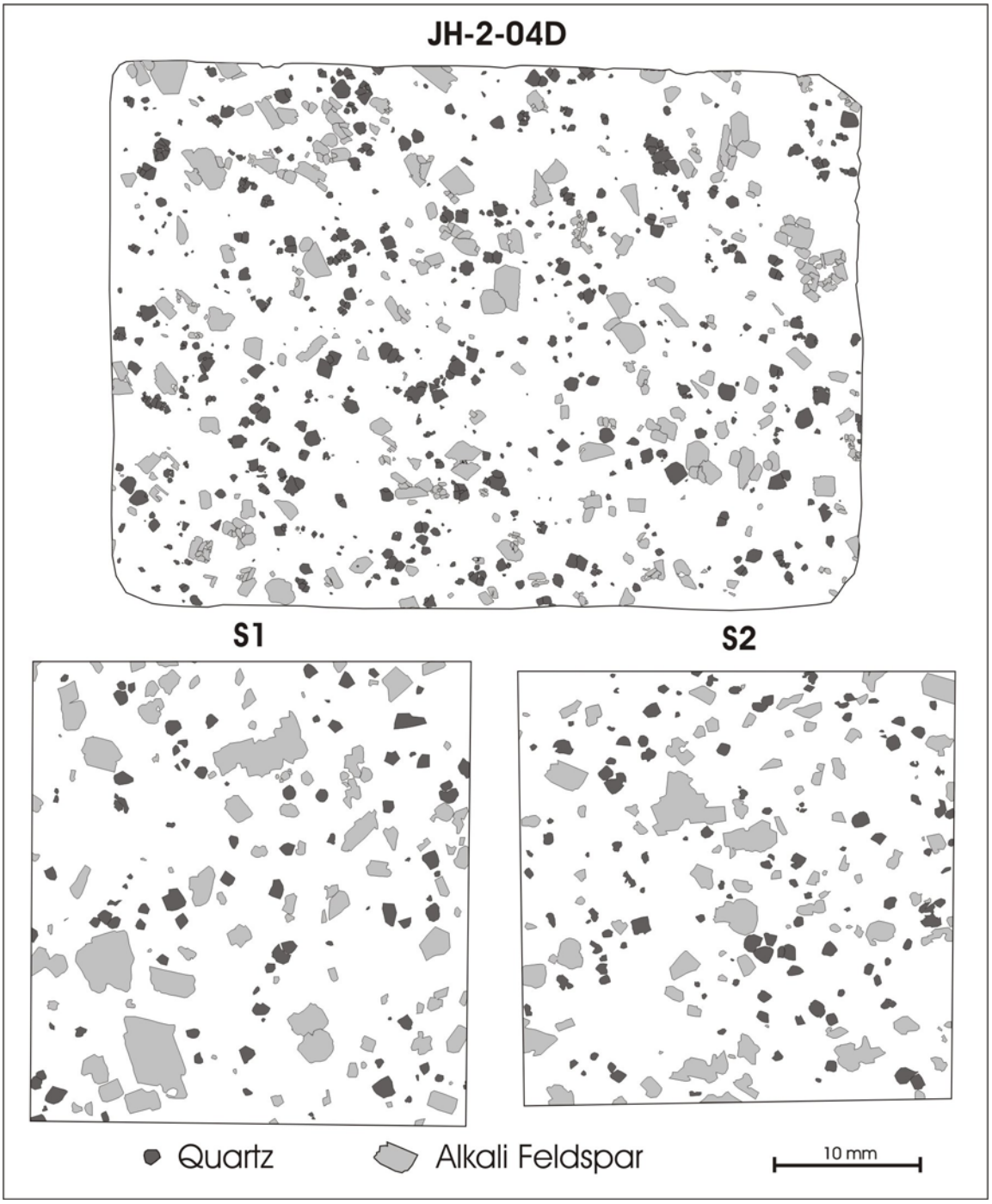

Fig. 9. Outlines of glomerocryst phenocrysts. JH-02-04D is a 50 mm x 75 mm thin section with the individual crystals in the glomerocrysts outlined as well as the individual crystal phenocrysts. S1 and S2 are approximately 30 mm x 30 mm rock slab outlines without the individual crystals in the glomerocrysts outlined.

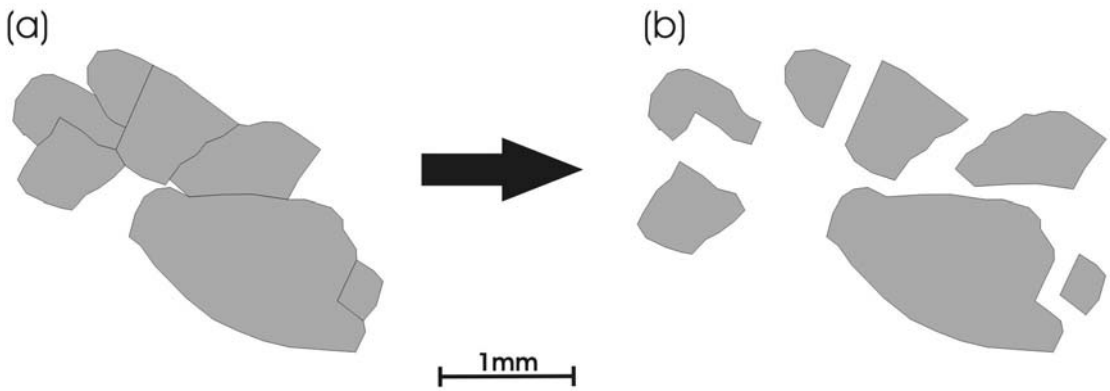

Fig. 10. Schematic deconstruction of a glomerocryst. (a) Digital outlines of alkali feldspar glomerocryst. (b) Deconstructed alkali feldspar glomerocryst after manually separating individual crystals.

the individual crystals comprising the glomerocryst were outlined and then manually deconstructed, or separated (Fig. 10b), to provide a proxy for the size and shape of phenocrysts prior to glomerocryst formation.

The resolution of the rock slabs' digital images placed restrictions on the lower size limit of the phenocrysts that could be resolved (~0.20 mm for alkali feldspar and ~0.25 mm for quartz) and also hampered the ability to accurately determine the boundaries of the phenocrysts, especially the interior shared crystal boundaries within glomerocrysts. To overcome these limitations a large 50 mm x 75 mm thin section of the rhyolite dike was made. A digital image of this thin section was acquired using a flatbed scanner. In addition, photomicrographs, using a transmitted light petrographic microscope, were then acquired of the whole thin section. Individual phenocrysts and glomerocrysts present in the digital photomicrographs were then outlined in CorelDRAW. These outlines were then transferred and rectified to the scanned image of the entire thin section as a place setter to guarantee that all crystals were counted. To define the individual glomerocryst crystals, extinction angles and relict borders (Fig. 6a-c and Fig. 7a-c) were used while tracing the phenocrysts. Data cannot be obtained for

phenocryst crystal sizes that approach the devitrified matrix size (~0.08 mm), especially in quartz due to resorption, which creates difficulties when determining the lower phenocryst size limit. However, a distinction between phenocrysts and matrix crystals can be made since the devitrified glass is equigranular (e.g., Fig. 7d-e). Crystals that are larger than 0.08 mm are considered phenocrysts and anything below this limit is part of the matrix. A caveat is that phenocrysts that have been resorbed to a size that is below 0.08 will be counted as part of the matrix and are obviously not part of the analysis. Fig. 9 shows the glomerocryst outlines and individual crystal phenocrysts of both the thin section and slabs.

Sizes, shapes and percentages of phenocrysts phases, as well as percentages of matrix and miarolitic cavities, are then readily determined from tracings using an image analysis program. For both techniques, the outlines produced in CorelDRAW were imported into ImageJ (Abramoff *et al.*, 2004), the Java based analogue to the image analysis program NIHImage, as an 8-bit grayscale Tiff Bitmap. Crystals lying on the edge of the area being analyzed were discounted since exclusion of these crystals has little affect on the final results. This because the number of partial crystal outlines along the edge of the analyzed area is considerably less than the total number of crystals counted. The images were then converted to binary images and the areas and lengths of the minor and major axes of the crystals were measured. ImageJ applies a best fit ellipse to each crystal where the area as the crystal is conserved. The major and minor axes of the ellipses will be considered the measurement of the crystal's major and minor axes (Fig. 11); this will be explained in subsequent sections.

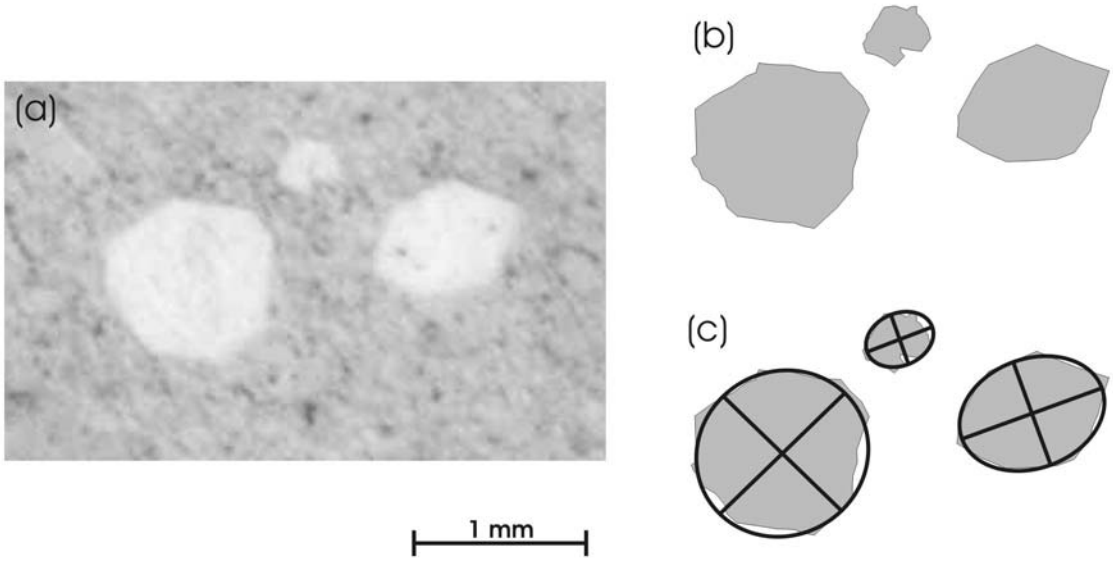

Fig. 11. Example of the application of a best fit ellipse to crystals in ImageJ. (a) Single quartz crystals in a rhyolite dike slab. (b) Outline of quartz crystals. (c) Fitted ellipse with major and minor axes calculated from ImageJ.

Size Measurements

Crystal sizes of the rhyolite dike (determined from ImageJ) were processed using CSD Corrections 1.36 (Higgins, 2000). This program converts the 2-dimensional data processed from the slabs and thin section to 3-dimensions, a process called stereology. This conversion is necessary as direct measurement of crystal sizes are limited to 3-dimensional (3D) analytical methods, such as serial grinding, mineral separation (Bindeman, 2003), and X-ray tomography (Castro *et al*., 2003), and are not always feasible. For objects more complex than a sphere, this conversion is mathematically quite difficult and has no unique solution for real data (Higgins, 2000). Difficulties that arise in the transformation of 2D data to 3D data (e.g., the intersection probability effect and the cut section effect) have been summarized by Higgins (2000) and Peterson (1996). The intersection probability effect states that in a polydispersed system, smaller crystals are less likely to be intersected by a 2-dimensional plane (e.g. a thin section or a slab) than larger crystals. The cut section effect states that the plane that cuts through a crystal

rarely contains the exact center of the crystal, which is needed for this conversion, but instead can intersect an infinite number of other possible orientations - consequently, crystal sizes can range from those approaching zero to those approaching the largest 3D lengths (this length would not have to intersect the center of the crystal). CSD Corrections (Higgins, 2000) accounts for these effects, and other possible effects, and calculates the long dimension, major axis, or diameter for three dimensional ideal crystal shapes (parallelepiped, ellipsoid, or sphere, respectively) from two dimensional measurements based upon the following input parameters: 2D measured length (box width or length, ellipse width or length, or maximum length), crystal shape, crystal roundness, and rock fabric (i.e., preferred alignment of crystals).

Determination of Crystal Shape

Following Higgins (1994) and Higgins (2000), the crystal shape is determined by finding the short (S), intermediate (I), and long (L) dimensions of the crystals, as well as defining the crystal, roundness, and the rock fabric. The S and I dimensions of the crystals are found by plotting the frequency distribution for width/length ratios (w/l) of measured crystals (Fig. 12) using the minor axis (w) and the major axis (l) of the best fit ellipses calculated from ImageJ (Fig. 11). The mode of the distribution corresponds to the S/I ratio, and by normalizing the S dimension to 1, a relative dimension for I can be determined (Table 2). Dimension L is determined using the following two equations:

$$\text{skewness} = \frac{\text{mean}(w/l) - \text{mode}(w/l)}{\text{standard deviation}(w/l)} \quad (1)$$

$$I/L = \text{skewness} + 0.5 \quad (2)$$

For alkali feldspar phenocrysts from the rhyolite dike this analysis yields an aspect ratio is 1:1.5:5.5 (S:I:L). This 3D aspect ratio is in agreement with 2D manually measured

alkali feldspar crystals in thin section with a mean aspect ratio of 1:2. The 2D w:l aspect ratio correlates to the 3D S:I aspect ratio since the most common width and length measurements correspond to S and I, respectively (Higgins, 2000).

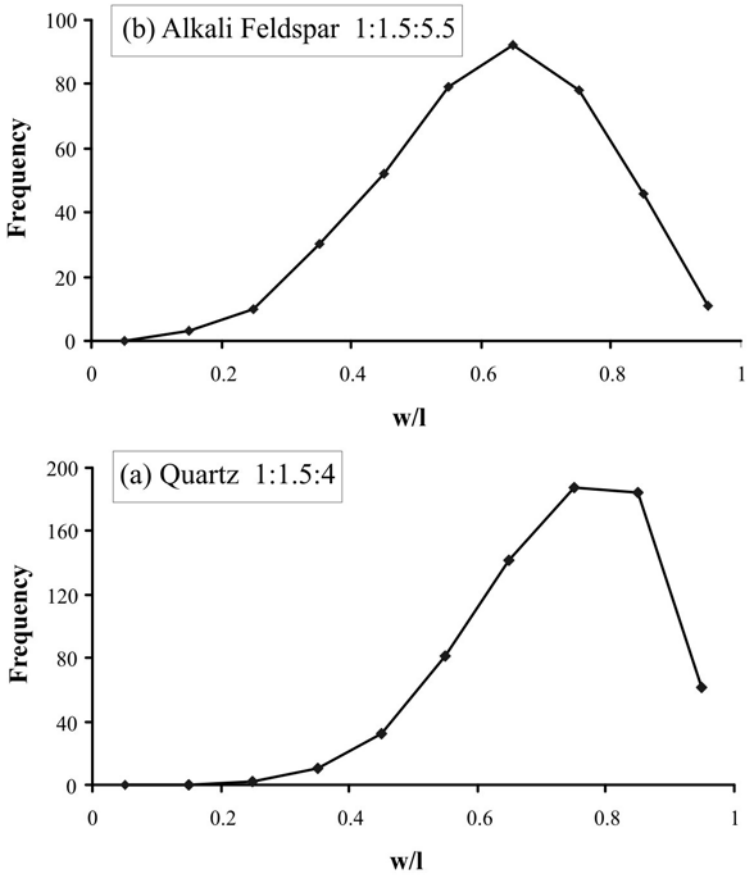

Fig. 12. Frequency vs. width (w) to length (l) ratios of the measured crystals to determine the short (S) and intermediate (I) dimensions of the crystal in 3-dimensions. The width and length correspond to the minor and major axis, respectively, of the measured crystals. (a) Alkali feldspar with a resultant aspect ratio of 1:1.5:5.5 and (b) quartz with an aspect ratio of 1:1.5:4. The quartz dimensions cannot be calculated graphically since they are equant grains and the dimensions 1:1.5:4 are, therefore, incorrect.

The calculated aspect ratio of quartz is 1:1.5:4. However, this aspect ratio is inconsistent with petrographic observations of quartz phenocrysts in the rhyolite dike. As noted by Higgins (1994), this analytical approach is unreliable for estimating aspect ratios of near equant grains, such as quartz. The aspect ratio of quartz was manually

determined by measuring euhedral or nearly euhedral (partially resorbed) quartz phenocrysts from a thin section using a transmitted light microscope in cross-polarized light. The a- and b-axis lengths of the quartz crystals were measured from crystals that were at complete extinction at all angles so that the c-axis is perpendicular to the plane of the thin section. Only one euhedral quartz crystal (Fig. 7f) was found so that the c-axis is parallel to the plane of the thin section (i.e. the crystal exhibits maximum birefringence

Table 2. Measured and calculated 2D dimensions of the quartz and alkali feldspar phenocrysts and their respective calculated 3D dimensions.

Measured Dimensions of Quartz Crystals

	⊥ c												|| c
	1	2	3	4	5	6	7	8	9	10	11	12	1
w	60	76	45	23	32	89	25	29	33	44	35	43	10
l	70	70	48	28	39	100	24	31	39	40	40	47	23
notes	e	e	e	e	e	pr	pr	pr	pr	pr	pr	pr	e

	⊥ c (mean)	|| c
w/l	0.90	0.43
l/w	1.1	2.3

Calculated Dimensions of Quartz and Alkali Feldspar Crystals

	Alkali Feldspar	Quartz
Population	401	700
Mode (w/l)	0.65	0.75
Mean (w/l)	0.61	0.73
Std. Dev. (w/l)	0.17	0.14
Skewness	-0.21	-0.14

3D dimensions

	Alkali Feldspar	Quartz (meas.)	Quartz (calc.)
S	1	1	1
I	1.5	1	1.5
L	5.5	2	4

Measurements for the quartz grains were determined using a transmitted light microscope under cross-polarized light. Measured grains were at complete extinction so that the a- and b-axis could be measured (looking down the c-axis: Quartz ⊥ c). Only one completely euhedral quartz crystal was found oriented so that the crystal exhibits maximum birefringence and an optical flash figure (Quartz || c). Abbreviations: e - euhedral and pr - partially resorbed. All dimensions have been rounded to the closest half number and units of the dimensions are arbitrary. Skewness for the calculated dimensions was calculated using Equation 1. Description of determining the short (S), intermediate (I), and long (L) dimensions are included in the text.

and an optical flash figure). The measurements are displayed in the Measured Dimensions section of Table 2 and the resultant new dimensions for quartz are 1:1:2.

The roundness parameters used for quartz and feldspar are 0.4 and 0.3, respectively, and are determined from visual inspection using the CSD Corrections (Higgins, 2000) scale of 0 representing blocky crystal shapes and 1 representing elliptical crystal shapes. As previously discussed, the rock fabric of the rhyolite dike is massive.

RESULTS

Geochemistry and the SiO_2-$NaAlSi_3O_8$-$KAlSi_3O_8$ Diagram

Bulk Composition

In general, comparisons of normative compositions of granitic/rhyolitic rocks with experimentally determined liquidus boundary curves, minima, and eutectics in the SiO_2-$NaAlSi_3O_8$-$KAlSi_3O_8$-H_2O (Q-Ab-Or; Fig. 13) system can suggest crystallization conditions for the magma. These comparisons are tentatively used since the composition of the rock does not a priori represent the original composition of the melt and the position of the boundary curves, minima, and eutectic are sensitive to additional components, such as anorthite and fluorine, which may be present in the natural melt and not in the experimental studies. For the rhyolite dike, direct comparisons with this system are warranted because the presence of miarolitic cavities indicate vapor saturation (at least at the time of emplacement), the anorthite component is low ($An_{<1}$), and the sum of the normative Q, Ab, and Or components is >95% (Hogan & Gilbert, 1997). The whole rock bulk composition data of the rhyolite dike determined by XRF (X-ray fluorescence) and the normative mineralogy are displayed in Table 3 (Hogan, unpublished data). Normalized bulk compositions of 35% Q, 39% Ab, and 26% Or

(Higgins, 1994) are plotted on the SiO_2-$NaAlSi_3O_8$-$KAlSi_3O_8$-H_2O diagram (point *X* of Fig. 13).

Feldspar Phenocryst Composition

The chemical composition of the alkali feldspar phenocrysts are displayed in Table 4 and Appendix A. The average individual phases, albite and orthoclase, and the proportions of seven perthitic alkali feldspar crystals were calculated using ImageJ (see Analytical Methods). The phase proportions, or weighting factors, for the individual feldspars range from 66% to 86% for the orthoclase host phase (albite weighting factors are

Table 3. Rhyolite dike whole rock chemical analysis of major and trace element compositions and normative mineralogy.

Major Element (wt.%)		CIPW Norm (wt %)	
SiO_2	76.2	Quartz	32.6
TiO_2	0.13	Plagioclase	37.4
Al_2O_3	11.9	Orthoclase	25.3
Fe_2O_3	2.07	Diopside	0.16
MnO	0.01	Hypersthene	2.02
MgO	0.07	Acmite	0.89
CaO	0.05	Ilmenite	0.25
Na_2O	4.54	Magnetite	0.45
K_2O	4.25	Apatite	0.02
P_2O_5	0.01	Zircon	0.06
Total	99.2	Total	99.1
Trace Element (ppm)		**Selected Normalized Phases**	
Ba	140	Quartz	34%
Nb	58	Albite	39%
Rb	172	Anorthite	0%
Sr	7	Orthoclase	27%
Y	94		
Zr	317		

Whole rock analysis determined by X-ray fluorescence using a Rigaku SMAX 3080 spectrometer at the School of Geology and Geophysics, University of Oklahoma (Hogan, unpublished data).

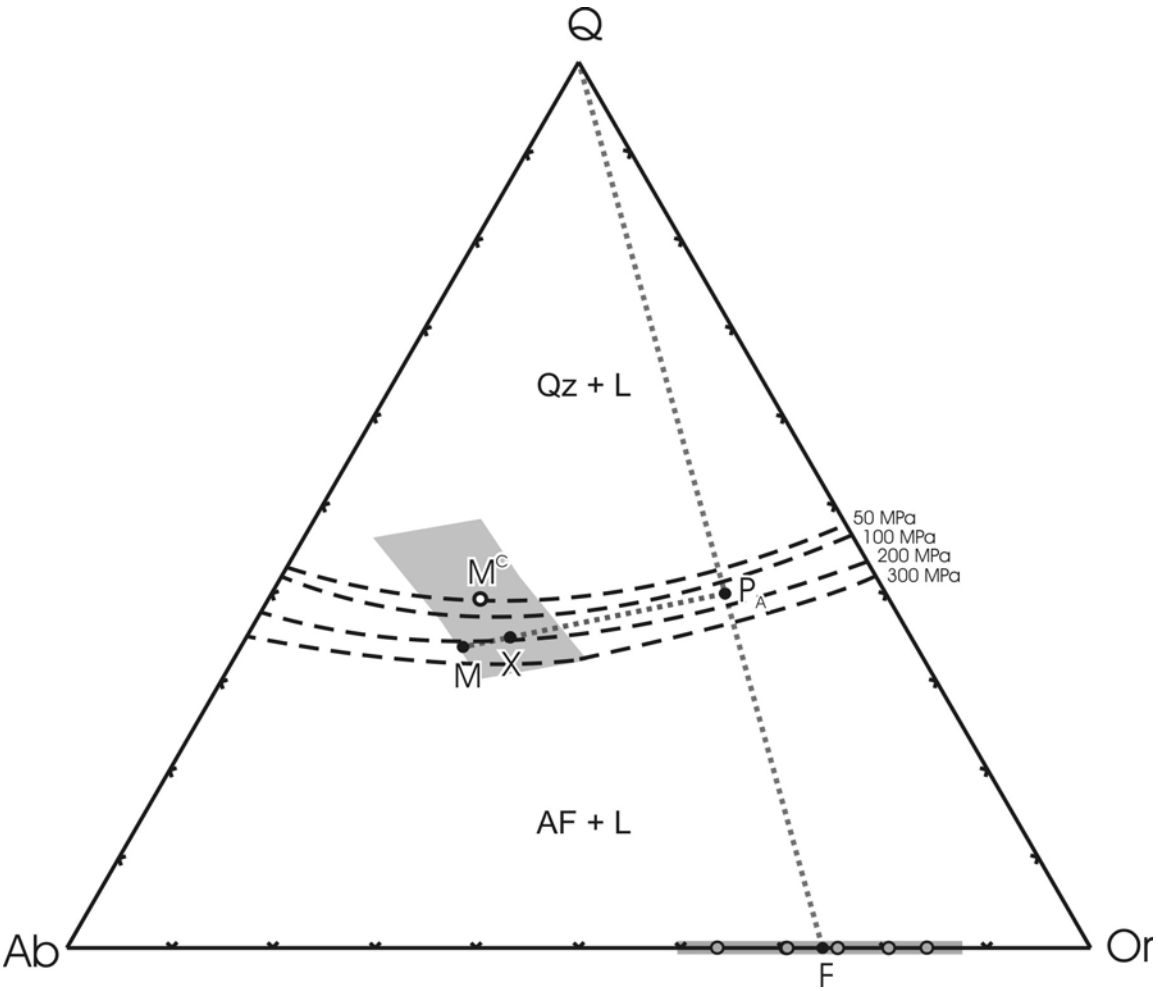

Fig. 13. Selected equilibrium phase relationships in the system SiO_2-$NaAlSi_3O_8$-$KAlSi_3O_8$-H_2O as modified from Tuttle & Bowen (1958). Qz + L is the quartz + liquid region and AF + L is the alkali feldspar + liquid region. The long dashed lines are pressure dependent cotectics. Point *X* is the projection of the whole rock bulk composition based upon the normative components quartz (Q), albite (Ab), and orthoclase (Or;Table 3), point *F* is the average composition of reconstituted alkali feldspar (Table 4), point P_A is the ratio of the quartz to alkali feldspar based upon the modal abundances of these phases as determined from image analysis of the thin section (Table 1), and *M* is the melt composition calculated from ratio between phenocrysts and matrix in the thin section JH-02-04D (Table 1). M^c is the CIPW normative composition of the melt derived from electron microprobe analysis of the matrix composition (Table 5). Grey open circles along the Ab-Or feldspar line are individual reconstituted alkali feldspars. The gray areas represent the 2σ deviation for the averages of average alkali feldspar composition (*F*) which varies along the Ab and Or line and the normative matrix composition (M^c) which can vary in Q, Ab, or Or direction.

complimentary; Table 4). The resultant normalized average reintegrated alkali feldspar has a composition of Or_{91} (point *F* on Fig. 13).

Modal Abundance of Phenocrysts and Matrix

To calculate the modal abundance of the phenocrysts, the total areas of both individual phenocryst phases (quartz and alkali feldspar) and the proportion of phenocrysts and matrix (18% and 82%, respectively) can be measured using Fig. 9 and ImageJ. Results are summarized in Table 1. For accuracy, only the TS sample (JH-2-04D) was used to calculate the quartz abundance. The quartz abundances in the rock slabs will be systematically underestimated relative to alkali feldspar due to the rock slabs' lower limits of resolution of the scanned images which makes accurately tracing quartz phenocrysts difficult. Point P_A of Fig. 13 represents the phenocrysts proportions of alkali feldspar and quartz (59.5% and 40.5%, respectively).

Composition of the Melt during Crystallization

The composition of the melt during crystallization of the rhyolite dike has been constrained using two independent approaches: (1) electron microprobe analysis (EMPA) using a wide beam (30 μm) integrated over large areas of phenocryst free matrix, which serves as a proxy of the former interstitial melt (Table 5 and Appendix A), and (2) graphical calculation from reconstruction of the topology of the three phase equilibrium triangle (SiO_2-$NaAlSi_3O_8$- $KAlSi_3O_8$-H_2O system). The normative abundances of the quartz (39%), albite (40%), and orthoclase (21%) components of the matrix, as determined from EMPA (Table 5), plot at point M^c adjacent to the 50 MPa quartz-feldspar cotectic when projected into the SiO_2-$NaAlSi_3O_8$- $KAlSi_3O_8$-H_2O system. Point M^c represents the composition of the melt at the time of quenching during emplacement.

Graphical reconstruction of the composition of the melt utilizes the principles of the lever rule which relates the proportions and compositions of the phases present in the

Table 4. Chemical composition analysis of the average alkali feldspar phases.

	Feldspar 1		Feldspar 2		Feldspar 3		Feldspar 4		Feldspar 5		Feldspar 6		Feldspar 7		Average Feldspar	
	Average	Std Dev	Average	Std Dev	Average	Std Dev	Average	Std Dev	Average	Std Dev	Average	Std Dev	Average	Std Dev	Average	2σ
	Chemical Composition (Weight Percent)															
	K Phase															
WF	0.78		0.83		0.73		0.73		0.86		0.66		0.73			
SiO_2	65.1	0.29	64.8	0.25	65.1	0.22	64.8	0.24	64.6	0.35	64.7	0.24	64.8	0.09	64.8	0.35
Al_2O_3	18.9	0.08	18.9	0.08	19.0	0.04	18.9	0.13	18.8	0.12	18.8	0.15	18.9	0.10	18.9	0.12
Fe_2O_3	0.05	0.04	0.04	0.03	0.03	0.02	0.03	0.01	0.05	0.02	0.02	0.01	0.03	0.02	0.03	0.02
CaO	0.00	0.00	0.00	0.00	0.00	0.00	0.00	0.00	0.00	0.01	0.00	0.00	0.00	0.00	0.00	0.00
BaO	0.03	0.03	0.03	0.03	0.01	0.02	0.03	0.02	0.03	0.02	0.02	0.02	0.04	0.02	0.03	0.02
Na_2O	0.24	0.04	0.20	0.04	0.21	0.05	0.25	0.04	0.23	0.04	0.19	0.04	0.25	0.14	0.22	0.05
K_2O	16.2	0.06	16.3	0.11	16.2	0.07	16.2	0.07	16.2	0.07	16.3	0.09	16.1	0.48	16.2	0.14
Total	100.6	0.29	100.2	0.26	100.5	0.22	100.3	0.32	100.0	0.45	100.1	0.31	100.1	0.34	100.24	0.46
	Na Phase															
WF	0.22		0.17		0.27		0.27		0.14		0.34		0.27			
SiO_2	69.0	0.24	69.2	0.20	68.8	0.37	69.0	0.27	68.4	0.31	68.5	0.43	68.5	0.42	68.8	0.60
Al_2O_3	20.1	0.12	20.1	0.20	20.1	0.18	20.2	0.08	20.0	0.10	20.0	0.21	20.0	0.15	20.1	0.12
Fe_2O_3	0.28	0.25	0.21	0.23	0.26	0.34	0.22	0.23	0.24	0.13	0.22	0.30	0.25	0.05	0.24	0.05
CaO	0.04	0.04	0.09	0.10	0.06	0.05	0.06	0.03	0.05	0.03	0.06	0.04	0.04	0.02	0.06	0.03
BaO	0.01	0.01	0.01	0.01	0.01	0.01	0.01	0.01	0.00	0.01	0.01	0.01	0.01	0.02	0.01	0.01
Na_2O	11.7	0.21	11.5	0.19	11.7	0.12	11.6	0.21	11.6	0.13	11.7	0.13	11.7	0.03	11.6	0.14
K_2O	0.23	0.27	0.11	0.04	0.13	0.09	0.26	0.37	0.36	0.46	0.08	0.02	0.17	0.21	0.19	0.20
Total	101.3	0.30	101.2	0.34	101.1	0.59	101.3	0.53	100.6	0.21	100.6	0.49	100.7	0.52	100.97	0.66
	Recombination															
SiO_2	65.9		65.6		66.1		66.0		65.1		66.0		65.8		65.8	0.66
Al_2O_3	19.2		19.1		19.3		19.3		19.0		19.2		19.2		19.2	0.22
Fe_2O_3	0.10		0.07		0.09		0.08		0.07		0.09		0.09		0.08	0.02
CaO	0.01		0.02		0.02		0.02		0.01		0.02		0.01		0.01	0.01
BaO	0.03		0.03		0.01		0.03		0.02		0.01		0.03		0.02	0.01
Na_2O	2.75		2.17		3.30		3.30		1.76		4.08		3.29		2.95	1.57
K_2O	12.7		13.4		11.9		11.9		14.1		10.8		11.8		12.4	2.23
Total	100.7		100.4		100.7		100.6		100.1		100.2		100.2		100.4	0.50
	Endmember Calculations (%)															
An	0.05		0.08		0.08		0.08		0.05		0.11		0.05		0.07	
Ce	0.05		0.05		0.03		0.05		0.04		0.03		0.06		0.04	
Ab	24.7		19.7		29.7		29.6		16.0		36.4		29.7		26.6	
Or	75.2		80.2		70.2		70.3		83.9		63.5		70.2		73.3	

WF is the weight factor which corresponds to the phase proportion in each respective alkali feldspar phenocryst.

system at equilibrium to the ratio of the lengths of the line segments connecting these phases (Fig. 13). Projection of the equilibrium tie line from the bulk composition of the phenocryst assemblage (P_A) must pass through the bulk composition of the rhyolite dike (X) and terminate at the composition of the melt (M). The ratio of the length of the line segment $\overline{P_A X}$ to the total length of the equilibrium tie line $\overline{P_A M}$ is equivalent to the proportion of "melt" present in the system:

$$\overline{P_A X} / \overline{P_A M} = \%\ Melt \tag{3}$$

Similarly, the ratio of the length of the line segment $\overline{XM}$ to the total length of the equilibrium tie line $\overline{P_A M}$ is equivalent to the proportion of phenocrysts present in the system:

$$\overline{XM} / \overline{P_A M} = \%\ Phenocrysts \tag{4}$$

In order to make this construction, the location of the back leg (line segment $\overline{QF}$) of the equilibrium three phase triangle Quartz (Q)–Alkali Feldspar (F)-Melt (M) must be fixed by constraining the composition of the alkali feldspar phenocrysts (F) in equilibrium with the melt. This is accomplished by using the reintegrated feldspar compositions (Table 4) and the assumption the quartz phenocrysts are pure SiO_2. The position of point P_A on the back leg of the three phase triangle is fixed by using either the modal abundance of alkali feldspar (59.5%) or quartz (40.5%) phenocrysts (see Table 1), the length of the line segment $\overline{QF}$ (measured from the graph), and the lever rule. For example,

$$\overline{P_A F} / \overline{QF} = \%\ Quartz\ Phenocrysts \tag{5}$$

Rearranging and solving for line segment $\overline{P_A F}$:

$$\overline{P_A F} = \left(\%\ Quartz\ Phenocrysts\right) * \overline{QF} \tag{6}$$

Table 5. Chemical composition analysis and normative mineralogies of rhyolite matrix.

Oxide (wt.%)	C1	Std Dev	C2	Std Dev	C3	Std Dev	Average	2σ
	Chemical Composition (weight percent)							
SiO_2	77.7	9.31	80.8	8.17	79.8	8.51	79.5	3.19
TiO_2	0.04	0.11	0.02	0.03	0.02	0.02	0.03	0.03
Al_2O_3	12.1	4.90	10.8	4.82	11.4	4.89	11.4	1.32
Fe_2O_3	1.15	2.54	0.80	1.24	0.57	0.84	0.84	0.59
MnO	0.01	0.01	0.01	0.01	0.01	0.01	0.01	0.00
MgO	0.01	0.01	0.00	0.00	0.00	0.01	0.00	0.00
CaO	0.04	0.03	0.04	0.03	0.04	0.02	0.04	0.01
SrO	0.03	0.03	0.03	0.03	0.03	0.03	0.03	0.00
BaO	0.01	0.02	0.01	0.01	0.01	0.01	0.01	0.00
Na_2O	4.35	2.48	4.84	2.60	4.82	2.43	4.67	0.55
K_2O	4.49	2.73	2.57	2.10	3.25	2.45	3.44	1.94
P_2O_5	0.01	0.02	0.01	0.02	0.01	0.02	0.01	0.00
F	0.05	0.06	0.05	0.06	0.05	0.06	0.05	0.00
Cl	0.01	0.01	0.01	0.01	0.01	0.01	0.01	0.00
Total	99.98	0.03	99.98	0.03	99.98	0.03	99.98	0.00
	Normative Minerals (weight percent)							
Quartz	34.8		42.6		39.2		38.9	4.09
Albite	36.7		40.8		40.3		39.2	1.59
Anorthite	0.00		0.00		0.00		0.00	0.00
Orthoclase	26.7		15.3		19.3		20.4	5.41
Corundum	0.08		0.04		0.60		0.24	0.57
Hypersthene	1.02		0.72		0.33		0.69	0.43
Ilmenite	0.08		0.04		0.04		0.05	0.02
Magnetite	0.49		0.35		0.08		0.31	0.29
Apatite	0.02		0.02		0.02		0.02	0.00
Halite	0.02		0.02		0.02		0.02	0.00
Fluorite	0.12		0.12		0.12		0.12	0.00
Total	99.93		99.95		99.99		99.96	0.04
Matrix composition normalized to quartz and feldspar (%). 2σ deviation in 2nd column.								
Quartz	39.4	7.7						
Albite	39.9	4.3						
Anorthite	0.0	0.0						
Orthoclase	20.7	11.9						

The location of the bulk composition of the system (*X*) was determined by projecting the whole rock analysis of the rhyolite dike into the SiO_2-$NaAlSi_3O_8$-$KAlSi_3O_8$-H_2O system using the normalized abundances of the normative phases: quartz (34%), albite (39%), and orthoclase (27%; Table 3). The location of the melt (*M*) can now be constrained graphically by rearranging (3) and solving for the length of the equilibrium tie line that connects the bulk composition of the phenocryst assemblage (P_A) and the melt composition (*M*). $\overline{P_A M}$ can be determined by using the modal abundance of the matrix (81.9%) as a proxy for the percent melt present in the system and the length of line segment $\overline{P_A X}$ as measured from the graphical construction of the phase relationships in the SiO_2-$NaAlSi_3O_8$-$KAlSi_3O_8$-H_2O system (Table 1; Fig. 13):

$$\overline{P_A M} = \overline{P_A X} / (\%\ Melt) \tag{3a}$$

Having determined the length of line segment $\overline{P_A M}$, the composition of the melt can be plotted from construction of this line on the ternary diagram. For the rhyolite dike, the melt (*M*) has the normative composition Q = 34%, Ab = 46%, Or = 20% and plots adjacent to the 200 MPa quartz-feldspar cotectic (Fig. 13). This represents the composition of the melt just prior to the onset of ascent.

Crystal Size Distribution (CSD) Analysis

The crystal size distribution (CSD) of alkali feldspar and quartz in the rhyolite dike was determined using the 2D major axis of the ellipse determined by ImageJ (Abramoff *et al.*, 2004). This data is organized by CSD Corrections (Higgins, 2000) into size intervals or bins (Table 6). Each bin in Table 6, denoted by the 2D Length column, represents the upper limit of the bin size. For example, in Table 6 the first alkali feldspar bin is 0.158 mm, where the bin range is from 0 mm to 0.158 mm; the next bin is 0.251 mm and the

Table 6. Frequency of 2D intersection lengths used to construct Fig. 14 and Fig. 15 from CSD Corrections 1.36.

Alkali Feldspar

		Slabs (S1 & S2)		Thin Section (JH-02-04D)	
	2D Length (mm)	Unseparated	Separated	Unseparated	Separated
Logarithmic Size Bins	*0.158*			(1)	(3)
	0.251	(1)	8	15	33
	0.398	14	38	26	60
	0.631	20	72	27	83
	1.000	44	114	31	93
	1.580	46	94	55	84
	2.510	37	37	38	40
	3.980	15	11	16	5
	6.310	4	(1)	(1)	
	10.00	(1)			
	Total	180	374	208	398

Quartz

		Slabs (S1 & S2)		Thin Section (JH-02-04D)	
	2D Length (mm)	Unseparated	Separated	Unseparated	Separated
Logarithmic Size Bins	*0.100*			(3)	(5)
	0.147			19	25
	0.215			27	58
	0.316	(5)	(7)	48	115
	0.464	29	33	81	176
	0.681	39	49	81	166
	1.000	71	86	75	108
	1.470	33	40	70	47
	2.150	11	(4)	17	
	3.160	(3)	(1)		
	4.640			(1)	
	Total	183	208	418	695

The slab sample is results from both slabs (S1 & S2) and JH-02-04D is the thin section sample. Unseparated crystals denote both glomerocrysts and single crystal phenocrysts. Separated crystals include both the separated glomerocrysts and the original single crystal phenocrysts. Numbers with parentheses denote bins that are not included in the graphical analysis because of insufficient population density at that size bin which results in high errors. Each bin interval for quartz and alkali feldspar is $10^{0.20}$ and $10^{0.16}$, respectively, larger than the previous bin.

bin range is from 0.159 mm to 0.251 mm, etc (each alkali feldspar interval is sequentially $10^{0.20}$ larger than the previous bin and quartz intervals are increasing by a factor of $10^{0.1\bar{6}}$). The abundance of quartz and alkali feldspar phenocrysts (this includes the unseparated glomerocrysts cases and the deconstructed glomerocrysts cases for the combined slabs and the thin section) per bin size are reported in Table 6.

Alkali Feldspar Bins

Similar frequencies were calculated for the combined deconstructed slab and TS alkali feldspar samples for bins greater than the 0.398 mm bin indicating good agreement between these two techniques for crystals within this size range. However, at bin sizes of 0.398 mm and smaller, agreement between the deconstructed slab and TS numbers is not as clear. This difference reflects the increased accuracy in representing smaller crystal sizes provided by the higher resolution of the thin section and petrographic microscope and the decreased accuracy in resolving smaller crystal sizes using digital images due to poor resolution.

Quartz Bins

There is considerable discrepancy between the frequencies of quartz phenocrysts per bin size as determined by the two techniques that was not observed for the feldspar data. This reflects the difficulty in detecting and accurately tracing quartz phenocrysts in the scanned images of the slabs due to the quartz phenocrysts' overall smaller size and limits of resolution of the digital images. Thus the number of quartz phenocrysts per bin size for the rock slabs appear to be underestimated in comparison to the analysis using the large thin section.

CSD Graphs

The CSD graphs (Fig. 14 and Fig. 15) are constructed by converting the 2D intersection lengths (Table 6) to the projected true 3D lengths by the stereology algorithms in CSD Corrections 1.36 (see Higgins, 2000). CSD graphs plot the crystal frequency for a given size interval (i.e. population density per volume per size bin) and has units of mm^{-4} against the 3D size interval (major axis of the predicted ellipsoids), or size bin, and has units of mm. The 3D major axis length data are grouped into their respective logarithmic size bins and are translated to points on the CSD graphs where each point is the mean size of the size interval or bin. A linear regression is applied to the size bin points or a

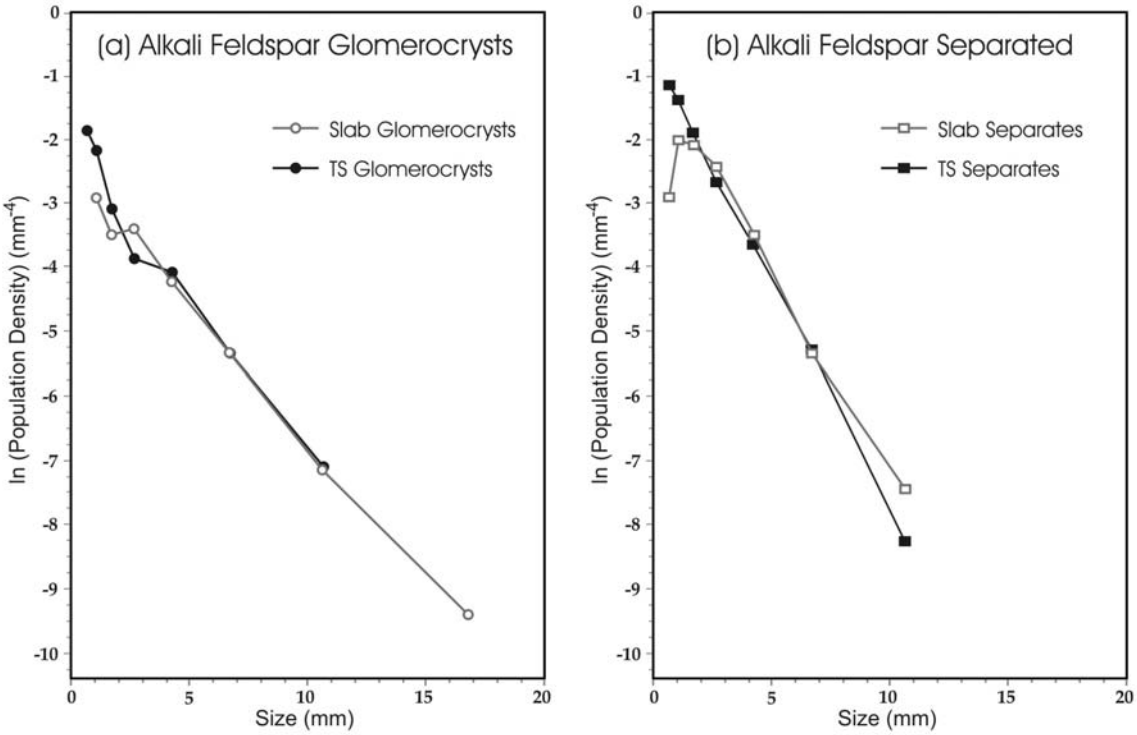

Fig. 14. CSDs of (a) alkali feldspar glomerocrysts and (b) deconstructed alkali feldspar glomerocrysts. Data for (a) contains both glomerocrysts and single phenocrysts in the samples and (b) contains both the separated glomerocryst and the original single phenocrysts. Each alkali feldspar size bin is $10^{0.20}$ larger than the previous bin. Error bars have not been displayed for visual ease and bins containing too few crystals have been omitted from the diagram and the regression analysis. See Appendix B for graphs with regression curves, omitted error bars, and omitted data points.

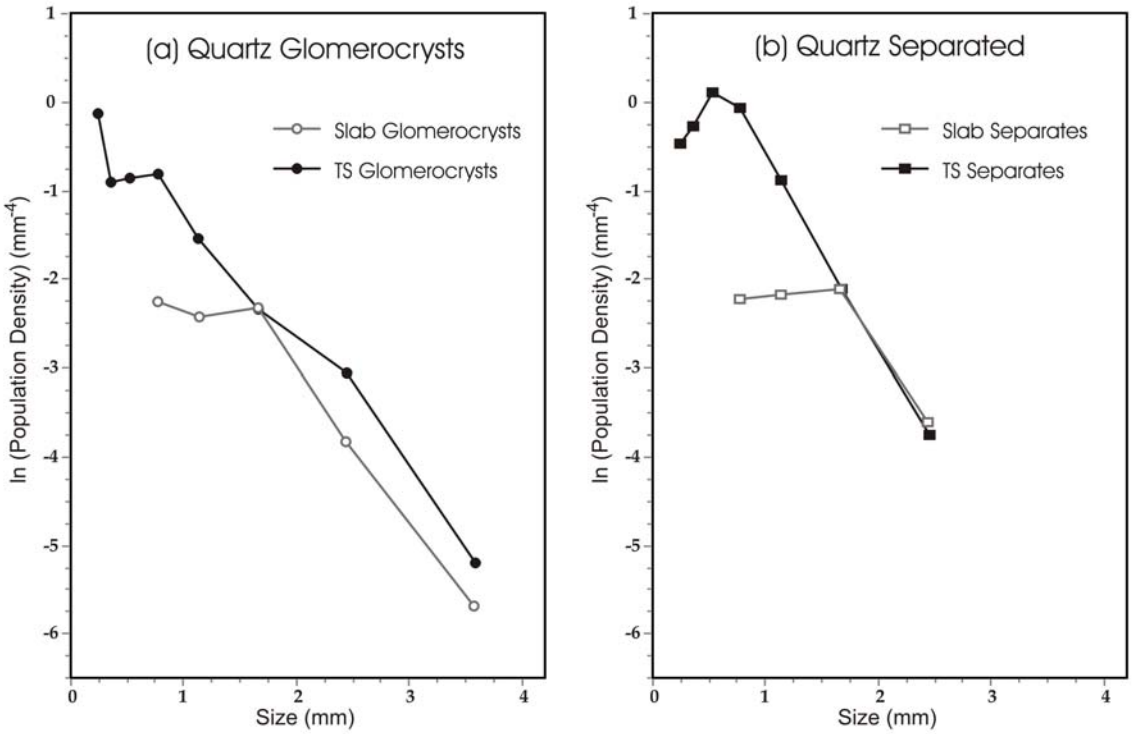

Fig. 15. CSDs of (a) quartz glomerocrysts and (b) deconstructed quartz glomerocrysts. Data for (a) contains both glomerocrysts and single phenocrysts in the samples and (b) contains both the separated glomerocryst and the original single phenocrysts. Each quartz size bin is $10^{0.1\bar{6}}$ larger than the previous bin. Errors bars have not been displayed for visual ease and bins containing too few crystals have been omitted from the diagram and the regression analysis. See Appendix B for graphs with regression curves, omitted error bars, and omitted data points.

subset of the points to calculate the trend of the data. The y-intercept of the linear regression curve is the nucleation density (n°) for the respective mineral in the system and the slope is the negative reciprocal of the product of the crystal growth rate and residence time (-1\Gτ) in the system (Fig. 17a and Equation 7; see Discussion for more detail). The smallest bin sizes for slab CSDs are not representative of the smallest 3D phenocrysts in the system since these crystals are not accurately resolved at this size. The smaller population densities for the slab curves at the smaller bin sizes (the slab curve deviation from the TS curve) compared to the TS curve are representative of the inaccuracy of using the slabs to represent smaller crystals sizes. The CSD graphs for

alkali feldspar and the quartz phenocrysts of the rhyolite dike are displayed in Fig. 14 and Fig. 15 with the results in Table 7 and raw data in Appendix B. Data points that were excluded from the regression analysis (Fig. 14, Fig. 15, and Table 7) due to large stereological errors as a result of insufficient population density (usually the smallest or largest bin) are denoted by parentheses in Table 6.

Table 7. CSD characteristics calculated from CSD Corrections 1.36.

Sample	Phenocryst Type	n	Area (mm^2)	Intercept (n°) (mm^{-4})	CSD Slope	r^2
Alkali Feldspar						
Slab	Glomerocrysts	180	1800	-2.41 ± 0.16	-0.434 ± 0.027	0.83
Slab	Separated	374	1800	-0.93 ± 0.12	-0.620 ± 0.028	0.061
JH-02-04D	Glomerocrysts	208	1824	-2.03 ± 0.14	-0.491 ± 0.028	0.073
JH-02-04D	Separated	398	1824	-0.72 ± 0.11	-0.686 ± 0.028	0.94
HVC	Individual	1251	5879	-1.2	-1.16	0.98
Quartz						
Slab	Glomerocrysts	183	1800	-0.42 ± 0.26	-1.35 ± 0.13	0.00034
Slab	Separated	208	1800	-0.60 ± 0.31	-1.11 ± 0.17	0.00014
JH-02-04D	Glomerocrysts	418	1824	0.09 ± 0.12	-1.39 ± 0.07	0.20
JH-02-04D	Separated	695	1824	1.31 ± 0.11	-1.91 ± 0.08	0.0019
HVC	Individual	716	5879	-1.7	-1.4	0.98

The slab sample is a combination of both S1 and S2 slabs. JH-02-04D is the thin section sample. HVC is a rhyolite from the Petersburg laccolith of the Halle Volcanic Complex (Mock and Jerram, 2005). The HVC also has plagioclase feldspar phenocrysts which is omitted here.

Alkali Feldspar CSD

Unseparated Glomerocrysts – Slab unseparated glomerocrysts CSD size data (major axis of the predicted ellipsoid; Fig. 14a) for alkali feldspar ranges from 1.063 mm (minimum bin size) to 16.85 mm (maximum bin size). It is important to note that the slab technique was unable to resolve the sizes of the smaller alkali feldspar phenocrysts. Thus the calculated lower size limit of 1.063 mm is an artifact imposed by the limit of resolution rather than an accurate representation of the true size of the smallest alkali feldspar

phenocryst. The slab unseparated glomerocrysts curve (Fig. 14a) is smooth with a very slight concave up shape for the largest 5 size bins and minor deviations from this trend at the two smallest size bins. The intercept and slope of a best fit trend line that fits this data is -2.41 ± 0.16 mm^{-4} and -0.434 ± 0.027 (Table 7), respectively, from 180 data points (2 data points have been excluded from the regression analysis; Table 6) and has an r^2 of 0.83.

TS unseparated glomerocrysts CSD size data for alkali feldspar ranges from 0.671 mm to 10.63 mm (Fig. 14a). Error in resolution does not occur in the TS CSD data and so the minimum size calculated from the CSD analysis is interpreted to be a measurement of the smallest length of the alkali feldspar phenocryst. The shape of the TS glomerocryst curve (Fig. 14a) has a slight concave up shape with deviations from the overall shape at the 2nd and 3rd smallest bin sizes. The intercept and slope of the best fit line that fits this data is -2.03 ± 0.14 mm^{-4} and -0.491 ± 0.028 (Table 7), respectively, from 208 data points (2 data points have been excluded from the regression analysis; Table 6) and has an r^2 of 0.073.

The results of both methods (slab and thin section) display very similar overall trends, with good agreement at the larger crystal sizes, and slight discrepancies at the smaller crystal sizes where the resolution afforded by the petrographic microscope and thin section is substantially improved by the accuracy of the size measurements.

Deconstructed Glomerocrysts – CSD analysis was performed again on these samples after the glomerocrysts were deconstructed by manually separating the joined crystals into individual phenocrysts using an image editing program. Slab separated glomerocrysts CSD size data for alkali feldspar ranges from 0.671 mm to 10.63 mm

(major axis of the predicted ellipsoid; Fig. 14b). The curve has a very slight concave up shape at large bin sizes and a tight concave down tail at the smaller crystal sizes. The intercept of a trend line that is fitted to this data is -0.93 ± 0.12 mm^{-4} and the slope is -0.620 ± 0.028 (Table 7) that is derived from 374 points (1 data point has been excluded from the regression analysis; Table 6) and has an r^2 of 0.061.

The thin section separated glomerocrysts CSD crystal size data for alkali feldspar ranges from 0.671 mm to 10.63 mm, also. However, the CSD curve based on this data set (Fig. 14b) is nearly linear over the entire data set with an intercept of -0.72 ± 0.11 mm^{-4} and a slope of -0.686 ± 0.028 (Table 7) from 398 data points (3 data points from the smallest bin size have been excluded from the regression analysis; Table 6) with an r^2 value of 0.94.

CSD curves from both techniques are similar in shape at the larger bin sizes where the resolution of the two techniques overlap. However, at the smaller alkali feldspar crystal sizes the slab curve tails downward and deviates from the more linear TS curve (Fig. 14b). This deviation from linearity appears to be an artifact of the lower limit of resolution of the slab technique rather than reflecting true size characteristics of the alkali feldspar phenocryst population.

Quartz CSD

Unseparated Glomerocrysts – Slab unseparated glomerocrysts CSD size data for quartz ranges from 0.771 mm to 3.58 mm. The curve is a straight line with a negative slope for the 3 largest size bins with the line becoming nearly horizontal at the smaller bin sizes (Fig. 15a). This is likely a reflection of the difficulty in resolving crystals at smaller sizes from the slabs rather than a true size characteristic of the quartz phenocryst population.

The intercept and slope from a trend line is -0.42 ± 0.26 mm^{-4} and -1.35 ± 0.13 (Table 7), respectively, from 183 data points (8 points excluded from the regression analysis; Table 6) and has an r^2 of 0.00034. Excluding the two smaller bin sizes to fit a linear regression to the three points that closely resemble a straight line, the intercept and slope from a trend line is changed to 0.65 ± 0.36 mm^{-4} and -1.80 ± 0.17, respectively, from 115 data points (73 points have been excluded from the regression analysis) and has an r^2 of 0.55.

TS unseparated glomerocrysts CSD size data for quartz ranges in size from 0.244 mm to 3.58 mm (Fig. 15a). In contrast to the data from the rock slabs, the major axes of the predicted ellipsoids at the lower size bins represent the true glomerocryst size population characteristics because of the increased resolution afforded by the thin section and petrographic microscope. The curve is complex, and although it exhibits an overall negative slope, there are several changes in slope along the curve especially at the smaller bin sizes (Fig. 15a). The intercept and slope from a trend is 0.09 ± 0.12 mm^{-4} and -1.39 ± 0.07 (Table 7), respectively, from 418 data points (4 being excluded from the regression analysis; Table 6) with an r^2 value of 0.2.

Deconstructed glomerocrysts - Slab separated crystals for quartz range in size from 0.771 mm to 2.44 mm (Fig. 15b). The two largest bin sizes define a line with a negative slope that closely corresponds with the line defined by the deconstructed quartz glomerocrysts of the thin section data set (see below). The horizontal line, similar to the quartz unseparated glomerocrysts CSD curve, defined by the smaller bin sizes is likely due to the lack of ability of the slab technique to resolve the smaller crystals. The intercept and slope from a trend line is -0.60 ± 0.31 mm^{-4} and -1.11 ± 0.17 (Table 7), respectively, with

an r^2 value of 0.00014 from 208 data points (12 data points being excluded from the regression analysis; Table 6).

TS separated quartz crystals range in size from 0.244 mm to 2.44 mm (Fig. 15b). The curve produced is a linear and negatively sloped at the larger bin sizes and has a concave down tail at the smaller bin sizes. This concave down tail is interpreted to reflect actual characteristics of these size populations because of the high resolution afforded by the thin section and petrographic microscope. The intercept of the trend line is 1.31 ± 0.11 mm^{-4} and the slope is -1.91 ± 0.08 (Table 7), with an r^2 value of 0.0019 from 695 data points (excluding 5 data points from the regression analysis; Table 6). Excluding the three smallest bin sizes to fit a linear regression to the four points of the larger bin sizes to create a line that closely resemble a straight line, the intercept and slope from a trend line is changed to 1.60 ± 0.13 mm^{-4} and -2.09 ± 0.10, respectively, from 497 data points (203 points have been excluded from the regression analysis) and has an r^2 of 0.89.

Unseparated Glomerocrysts vs. Deconstructed Glomerocrysts

Comparisons of the TS CSDs for the unseparated glomerocrysts and deconstructed glomerocrysts for both alkali feldspar and quartz phenocrysts are illustrated in Fig. 16. While there is good agreement between the slab and the thin section technique at the larger bin sizes, which demonstrates the robust nature and reproducibility of the CSD analysis, data from the slab samples have been excluded because, as stated previously, the inadequate resolution of the smaller crystal sizes can lead to artifacts rather than a true reflections of the characteristics of the size populations at smaller bin sizes.

The alkali feldspar glomerocryst curve (Fig. 16a) exemplifies the effects of separating the crystals. Both the unseparated glomerocrysts curve and the separated

(deconstructed) curves pivot around a single point (the 6.71 mm size bin) where the unseparated glomerocrysts population density is greater than the separated population density for sizes greater than the pivot point and the glomerocryst population density is less than the separated population density for sizes smaller than this pivot point. Separating the crystals decreases the size of the original unseparated glomerocrysts population and distributes them among smaller size bins, thus increasing their population. This process occurs in all the size bins and causes a cumulative effect of an increase in population density at the smaller size bins. Deconstruction of the alkali feldspar glomerocrysts also yields a good linear correlation (r^2=0.94; n= 398) among all the size populations as is predicted by CSD theory for homogeneous nucleation and growth of crystals.

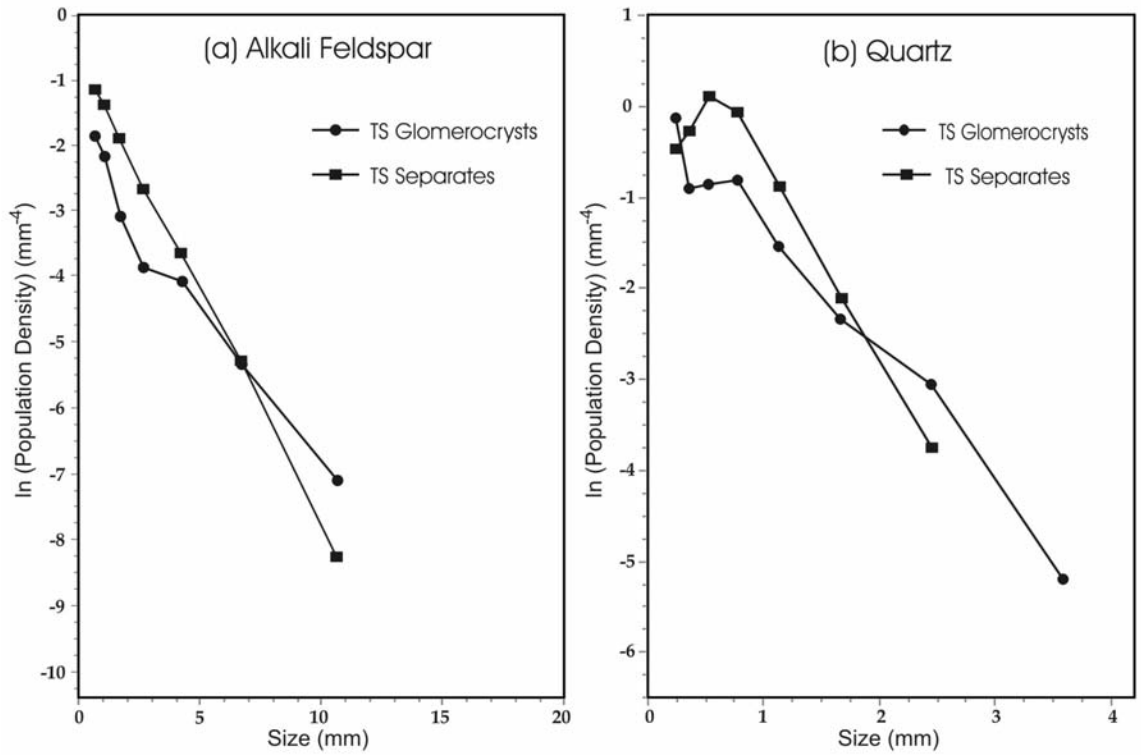

Fig. 16. CSD graphs of thin section data of (a) alkali feldspar and (b) quartz CSD comparing glomerocrysts and the subsequent separated crystals. Curves are the same as Fig. 14 and Fig. 15. See Appendix B for graphs with regression curves, omitted error bars, and omitted data points.

The same process occurs for the quartz TS CSD (Fig. 16b) where the deconstruction of the larger glomerocrysts increases the population density of the smaller crystal sizes creating another pivot point between these two curves. This yields a CSD that is highly linear over the four largest bin sizes ($r^2 = 0.89$; n= 497) and tails downward at the smaller crystal sizes. This concave down tail at the smaller sizes represent the true size characteristics of the quartz phenocryst population, rather than an artifact of the technique, because of the higher resolution afforded by the thin section and petrographic microscope.

DISCUSSION

Crystal Size Distribution

Theory

Petrologists have successfully extracted information regarding the crystallization of magma (pressure, temperature, nucleation rates, growth rates, residence time, etc.) from quantitative analysis of the size, shape, abundance, and distribution of crystals present in igneous rocks (Marsh, 1988; Waters & Boudreau, 1996; Higgins, 2000). The quantification of rock textures in igneous rocks can be accomplished through the use of crystal size distribution (CSD) analyses. CSD's are a relatively recent way to look at geologic systems using crystal size (length, area, or volume) to decipher the evolution of crystals (Marsh, 1988; Mangan, 1990; Higgins, 2000). Originally applied to study crystallization systems in chemical engineering, CSD theory can be used to extract information from geologic systems that describes crystal growth rate, nucleation density, nucleation rate, cooling histories, magmatic processes (e.g., crystal settling, resorption,

magma mixing), and estimation of magma storage times (Randolph & Larson, 1971; Marsh, 1988; Mangan, 1990; Castro *et al.*, 2003).

Marsh (1988) recognized that by plotting population densities against crystal size a log-linear distribution can be predicted (Fig. 17a). The CSD diagram can be used to extract quantitative data of geologic systems regarding crystal populations' nucleation density, growth rate, contamination (i.e. magma mixing), and residence time. Mathematically, the population density (n) of a simple open steady-state system can be expressed as

$$n = n°\exp\left(-\frac{L}{G\tau}\right) \tag{7}$$

where n° is nucleation density, L is crystal size, G is growth rate, and τ is residence time (Marsh, 1988; Marsh, 1998). In a steady-state system, G and τ are assumed to be constant (Peterson, 1996; Marsh, 1998). The log-linear curve is based on the exponential increase in nucleation rate (J) with time (Marsh, 1998) and is related to Equation (7) where

$$J = n°G. \tag{8}$$

From Fig. 17a, the y-intercept is n° and the slope of the curve is -1\Gτ. For a more detailed mathematical analysis see Marsh, 1988; Peterson, 1996; Marsh, 1998; and, Higgins, 2000.

A departure from an ideal CSD straight curve indicates perturbation of a steady state system, modification of crystal sizes by processes other than crystallization (e.g., Ostwald ripening, fig. 8b) or mixture of unique populations of phenocrysts (e.g., as a result of magma mixing, fig 8c). The formation of glomerocrysts will also result in CSD curves that exhibit distributions similar to Ostwald ripening reflecting an increase in the

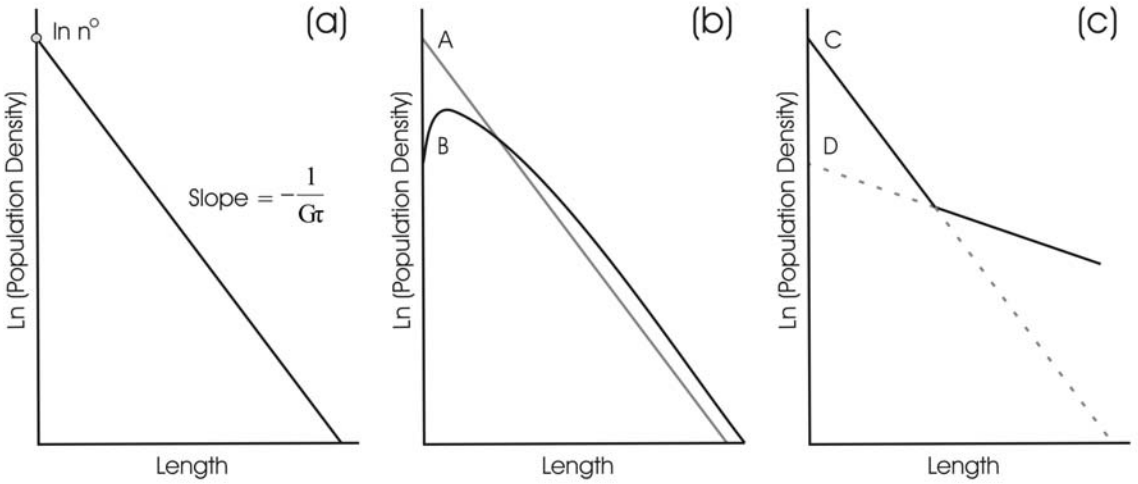

Fig. 17. Examples of crystal size distribution (CSD) semi-logarithmic graphs. The x-axis is the crystal length; the y-axis is the crystal population density; the y-intercept (n^o) represents the nucleation density; the slope is the negative inverse product of the crystal growth rate and residence time (-1\Gτ). (a) Ideal CSD with straight slope (constant nucleation and growth rate). (b) Generic curve for glomerocryst formation or Ostwald ripening where curve A represents the ideal straight slope CSD and curve B represents a system where there is an increase in larger crystal sizes and a decrease in smaller crystal sizes. (c) CSD curve (solid line) modeled for magma mixing with two different crystal populations (C and D) in the same rock. Modified from Marsh (1988).

population density of "apparent" larger crystal sizes (i.e., the size of the glomerocrysts) at the expense of smaller crystal sizes now associated with the glomerocrysts (Curve B in Fig. 17). With Ostwald ripening, large crystals grow at the expense of the resorption of smaller crystals to reduce the interfacial area and bring the system to its lowest energy state (Voorhees, 1992). Ostwald ripening and CSDs affected by glomerocrysts can easily be distinguished in thin section. A crystal population where resorption occurs will have a similar shape as Fig. 17b caused by the decrease in the number of smaller crystal. However, the larger crystal populations will stay static or decrease instead of the increase that is seen in Ostwald ripening or glomerocrysts. It is possible when magma mixing occurs that two different crystal populations (curves C and D in Fig. 17) will combine and produce a resultant CSD curve that shows the characteristics unique to each original magma (e.g. the crystal populations may have contrasting size ranges and abundances

that would be indicated on their respective CSD curve). This type of curve is easily identified by having two different slopes and intercepts which will result in a kink in the CSD (Marsh, 1988).

Rhyolite Dike at Medicine Park

The slight differences in the separated slab and TS CSDs (Fig. 14 and Fig. 15) at the larger crystal sizes can be attributed to localized variations in population density within the rhyolite dike (e.g., see Fig. 9). The larger bins have smaller numbers of crystals and are, therefore, more sensitive to changes in population. However, taking into account that the slab and thin section samples were taken from different portions of the rhyolite dike and that the separated slab and TS CSD curves at the larger crystal sizes are in close agreement with each other, these CSDs represent the reproducibility of the CSD technique and the robustness of the data set.

The CSDs presented in this study show unique histories for the alkali feldspar and quartz phenocrysts in the rhyolite dike. The deconstructed TS alkali feldspar glomerocryst population yields a straight CSD curve (Fig. 14b; Table 7) as predicted by CSD theory (Marsh, 1988) and represents steady state nucleation and growth of alkali feldspar up to the time when the magma quenched. The quartz phenocrysts record a more complex crystallization history. The resorption of quartz phenocrysts that is evident in thin section (Fig. 7d-e) is also reflected in the TS separated CSD curve (Fig. 15b) by the abrupt downward turn in the curve at the lower crystal sizes. Note that the concave down curve caused by resorption and one produced by inadequate resolution, as seen in the deconstructed alkali feldspar slab CSDs (Fig. 14b), can be distinguished by the use of thin sections to resolve the smaller crystal sizes. Resorption, while affecting

nearly all quartz crystals present in the dike, had a much greater, and therefore noticeable, effect on the population density of the smaller crystal sizes because of the considerably larger surface area to volume ratio for the smaller crystals sizes (i.e., bin sizes less than 0.771 mm, see Fig. 15b). Based upon the CSD analysis, quartz phenocrysts less than 0.244 mm in size (the 3-dimensional longest axis length) were entirely resorbed back into the melt. The larger crystal sizes, which are the least affected by resorption, retain a straight CSD curve (Fig. 15b) indicating steady state nucleation and growth of quartz occurred prior to initiation of resorption during magma ascent.

Glomerocryst Formation

Glomerocrysts are a common textural feature in plutonic and volcanic rocks. The formation of glomerocrysts, though not completely understood, has been attributed to a number of processes that occur during crystallization of the magma include synneusis (Vogt, 1921; Vance, 1969), resorption (Hogan, 1993), and flow differentiation (Coetzee *et al.*, 1995). Synneusis is a process in which minerals in a liquid rich magma "drift" or "swim" together during crystal settling and join along preferred crystal orientations (e.g., orientations with the lowest interfacial energy) usually being the broader crystal faces (Vogt, 1921; Vance, 1969; Schwindlinger & Alfred T. Anderson, 1989). As a result, glomerocrysts form during crystallization and new material can crystallize as an overgrowth on the glomerocryst. Hogan (1993) describes a process where glomerocrysts form when two or more crystals come together while the crystals are undergoing resorption rather than during crystallization. The driving force for resorption can be due to a change in an intensive variable such as pressure, temperature, or aH_2O. The resorption leads to the development of a boundary layer at the dissolving crystal surface

that is rich in the chemical constituents of the crystals. Overlap of the boundary layers of two or more crystals creates an intervening melt composition that crystallizes and "glues" the crystals together which can result in glomerocrysts. Coetzee *et al*. (1995) postulates that, within the Annas Rust dolerite sill, regions that have grain inertias at low velocities facilitate coagulation of crystals leading to development of glomerocrysts. Flow differentiation will force the crystals away from the sill walls and migrate down a velocity gradient towards the central region of the sill creating regions of high crystal density at the edges of the core. Within this region of the sill the crystals are in constant motion leading to multiple collisions with each other and the formation of glomerocrysts.

Post crystallization processes, such as annealing, can also alter the original magmatic fabric of the rock. Textural coarsening, or Ostwald ripening, occurs when polycrystalline mixtures are not at their lowest energy state (Voorhees, 1992; Higgins, 1998). To minimize the total interfacial energy, crystals smaller than a certain size limit dissolve and larger grains that are above the size limit continue to grow (Cabane *et al.*, 2001). However, textural coarsening is not thought to occur in volcanic rocks (Berger & Roselle, 2001). Thus while the original matrix of the rhyolite dike is likely to have been glassy and subsequently devitrified into the present microgranular state, there is little other evidence to support that post crystallization processes have selectively modified the sizes of some phenocrysts and not others.

The process that forms glomerocrysts in the rhyolite dike can be ascertained through integration of petrographic observations, experimental phase relationships, and the CSD analyses. The downturn that is present in the CSD curve for deconstructed quartz glomerocrysts (Fig. 15) indicates a "depletion" of the smaller crystals size

populations – a feature indicating resorption of quartz phenocrysts back into the melt was already in progress before glomerocrysts had started to form. This is consistent with petrographic observations as quartz glomerocrysts are commonly comprised of crystals with irregular to embayed margins, a feature that can be produced during dissolution (Fig. 7). The driving force for resorption of quartz is the decrease in the stability field for quartz with decreasing pressure. Accompanying the ascent of the magma from the storage chamber at 200 MPa to the emplacement level at 50 MPa is the concomitant displacement of the quartz-feldspar cotectic towards quartz (Fig. 13). This displacement of the cotectic places the composition of the melt solely in the feldspar stability field leading to resorption of quartz phenocrysts until the composition of the melt coincides with the cotectic at the emplacement level, approximately that of the 50 MPa cotectic. The formation of quartz glomerocrysts in the rhyolite dike is well explained as a result of resorption (Hogan, 1993) as the timing of resorption of quartz and formation of quartz glomerocrysts in the rhyolite dike coincide with magma ascent.

Alkali feldspars phenocrysts in the rhyolite dike show considerably less evidence of having undergone any significant period of resorption during crystallization (Fig. 6a-e) and there is little evidence to support reduction of the population densities of alkali feldspar crystals that are 1 mm or larger in size. In contrast to quartz, deconstructed alkali feldspar glomerocrysts produce a nearly straight CSD curve (Fig. 14b) as predicted for steady state nucleation and growth of this mineral during crystallization. This indicates that alkali feldspar glomerocrysts formed after this crystal size population distribution was established and before the matrix quenched. In addition, evidence for precipitation of new alkali feldspar that is shared across several contacts between individual alkali

feldspars associated together in a multi-crystal glomerocryst has been observed (Fig. 6a). This would indicate that the formation of these glomerocrysts occurred while alkali feldspar was still crystallizing. Since decompression of the rhyolite dike magma does not cause alkali feldspar to become unstable (Fig. 13), it is possible for crystallization to occur as the magma ascends through the overlying crust. Similar to quartz, it is likely that the formation of this texture is associated with the rise of this magma through the crust, but alternative explanations to resportion need to be explored.

Schwindlinger (1999) outlines a variation of the synneusis model where the settling of hypothetically similar spheres in a magma chamber can aggregate, but not necessarily touch, because inertia reduces the settling velocity of the leading sphere allowing the trailing sphere to "draft". At low Reynolds numbers (the ratio of inertial forces to viscous forces) two horizontally aligned spheres will increase their velocities by decreasing their distance from each other and will cause the spheres to cluster. Either increasing the Reynolds number to make the fluid more turbulent or increasing the number of spheres in the cluster can destabilize the cluster and cause one of the spheres to detach from the cluster and trail it. In a two phase system with different densities, clusters will collide with each other and eject any dissimilar particles. Schwindlinger's (1999) model can explain the formation of the monomineralic alkali feldspar glomerocrysts within the rhyolite dike without requiring resorption. Continued crystal growth will tightly bind the glomerocryst formation together and create crystal overgrowths onto one another (Fig. 6a-c). However, the crystals that constitute the glomerocrysts still retain their crystal boundaries and are still readily seen because there

is interstitial material in between the crystals (Fig. 6a-c and Fig. 7a-c) or, in the tightly clustered case, the orientations of the crystals are misaligned.

Magma Emplacement Analysis

Transport and emplacement of the rhyolite dike can be interpreted from a SiO_2-$NaAlSi_3O_8$-$KAlSi_3O_8$-H_2O system ternary phase diagram (Fig. 13) and is directly related to its textures. The graphically determined melt composition (M), projected from the ratio of phenocrysts to matrix, plots just below the 200 MPa quartz-alkali feldspar cotectic curve. Using a pressure of 225 MPa and an average felsic rock density of 2.67 g cm^{-2}, the depth at which the phenocrysts crystallized was ~8.6 km. The graphically projected depth of phenocryst crystallization for the rhyolite dike is similar to depths that have been calculated for a temporary storage chamber, or crustal magma trap, for the Mount Scott granite at 7-8 km from amphibole phenocrysts (Hogan & Gilbert, 1995). A depth of 7-8 km corresponds closely with the estimated depth of the brittle-ductile transition and the Proterozoic basement – Cambrian cover contact at the time of formation of the Southern Oklahoma Aulacogen, which Hogan & Gilbert (1995) propose was temporarily activated as a crustal magma trap for the Mount Scott granite magma. A reduction in the magma driving pressure as a result of change in the regional horizontal tectonic stress, magma supply rate, magma source depth, or some combination relaxes the crustal magma trap which may trigger the rise of magma to its final emplacement level (Hogan & Gilbert, 1995).

The magma that formed the rhyolite dike intruded the Rush Lake granite, which is texturally and temporally similar to the Mount Scott granite (Price, 1998), and quenched to the porphyritic rhyolite texture (Fig. 4). The bulk composition (Table 5) of the very

fine grained matrix of the dike serves as a proxy for the composition of the melt at the time of emplacement. The matrix (melt) composition, as determined from EMP analysis (M^c) plots on the 50 MPa quartz-alkali feldspar cotectic curve, which corresponds to a depth of ~1.9 km. The shift in the composition of the melt at 200 MPa, as determined from topological construction of the equilibrium phase relationships in the ternary system Q-Ab-Or-H_2O, to the measured composition of the matrix reflects an increase in the SiO_2 component of the melt as a result of quartz dissolution with decreasing pressure during magma ascent from the storage chamber to the final emplacement level in the crust.

Using the mechanisms for the stall of magma and subsequent rise to shallower levels in the crust of the Rush Lake granite, described above, the rhyolite dike's path to its emplacement has two stages. First, the late stage felsic magma rises in the crust as dikes and stalls at the approximate level of the brittle-ductile transition of ~8.6 km to begin crystallizing alkali feldspar and quartz under steady state conditions as determined by the calculated melt composition (point M in Fig. 13) from topological reconstruction of the equilibrium phase assemblage in the ternary system Q-Ab-Or-H_2O. Crystallization of this magma is interrupted, after forming only 18% phenocrysts, as it begins to ascend in the crust once more. During this ascent, glomerocrysts form, quartz glomerocrysts as a result of resorption with possible affect from synneusis and alkali feldspar glomerocrysts as a result of synneusis. The magma is emplaced as a dike and quenches to form an intrusive porphyritic rock with the texture of rhyolite. The composition of the matrix, which serves as a proxy for the composition of the melt at the time of emplacement (M^c) reflects the final emplacement level of the rhyolite dike (~1.9 km) at the time of intrusion into the Rush Lake granite.

Crystal Growth

Volcanic and hypabyssal rocks' crystal growth rates parallel the early stages of crystal growth for plutonic rocks. Crystal growth in a magmatic system where crystals are suspended in the melt will undergo unconstrained crystal growth (Kirkpatrick, 1975) which volcanic or hypabyssal rocks will do throughout their lifetime unless glomerocrysts form. Volcanic or hypabyssal rocks range in magmatic settings of low undercooling and few nucleation sites (few large phenocrysts) to high undercooling and many nucleation sites (many small phenocrysts), such as when magma ascends through the crust (Swanson, 1977).

Crystal growth rates depend upon the axis of the crystal geometry and, for quartz, are fastest along the c-axis (Swanson & Fenn, 1986). Swanson and Fenn (1986) experimentally calculated a c-axis growth rate for quartz in a system with a bulk composition of $Ab_{60}Q_{40}$, temperature of 850 °C, and 2% wt% H_2O to be 3×10^{-8} cm/s. A rough estimate of the residence time in a pre-erupted magma chamber can be calculated from this growth rate. Assuming that the largest quartz crystals have only small amounts of resorption (crystals similar to Fig. 7f), the largest measured half length in the rhyolite dike is 0.7 mm which yields a residence time for quartz of ~27 days.

Similar calculations can be estimated for alkali feldspar. Using an alkali feldspar haplogranodiorite composition, a growth rate of 2×10^{-7} cm/sec is calculated by Swanson (1977). A maximum half length of 1.7 mm obtained from the rhyolite dike alkali feldspar population corresponds to a maximum residence time of ~10 days.

Quartz Resorption

In most hypabyssal rocks, quartz grains are allowed to grow to subhedral and euhedral forms without the restriction from other crystals, contrary to deeper plutonic rocks (Swanson & Fenn, 1986). Since the quartz crystals of the rhyolite dike show evidence of resorption or embayment (Fig. 7d-e), other processes are occurring. Dissolved quartz material can clearly be seen migrating away from the crystal creating a quartz saturated corona around the crystal. However, why there is a range in the level to which some of the crystals are being resorbed to the point of being excluded from the effects of resorption (Fig. 7f) is unclear. Since euhedral crystals that do not exhibit any dissolution are extremely rare (Fig. 7f is the only euhedral crystal in the thin section studied), this point will not be examined. A corona of dissolved material forming around a crystal is the first step in glomerocryst formation outlined by Hogan (1993). The problem arises, however, in that the alkali feldspar glomerocrysts do not show resorption, which would be necessary for Hogan's (1993) glomerocryst formation model. However, as stated previously, Schwindlinger's (1999) synneusis model is entirely plausible for the formation of the alkali feldspar glomerocrysts. The lack of evidence for overgrowths on the resorbed quartz indicates rapid quenching of magma with little or no time for quartz to reequilibrate and continue crystal growth.

Contrary to crystal growth, dissolution (resorption) rates are not dependant upon the crystal axis and crystallographic orientation (Cashman, 1990; Liang, 1999). The rate of resorption is dependant upon the composition of the melt at the time of resorption and the ability of the resorbed material to diffuse away from the crystal (Liang, 1999). The amount of resorbed quartz material in the system is directly related to the time and

distance that the magma ascended through the crust. If the rate of resorption can be constrained, then the time and distance can also be constrained.

Table 8 and Fig. 18 show the calculated amount of resorbed quartz material that was lost back into the magma system. Using the projected aspect ratio for quartz, 1:1:2, and the volume for an ellipse, volumes for each bin (interval) can be found. V_{proj} is the volume of quartz in the system that would exist if the quartz was not resorbed. Subtracting V_{proj} from the V_{calc}, the amount of material lost is 1.819 mm^3. The projected slope and intercept of the constant nucleation and growth quartz CSD (Fig. 18) is -2.09 ± 0.07 and 1.61 ± 0.09, respectively, with an r^2 value of 0.99.

Table 8. Projected data for an ideal quartz CSD.

Interval	n_{Calc}	n_{Proj}	n_{Diff}	L	I	S	V_1	V_{calc}	V_{proj}
2.44	47	47	0	2.94	1.47	1.47	3.326	156.343	156.343
1.661	108	108	0	2	1	1	1.047	113.097	113.097
1.132	166	166	0	1.362	0.681	0.681	0.331	54.901	54.901
0.771	176	176	0	0.928	0.464	0.464	0.105	18.412	18.412
0.525	115	148	33	0.632	0.316	0.316	0.033	3.800	4.890
0.358	58	113	55	0.43	0.215	0.215	0.010	0.604	1.176
0.244	25	72	47	0.294	0.147	0.147	0.003	0.083	0.240
						Total Volume =	4.85576	347.24	349.059

Interval is the midpoint of the logarithmic interval calculated by CSD Corrections 1.36. n_{Calc} is the actual population of quartz in the thin section, n_{Proj} is the projected population for a straight CSD curve, n_{Diff} is the difference between n_{Proj} and n_{Calc}, L, I and S are the long, intermediate and short axes' lengths, respectively. V_1 is the ellipsoid volume in mm^3 of one crystal, V_{calc} is the ellipsoid volume in mm^3 using n_{Calc} and V_{proj} is the elliptical volume in mm^3 using n_{Proj}.

Unfortunately, no studies of resorption rates for a rhyolitic composition have yet been done. Shaw (2004) has summarized previous studies of quartz dissolution in both natural and synthetic systems. In the convection free studies, there is a linear relationship between the amount of dissolution and the square root of time, indicating dissolution is

controlled by the rate of diffusion of material away from the crystal interface. This can be applied to the rhyolite dike system because the resorbed material is still in the immediate vicinity of the crystal (Fig. 7d-e), so little or no convection in the system can be assumed. Acosta-Vigil *et al*. (2006) calculated that the dissolution rate for quartz in a H_2O saturated haplogranitic melt at 800°C and 200 MPa is 1.5 x 10^{-11} cm/s by heating the source rock to these conditions. The process by which quartz was resorbed in the rhyolite dike is essentially an isothermal process (magma ascension through the crust) and so this dissolution rate does not directly apply to the rhyolite dike, but the ascension through the crust can be loosely constrained. The amount of dissolved quartz material in the rhyolite

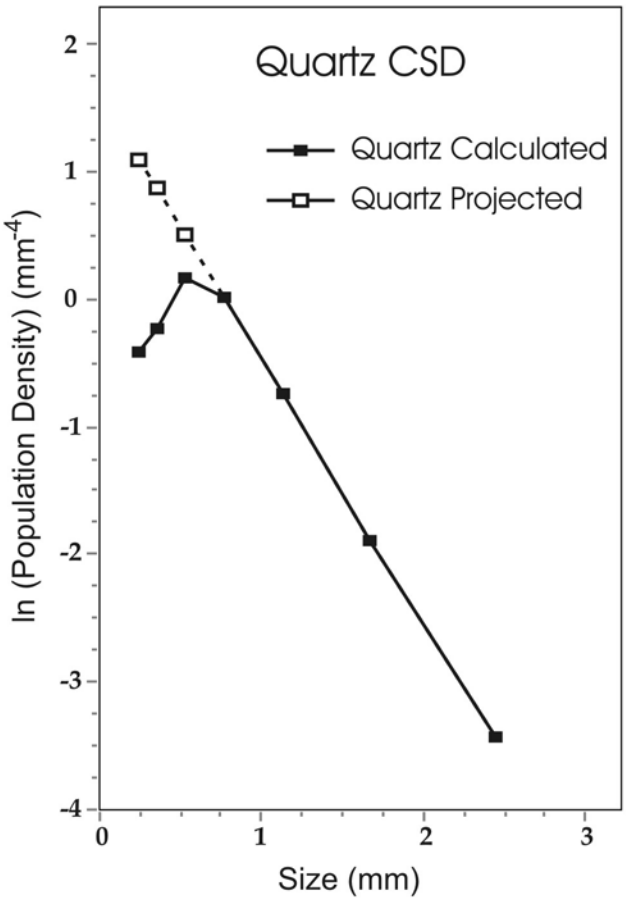

Fig. 18. CSD graph comparing the quartz CSD calculated from CSD Corrections 1.36 and the straight quartz CSD that is projected for constant nucleation and growth.

dike is projected to be 1.819 mm^3. Using the dissolution rate calculated by Acosta-Vigil *et al.* (2006) and calculating the semi-major axis of a sphere of the same volume, this amount of dissolved material would take ~160 years to produce.

The difference between the projected matrix composition (M) and the analyzed matrix composition (M^c) in Fig. 13 correspond to depths of ~8.6 km and ~1.9 km, respectively. The average rate of ascension can be calculated using the quartz dissolution time (160 y) assuming that all of the quartz material resorbed and the distance that the magma traveled (6.7 km). The rate of ascension is calculated to be 1.33 x 10^{-6} m/s (41.9 m/year). This is much smaller than the typical ascent rate of 0.1 m/s for crystal free non-eruptive granitic magma for dikes of 3 – 13 m in width (Clemens, 1998) and the average magma ascent rates for near surface silicic magmas of 0.001 m/s (Rutherford & Gardner, 2000). The slow ascent rate for the rhyolite dike could be explained by phenocrysts increasing the viscosity of the melt and that the rhyolite dike is not near surface, which would increase the volatile content in the melt and decrease viscosity. This, however, is not realistic. A magma intruding into the crust to form dikes will loose much of its heat to the surrounding bedrock and will quench deeper in the crust. Petrologically, at these long time scales quartz would return to equilibrium with the melt and would resume crystallization, which is not seen**.**

A slightly different approach to this problem is needed to create more realistic ascent rates that resemble rates stated above (0.1 to 0.001 m/s). If the dissolution rate is similar to a quartz crystallization rate of 3 x 10^{-8} cm/s (Swanson and Fenn, 1986), then more reasonable ascent rates are possible. Using the same sphere of resorbed material that was calculated above (1.819 mm^3), the dissolution time and ascent rate is ~29 days

and 0.0027 m/s, respectively. The ascent rate is in good agreement with Rutherford and Gardner's (2000) ascent rate (0.001 m/s) of near surface silicic magmas. With these estimations, 56 days is needed to crystallize quartz and alkali feldspar, create glomerocrysts and erupt through 6.7 km of overburden. However, 56 days should be considered a tentative time since it is based primarily on only one parameter: the quartz crystallization rate.

CONCLUSIONS

Characteristics of the rhyolite dike at Medicine Park can be established through petrography. Projecting the matrix and phase proportions, the whole rock composition, the phase compositions, and the matrix composition onto the SiO_2-$NaAlSi_3O_8$-$KAlSi_3O_8$-H_2O system and using graphical manipulation, the depth of crystallization (8.6 km) and depth of emplacement (1.9 km) are approximated.

CSD analysis allows quantification of textures. When determining the CSD, crystal lengths in the sample that range in size below 2 mm must be determined using thin sections to adequately characterize the CSD. Combining CSD with the deconstruction of glomerocrysts opens a window to conditions before the formation of clusters. Deconstructed alkali feldspar glomerocrysts yield a good linear correlation (r^2=0.94) on a CSD graph as is predicted by CSD theory for homogeneous nucleation and growth of crystals. Separating the quartz glomerocrysts reveals, through CSD analysis, a strong decrease in population density as the crystal sizes decrease below 0.77 mm. This decrease in population density with size is caused by resorption which occurred before or coeval with glomerocryst formation. Small overgrowths of a few alkali feldspar

glomerocrysts demonstrate that the time between the onset of glomerocryst formation and the quenching of the rhyolite dike magma was not immediate.

Constraining the timing of rhyolite dike's major events is difficult and ambiguous. The residence times of quartz and alkali feldspar are 27 days and 10 days, respectively, yet there is no petrographic evidence to support alkali feldspar crystallizing before quartz. Using the depth of crystallization and quenching, the amount of quartz material resorbed, and a quartz dissolution rate, the time elapsed from when the magma began its ascension through the crust from the crustal magma trap at ~8.6 km to the emplacement depth (~1.4 km) as well as the ascension rate can tentatively be determined. Experimentally derived dissolution rates produce ascension rates that are not probable for this system; however, using a crystal growth rate of 3×10^{-8} cm/s for the dissolution rate, a reasonable magma ascension rate of (0.0027 m/s) and a magma travel time (29 days) is produced for the rhyolite dike.

REFERENCES

Abramoff, M. D., Magelhaus, P. J. & Ram, S. J. (2004). Image Processing with ImageJ. *Biophotonics International* 11, 36-42.

Acosta-Vigil, A., London, D., Morgan, G. B. V. & Dewers, T., A. (2006). Dissolution of Quartz, Albite, and Orthoclase in H2O-Saturated Haplogranitic Melt at 800°C and 200 MPa: Diffusive Transport Properties of Granitic Melts at Crustal Anatectic Conditions. *Journal of Petrology* 47, 231-254.

Acosta-Vigil, A., London, D., VI, G. B. M. & Dewers, T. A. (2003). Solubility of excess alumina in hydrous granitic meltsin equilibrium with peraluminous minerals at 700–800 C and 200 MPa, and applications of the aluminum saturation index. *Contributions to Mineralogy and Petrology* 146, 100-119.

Berger, A. & Roselle, G. (2001). Crystallization processes in migmatites. *American Mineralogist* 86, 215-224.

Best, M. G. & Christiansen, E. H. (1997). Origin of broken phenocrysts in ash-flow tuffs. *GSA Bulletin* 109, 63-73.

Bindeman, I. N. (2003). Crystal sizes in evolving silicic magma chambers. *Geology* 31, 367-370.

Cabane, H., Laporte, D. & Provost, A. (2001). Experimental investigation of the kinetics of Ostwald ripening of quartz in silicic melts. *Contributions to Mineralogy and Petrology* 142, 361-373.

Cashman, K. V. (1990). Textural constraints on the kinetics of crystallization of igneous rocks. In: Nicholls, J. & Russell, J. K. (eds.) *Modern Methods of Igneous Petrology: Understanding Magmatic Processes*. Washington, D.C.: Mineralogical Society of America, 259-314.

Castro, J. M., Cashman, K. V. & Manga, M. (2003). A technique for measuring 3D crystal-size distributions of prismatic microlites in obsidian. *American Mineralogist* 88, 1230-1240.

Clemens, J. D. (1998). Observations on the origins and ascent mechanisms of granitic magmas. *Journal of the Geological Society, London* 155, 843-851.

Coetzee, M. S., Bate, M. D. & Elsenbroek, J. H. (1995). Flow differentiation - an explanation for the origin and distribution of plagioclase glomerocrysts in the annas rust dolerite sill, vredefort dome. *South African Journal of Geology* 98, 276-286.

Deggeller, M., Wright, J. E., Hogan, J. P., Gilbert, M. C. & Price, J. D. (1996). Age and source characteristics of Mount Scott Granite, OK. *Geological Society of America Abstracts with Programs* 28, 10.

Durand, S. R. & Sen, G. (2004). Preeruption history of the Grande Ronde Formation lavas, Columbia River Basalt Group, American Northwest: Evidence from phenocrysts. *Geology* 32, 293-296.

Gilbert, M. C. & Myers, J. D. (1986). Overview of the Wichita Granite Group. In: Gilbert, M. C. (ed.) *Petrology of the Cambrian Wichita Mountains Igneous Suite*, 107-116.

Gilbert, M. C. & Powell, B. N. (1988). Igneous geology of the Wichita Mountains, southwestern Oklahoma. In: Hayward, O. T. (ed.) *South-Central Section of the Geological Society of America*, 109-126.

Ham, W. E., Denison, R. E. & Merritt, C. A. (1964). *Basement Rocks and Structural Evolution of Southern Oklahoma*. Oklahoma Geological Survey Bulletin 95.

Higgins, M. D. (1994). Numerical Modeling of crystal shapes in thin sections: Estimation of crystal habit and true size. *American Mineralogist* 79, 113-119.

Higgins, M. D. (1998). Origin of Anorthosite by Textural Coarsening: Quantitative Measurements of a Natural Sequence of Textural Development. *Journal of Petrology* 39, 1307-1323.

Higgins, M. D. (2000). Measurement of crystal size distributions. *American Mineralogist* 85, 1105-1116.

Higgins, M. D. (2006). *Quantitative Textural Measurements in Igneous and Metamorphic Petrology*. Cambridge: Cambridge University Press.

Hogan, J. P. (1993). Monomineralic Glomerocrysts: Textural Evidence for Mineral Resorption During Crystallization of Igneous Rocks. *Journal of Geology* 101, 531-540.

Hogan, J. P. & Gilbert, M. C. (1995). The A-Type Mount Scott Granite sheet: Importance of crustal magma traps. *Journal of Geophysical Research* 100, 15,779-715,792.

Hogan, J. P. & Gilbert, M. C. (1997). Intrusive style of A-type sheet granites in a rift environment: The Southern Oklahoma Aulacogen. In: Ojakangas, R. W., Dickas, A. B. & Green, J. C. (eds.) *Middle Proterozoic to Cambrian Rifting, Central North America*: Geological Society of America Special Paper 312, 299-311.

Hogan, J. P. & Gilbert, M. C. (1998). The Southern Oklahoma Aulacogen: A Cambrian analog for Mid-Proterozoic AMCG (Anorthosite-Mangerite-Charnockite-Granite) complexes? In: Hogan, J. P. & Gilbert, M. C. (eds.) *Basement Tectonics 12: Central North America and Other Regions*: Kluwer Academic Publishers, 39 - 78.

Hogan, J. P., Gilbert, M. C., Hames, W. E. & Wright, J. E. (1995). Magmatic history of an ancient crustal rift. *Geological Society of America Abstracts with Programs* 27, 436.

Johannes, W. & Holtz, F. (1996). *Petrogenesis and Experimental Petrology of Granitic Rocks*. Berlin: Springer.

Kirkpatrick, R. J. (1975). Crystal growth from the melt: A review. *American Mineralogist* 60, 798-814.

Lambert, D. D., Unruh, D. M. & Gilbert, M. C. (1988). Rb-Sr and Sm-Nd isotopic study of the Glen Mountains layered complex: Initiation of rifting within the southern Oklahoma aulacogen. *Geology* 16, 13-17.

Liang, Y. (1999). Diffusive dissolution in ternary systems: Analysis with applications to quartz and quartzite dissolution in molten silicates. *Geochimica et Cosmochimica Acta* 63, 3983-3995.

Mangan, M. T. (1990). Crystal size distribution systematics and the determination of magma storage times: The 1959 eruption of Kilauea volcano, Hawaii. *Journal of Volcanology and Geothermal Research* 44, 295-302.

Marsh, B. D. (1988). Crystal size distribution (CSD) in rocks and the kinetics and dynamics of crystallization I. Theory. *Contributions to Mineralogy and Petrology* 99, 277-297.

Marsh, B. D. (1998). On the Interpretation of Crystal Size Distributions in Magmatic Systems. *Journal of Petrology* 39, 553-599.

Paulick, H. & Breitkreuz, C. (2005). The Late Paleozoic felsic lava-dominated large igneous province in northeast Germany: volcanic facies analysis based on drill cores. *International Journal of Earth Sciences* 94, 834-850.

Petersen, J. S. & Lofgren, G. E. (1986). Lamellar and patchy intergrowths in feldspars: Experimental crystallization of eutectic silicates. *American Mineralogist* 71, 343-355.

Peterson, T. D. (1996). A refined technique for measuring crystal size distributions in thin section. *Contributions to Mineralogy and Petrology* 124, 395-405.

Price, J. D. (1998). Petrology of the Mount Scott Granite. *Geology & Geophysics*. Norman, Oklahoma: University of Oklahoma, 240.

Randolph, A. D. & Larson, M. A. (1971). *Theory of particulate processes*. New York: Academic Press.

The Rock Color Chart Committee. (1964). *Rock Color Chart*. New York: Geological Society of America.

Rutherford, M. J. & Gardner, J. E. (2000). Rates of Magma Ascent. In: Sigurdsson, H. (ed.) *Encyclopedia or Volcanoes*. San Diego: Academic Press, 207-218.

Schaeben, H., Boogaart, K. G. v. d., Mock, A. & Breitkreuz, C. (2002). Inherited correlation in crystal size distribution: Comment and Reply. *Geology* 30, 282-283.

Schwindlinger, K. R. (1999). Particle dynamics and aggregation of crystals in a magma chamber with application to Kilauea Iki olivines. *Journal of Volcanology and Geothermal Research* 88, 209-238.

Schwindlinger, K. R. & Alfred T. Anderson, J. (1989). Synneusis of Kilauea Iki olivines. *Contributions to Mineralogy and Petrology* 103, 187-198.

Shaw, C. S. J. (2004). Mechanisms and rates of quartz dissolution in melts in the CMAS (CaO–MgO–Al2O3–SiO2) system. *Contributions to Mineralogy and Petrology* 148, 180-200.

Swanson, S. E. (1977). Relation of nucleation and crystal-growth rate to the development of granitic textures. *American Mineralogist* 62, 966-978.

Swanson, S. E. & Fenn, P. M. (1986). Quartz crystallization in igneous rocks. *American Mineralogist* 71, 331-342.

Tomiya, A. & Takahashi, E. (2005). Evolution of the Magma Chamber beneath Usu Volcano since 1663: a Natural Laboratory for Observing Changing Phenocryst Compositions and Textures. *Journal of Petrology* 46, 2395-2426.

Tuttle, O. F. & Bowen, N. L. (1958). *Origin of granite in the light of experimental studies in the system $NaAlSi_3O_8$-$KAlSi_3O_8$-SiO_2-H_2O*. Geological Society of America Memoir 74. New York: The Geological Society of America.

Vance, J. A. (1969). On Synneusis. *Contributions to Mineralogy and Petrology* 24, 7-29.

Vogt, J. H. L. (1921). The physical chemistry of the crystallization and magmatic differentiation of the igneous rocks. *Journal of Geology* 29, 318-350.

Voorhees, P. W. (1992). Ostwald Ripening of Two-Phase Mixtures. *Annual Review of Materials Science* 22, 197-215.

Waters, C. & Boudreau, A. E. (1996). A reevaluation of crystal-size distributions in chromite cumulates. *American Mineralogist* 81, 1452-1459.

Weaver, B., Kar, A., Davidson, J. & Colucci, M. (1996). Geochemical Characteristics of Volcanic Rocks from Ascension Island, South Atlantic Ocean. *Geothermics* 25, 449-470.

Wright, J. E. & Hogan, J. P. (1996). The Southern Oklahoma Aulacogen: not just another B.L.I.P. *Eos, Transactions, American Geophysical Union* 77, 845.

APPENDIX A.

NORMALIZED QUANTITATIVE ELECTRON MICROPROBE ANALYSES

Quantitative Electron Microprobe Analyses

Pre-run Standards for Analysis of Alkali Feldspar (Alkali Feldspar Run 1)

	AMAB-1	AMAB-2	AMAB-3	AMAB-4	SWAN-1	SWAN-2	SWAN-3	SWAN-4	SGKF-1	SGKF-2	SGKF-3	AUGI-1	AUGI-2	STR-1	STR-2	BRT-1	BRT-2
	Chemical Composition (Weight Percent)																
SiO_2	68.13	67.79	67.95	67.87	46.27	46.17	46.11	46.29	64.81	64.46	64.29	46.63	46.68	0.00	0.00	0.10	0.09
Al2O_3	19.60	19.57	19.61	19.38	33.96	33.75	33.94	34.20	18.38	18.47	18.43	0.57	0.61	0.01	0.00	0.68	0.71
Fe_2O_3	0.00	0.00	0.02	0.00	0.42	0.40	0.43	0.40	0.00	0.00	0.00	33.60	33.56	0.00	0.00	0.00	0.00
CaO	0.24	0.24	0.26	0.22	17.43	17.51	17.53	17.46	0.00	0.01	0.00	19.35	19.38	2.16	2.39	0.00	0.00
SrO	0.02	0.00	0.02	0.00	0.00	0.00	0.00	0.00	0.07	0.08	0.09	0.00	0.00	67.90	67.77	0.00	0.00
BaO	0.00	0.00	0.00	0.00	0.00	0.01	0.00	0.01	0.31	0.33	0.33	0.03	0.02	0.02	0.06	65.66	65.63
Na_2O	11.68	11.48	11.46	11.54	1.66	1.61	1.65	1.64	1.20	1.20	1.25	0.19	0.17	0.00	0.00	0.15	0.15
K_2O	0.26	0.24	0.24	0.17	0.04	0.05	0.05	0.05	15.15	14.89	15.02	0.00	0.00	0.02	0.00	0.00	0.01
P_2O_5	0.03	0.05	0.02	0.06	0.01	0.04	0.00	0.00	0.02	0.00	0.00	0.01	0.00	0.12	0.00	0.01	0.05
Total	99.97	99.36	99.59	99.24	99.79	99.54	99.72	100.04	99.94	99.45	99.43	100.37	100.42	70.22	70.21	66.60	66.64
	Ions per 8 Oxygen																
Si	2.983	2.983	2.984	2.989	2.135	2.136	2.131	2.131	2.995	2.991	2.988	2.436	2.437	0.000	0.000	0.030	0.027
Al	1.011	1.015	1.015	1.006	1.847	1.841	1.849	1.855	1.001	1.010	1.010	0.035	0.037	0.001	0.000	0.235	0.245
Fe	0.000	0.000	0.001	0.000	0.015	0.014	0.015	0.014	0.000	0.000	0.000	1.321	1.318	0.000	0.000	0.000	0.000
Ca	0.011	0.011	0.012	0.011	0.862	0.868	0.868	0.861	0.000	0.001	0.000	1.083	1.084	0.441	0.488	0.000	0.000
Sr	0.001	0.000	0.001	0.000	0.000	0.000	0.000	0.000	0.002	0.002	0.002	0.000	0.000	7.504	7.507	0.000	0.000
Ba	0.000	0.000	0.000	0.000	0.000	0.000	0.000	0.000	0.006	0.006	0.006	0.001	0.001	0.002	0.005	7.537	7.505
Na	0.992	0.980	0.976	0.986	0.148	0.145	0.148	0.146	0.107	0.108	0.113	0.019	0.017	0.000	0.000	0.083	0.083
K	0.015	0.013	0.014	0.009	0.003	0.003	0.003	0.003	0.893	0.881	0.891	0.000	0.000	0.004	0.000	0.000	0.002
P	0.001	0.002	0.001	0.002	0.000	0.002	0.000	0.000	0.001	0.000	0.000	0.001	0.000	0.020	0.000	0.004	0.013
Sum	5.013	5.004	5.002	5.002	5.009	5.008	5.013	5.009	5.004	4.999	5.009	4.895	4.894	7.972	8.000	7.889	7.874

Standard abbreviations are as follows: AMAB - Amelia albite (Virginia: Na); SWAN - anorthite (Stillwater: An_{84}); SGKF - adularia (St. Goddard Switzerland: K); AUG - Augite (AMAX R&D Laboratory); STR - strontionite (Sr); BRT - Barite (Ba).

Quantitative Electron Microprobe Analyses

Analyses of Alkali Feldspar

Circle Four - Alkali Feldspar 1 (K Phase)

	Afs1-KF-1	Afs1-KF-2	Afs1-KF-3	Afs1-KF-4	Afs1-KF-5	Afs1-KF-6	Afs1-KF-7	**Average**	Std Dev
				Chemical Composition (Weight Percent)					
SiO_2	64.26	64.11	64.37	64.24	64.49	64.25	64.16	**64.27**	0.13
$Al2O_3$	18.23	18.05	18.36	18.35	18.18	18.27	18.22	**18.24**	0.10
Fe_2O_3	0.06	0.04	0.03	0.03	0.03	0.02	0.02	**0.03**	0.01
CaO	0.00	0.01	0.00	0.00	0.00	0.00	0.00	**0.00**	0.00
SrO	0.00	0.00	0.06	0.00	0.00	0.05	0.02	**0.02**	0.03
BaO	0.05	0.01	0.04	0.06	0.04	0.03	0.04	**0.04**	0.02
Na_2O	0.24	0.24	0.17	0.17	0.26	0.20	0.17	**0.21**	0.04
K_2O	16.44	16.52	16.45	16.58	16.30	16.65	16.48	**16.49**	0.11
P_2O_5	0.03	0.02	0.03	0.00	0.02	0.05	0.00	**0.02**	0.02
Total	99.32	98.99	99.50	99.42	99.31	99.51	99.13	**99.31**	0.19
				Ions per 8 Oxygen					
Si	2.995	3.000	2.994	2.993	3.002	2.992	2.997	**2.996**	0.004
Al	1.002	0.995	1.006	1.007	0.997	1.003	1.003	**1.002**	0.004
Fe	0.002	0.001	0.001	0.001	0.001	0.001	0.001	**0.001**	0.000
Ca	0.000	0.000	0.000	0.000	0.000	0.000	0.000	**0.000**	0.000
Sr	0.000	0.000	0.002	0.000	0.000	0.001	0.001	**0.001**	0.001
Ba	0.001	0.000	0.001	0.001	0.001	0.001	0.001	**0.001**	0.000
Na	0.022	0.022	0.016	0.015	0.023	0.018	0.016	**0.019**	0.004
K	0.978	0.986	0.976	0.986	0.968	0.989	0.982	**0.981**	0.007
P	0.001	0.001	0.001	0.000	0.001	0.002	0.000	**0.001**	0.001
Sum	5.001	5.005	4.996	5.003	4.993	5.007	5.000	**5.001**	0.005
An	0.02	0.03	0.00	0.01	0.00	0.00	0.00	**0.01**	0.01
Ab	2.20	2.16	1.57	1.49	2.35	1.77	1.58	**1.87**	0.35
Or	97.68	97.79	98.20	98.39	97.58	98.06	98.28	**98.00**	0.32
Cel	0.10	0.02	0.07	0.11	0.07	0.05	0.07	**0.07**	0.03
Slaw	0.00	0.00	0.16	0.00	0.00	0.12	0.07	**0.05**	0.07

Circle Four - Alkali Feldspar 1 (Na Phase)

	Afs1-NF-1	Afs1-NF-2	Afs1-NF-3	Afs1-NF-4	Afs1-NF-5	Afs1-NF-6	**Average**	Std Dev
				Chemical Composition (Weight Percent)				
SiO_2	68.38	68.03	68.46	67.96	68.20	68.25	**68.21**	0.19
$Al2O_3$	19.53	19.37	19.33	19.40	19.44	19.43	**19.42**	0.07
Fe_2O_3	0.09	0.21	0.05	0.54	0.25	0.04	**0.20**	0.19
CaO	0.10	0.03	0.05	0.05	0.06	0.03	**0.05**	0.02
SrO	0.03	0.02	0.02	0.00	0.00	0.00	**0.01**	0.01
BaO	0.00	0.00	0.00	0.00	0.00	0.00	**0.00**	0.00
Na_2O	11.72	11.66	11.82	11.62	11.68	11.69	**11.70**	0.07
K_2O	0.15	0.09	0.03	0.09	0.08	0.05	**0.08**	0.04
P_2O_5	0.00	0.00	0.00	0.01	0.00	0.01	**0.00**	0.01
Total	99.99	99.41	99.77	99.68	99.70	99.50	**99.67**	0.20
				Ions per 8 Oxygen				
Si	2.990	2.991	2.998	2.984	2.990	2.995	**2.991**	0.005
Al	1.007	1.004	0.998	1.004	1.004	1.005	**1.004**	0.003
Fe	0.003	0.007	0.002	0.018	0.008	0.001	**0.007**	0.006
Ca	0.005	0.001	0.003	0.002	0.003	0.002	**0.003**	0.001
Sr	0.001	0.000	0.001	0.000	0.000	0.000	**0.000**	0.000
Ba	0.000	0.000	0.000	0.000	0.000	0.000	**0.000**	0.000
Na	0.993	0.994	1.003	0.989	0.992	0.995	**0.994**	0.005
K	0.008	0.005	0.002	0.005	0.005	0.003	**0.005**	0.002
P	0.000	0.000	0.000	0.001	0.000	0.000	**0.000**	0.000
Sum	5.006	5.003	5.005	5.002	5.002	5.001	**5.003**	0.002
An	0.45	0.13	0.25	0.24	0.27	0.16	**0.25**	0.11
Ab	98.67	99.31	99.51	99.26	99.28	99.54	**99.26**	0.31
Or	0.80	0.52	0.19	0.49	0.45	0.30	**0.46**	0.21
Cel	0.00	0.00	0.00	0.01	0.00	0.00	**0.00**	0.00
Slaw	0.08	0.04	0.05	0.00	0.00	0.00	**0.03**	0.03

Quantitative Electron Microprobe Analyses

Analyses of Alkali Feldspar

Circle Five - Alkali Feldspar 2 (K Phase)

	Afs2-KF-1	Afs2-KF-2	Afs2-KF-3	Afs2-KF-4	Afs2-KF-5	Afs2-KF-6	Afs2-KF-7	**Average**	Std Dev
				Chemical Composition (Weight Percent)					
SiO_2	64.05	64.06	64.20	63.95	64.28	63.99	64.01	**64.08**	0.12
$Al2O_3$	18.14	18.17	18.06	18.24	18.08	17.99	18.04	**18.10**	0.08
Fe_2O_3	0.03	0.01	0.03	0.03	0.03	0.03	0.03	**0.03**	0.01
CaO	0.00	0.00	0.00	0.01	0.00	0.02	0.00	**0.00**	0.01
SrO	0.02	0.00	0.01	0.00	0.05	0.00	0.03	**0.02**	0.02
BaO	0.05	0.00	0.06	0.04	0.03	0.04	0.06	**0.04**	0.02
Na_2O	0.28	0.20	0.26	0.20	0.21	0.27	0.27	**0.24**	0.03
K_2O	16.45	16.49	16.49	16.54	16.56	16.44	16.44	**16.49**	0.05
P_2O_5	0.00	0.01	0.00	0.03	0.00	0.07	0.01	**0.02**	0.03
Total	99.02	98.94	99.11	99.03	99.24	98.86	98.90	**99.01**	0.13
				Ions per 8 Oxygen					
Si	2.997	2.997	3.001	2.992	3.001	2.998	2.999	**2.998**	0.003
Al	1.000	1.002	0.995	1.006	0.995	0.993	0.996	**0.998**	0.005
Fe	0.001	0.000	0.001	0.001	0.001	0.001	0.001	**0.001**	0.000
Ca	0.000	0.000	0.000	0.000	0.000	0.001	0.000	**0.000**	0.000
Sr	0.001	0.000	0.000	0.000	0.001	0.000	0.001	**0.000**	0.000
Ba	0.001	0.000	0.001	0.001	0.001	0.001	0.001	**0.001**	0.000
Na	0.025	0.018	0.023	0.019	0.019	0.024	0.024	**0.022**	0.003
K	0.982	0.984	0.983	0.987	0.987	0.982	0.983	**0.984**	0.002
P	0.000	0.000	0.000	0.001	0.000	0.003	0.000	**0.001**	0.001
Sum	5.006	5.002	5.004	5.006	5.004	5.004	5.005	**5.005**	0.001
An	0.00	0.00	0.00	0.03	0.00	0.08	0.01	**0.02**	0.03
Ab	2.47	1.80	2.32	1.85	1.89	2.42	2.42	**2.17**	0.31
Or	97.38	98.20	97.53	98.06	97.94	97.42	97.38	**97.70**	0.35
Cel	0.09	0.00	0.11	0.06	0.05	0.08	0.11	**0.07**	0.04
Slaw	0.06	0.00	0.04	0.00	0.13	0.00	0.08	**0.04**	0.05

Circle Five - Alkali Feldspar 2 (Na Phase)

	Afs2-NF-1	Afs2-NF-2	Afs2-NF-3	Afs2-NF-4	Afs2-NF-5	Afs2-NF-6	**Average**	Std Dev
				Chemical Composition (Weight Percent)				
SiO_2	67.97	68.24	68.39	68.06	68.33	67.76	**68.13**	0.24
$Al2O_3$	19.17	19.27	19.18	19.12	19.23	19.24	**19.20**	0.06
Fe_2O_3	0.06	0.07	0.14	0.07	0.05	0.23	**0.10**	0.07
CaO	0.07	0.03	0.02	0.03	0.06	0.17	**0.06**	0.06
SrO	0.01	0.00	0.00	0.02	0.05	0.00	**0.01**	0.02
BaO	0.03	0.03	0.02	0.00	0.00	0.00	**0.01**	0.01
Na_2O	11.55	11.77	11.56	11.67	11.65	11.49	**11.62**	0.10
K_2O	0.12	0.12	0.11	0.14	0.12	0.12	**0.12**	0.01
P_2O_5	0.07	0.03	0.00	0.00	0.04	0.01	**0.02**	0.03
Total	99.06	99.57	99.43	99.11	99.51	99.01	**99.28**	0.25
				Ions per 8 Oxygen				
Si	2.997	2.996	3.004	3.001	2.999	2.992	**2.998**	0.004
Al	0.996	0.997	0.993	0.993	0.995	1.001	**0.996**	0.003
Fe	0.002	0.002	0.005	0.002	0.002	0.008	**0.003**	0.002
Ca	0.003	0.001	0.001	0.001	0.003	0.008	**0.003**	0.003
Sr	0.000	0.000	0.000	0.001	0.001	0.000	**0.000**	0.000
Ba	0.001	0.000	0.000	0.000	0.000	0.000	**0.000**	0.000
Na	0.988	1.002	0.985	0.998	0.991	0.983	**0.991**	0.007
K	0.007	0.007	0.006	0.008	0.007	0.007	**0.007**	0.000
P	0.003	0.001	0.000	0.000	0.001	0.000	**0.001**	0.001
Sum	4.997	5.007	4.993	5.004	4.999	4.999	**5.000**	0.005
An	0.34	0.13	0.09	0.13	0.26	0.80	**0.29**	0.27
Ab	98.88	99.14	99.23	99.04	98.96	98.54	**98.96**	0.24
Or	0.69	0.69	0.64	0.77	0.66	0.66	**0.69**	0.05
Cel	0.06	0.04	0.03	0.00	0.00	0.00	**0.02**	0.03
Slaw	0.03	0.00	0.00	0.06	0.12	0.00	**0.03**	0.05

Quantitative Electron Microprobe Analyses

Analyses of Alkali Feldspar

Circle Six - Alkali Feldspar 3 (K Phase)

	Afs3-KF-1	Afs3-KF-2	Afs3-KF-3	Afs3-KF-4	Afs3-KF-5	Afs3-KF-6	**Average**	Std Dev
				Chemical Composition (Weight Percent)				
SiO_2	64.40	64.21	64.38	64.11	64.10	64.31	**64.25**	0.13
$Al2O_3$	18.23	18.20	18.18	18.16	18.12	18.29	**18.20**	0.06
Fe_2O_3	0.02	0.04	0.05	0.05	0.04	0.03	**0.04**	0.01
CaO	0.01	0.01	0.00	0.00	0.00	0.00	**0.00**	0.00
SrO	0.04	0.00	0.04	0.06	0.00	0.00	**0.02**	0.02
BaO	0.03	0.06	0.00	0.01	0.02	0.05	**0.03**	0.02
Na_2O	0.26	0.33	0.26	0.22	0.29	0.33	**0.28**	0.04
K_2O	16.54	16.35	16.58	16.49	16.37	16.29	**16.44**	0.11
P_2O_5	0.03	0.00	0.01	0.02	0.00	0.00	**0.01**	0.01
Total	99.56	99.20	99.50	99.11	98.95	99.31	**99.27**	0.23
				Ions per 8 Oxygen				
Si	2.996	2.997	2.998	2.996	2.998	2.996	**2.997**	0.001
Al	1.000	1.001	0.997	1.000	0.999	1.004	**1.000**	0.002
Fe	0.001	0.002	0.002	0.002	0.001	0.001	**0.001**	0.000
Ca	0.000	0.000	0.000	0.000	0.000	0.000	**0.000**	0.000
Sr	0.001	0.000	0.001	0.002	0.000	0.000	**0.001**	0.001
Ba	0.001	0.001	0.000	0.000	0.000	0.001	**0.001**	0.000
Na	0.023	0.030	0.023	0.020	0.027	0.030	**0.025**	0.004
K	0.981	0.973	0.985	0.983	0.977	0.968	**0.978**	0.006
P	0.001	0.000	0.000	0.001	0.000	0.000	**0.000**	0.001
Sum	5.004	5.004	5.006	5.003	5.003	5.000	**5.003**	0.002
An	0.04	0.04	0.02	0.00	0.00	0.00	**0.02**	0.02
Ab	2.32	2.96	2.31	1.97	2.66	3.00	**2.54**	0.41
Or	97.48	96.89	97.55	97.87	97.29	96.91	**97.33**	0.38
Cel	0.05	0.11	0.01	0.01	0.04	0.09	**0.05**	0.04
Slaw	0.11	0.00	0.11	0.15	0.01	0.00	**0.06**	0.07

Circle Six - Alkali Feldspar 3 (Na Phase)

	Afs3-NF-1	Afs3-NF-2	Afs3-NF-3	Afs3-NF-4	Afs3-NF-5	Afs3-NF-6	**Average**	Std Dev
				Chemical Composition (Weight Percent)				
SiO_2	68.36	68.25	68.14	68.45	68.55	68.28	**68.34**	0.15
$Al2O_3$	19.38	19.33	19.36	19.40	19.41	19.27	**19.36**	0.05
Fe_2O_3	0.07	0.20	0.35	0.03	0.02	0.24	**0.15**	0.13
CaO	0.03	0.05	0.04	0.05	0.03	0.09	**0.05**	0.02
SrO	0.00	0.00	0.02	0.00	0.02	0.00	**0.01**	0.01
BaO	0.00	0.00	0.03	0.02	0.01	0.05	**0.02**	0.02
Na_2O	11.81	11.63	11.75	11.74	11.56	11.46	**11.66**	0.13
K_2O	0.07	0.10	0.06	0.10	0.06	0.11	**0.08**	0.02
P_2O_5	0.00	0.04	0.00	0.02	0.00	0.05	**0.02**	0.02
Total	99.73	99.61	99.74	99.80	99.67	99.56	**99.69**	0.09
				Ions per 8 Oxygen				
Si	2.995	2.994	2.989	2.996	3.001	2.996	**2.995**	0.004
Al	1.001	0.999	1.001	1.001	1.001	0.997	**1.000**	0.002
Fe	0.002	0.007	0.012	0.001	0.001	0.008	**0.005**	0.004
Ca	0.002	0.002	0.002	0.002	0.002	0.004	**0.002**	0.001
Sr	0.000	0.000	0.001	0.000	0.000	0.000	**0.000**	0.000
Ba	0.000	0.000	0.001	0.000	0.000	0.001	**0.000**	0.000
Na	1.003	0.989	0.999	0.997	0.981	0.975	**0.991**	0.011
K	0.004	0.006	0.003	0.005	0.003	0.006	**0.005**	0.001
P	0.000	0.001	0.000	0.001	0.000	0.002	**0.001**	0.001
Sum	5.007	4.999	5.006	5.003	4.990	4.989	**4.999**	0.008
An	0.16	0.24	0.19	0.22	0.15	0.43	**0.23**	0.10
Ab	99.46	99.18	99.39	99.20	99.45	98.84	**99.26**	0.24
Or	0.37	0.58	0.32	0.54	0.33	0.64	**0.46**	0.14
Cel	0.01	0.00	0.05	0.04	0.02	0.09	**0.04**	0.03
Slaw	0.00	0.00	0.05	0.00	0.04	0.00	**0.02**	0.02

Quantitative Electron Microprobe Analyses

Analyses of Alkali Feldspar

Circle Seven - Alkali Feldspar 4 (K Phase)

	Afs4-KF-1	Afs4-KF-2	Afs4-KF-3	Afs4-KF-4	Afs4-KF-5	Afs4-KF-6	**Average**	Std Dev
				Chemical Composition (Weight Percent)				
SiO_2	64.42	64.33	64.52	64.41	64.43	64.43	**64.42**	0.06
$Al2O_3$	18.29	18.28	18.25	18.35	18.22	18.20	**18.27**	0.05
Fe_2O_3	0.06	0.03	0.06	0.02	0.03	0.00	**0.03**	0.03
CaO	0.00	0.03	0.00	0.00	0.00	0.00	**0.01**	0.01
SrO	0.04	0.05	0.02	0.04	0.00	0.00	**0.02**	0.02
BaO	0.00	0.02	0.07	0.01	0.04	0.03	**0.03**	0.02
Na_2O	0.29	0.38	0.27	0.27	0.25	0.32	**0.30**	0.05
K_2O	16.71	16.40	16.53	16.45	16.36	16.39	**16.47**	0.13
P_2O_5	0.00	0.00	0.02	0.02	0.01	0.01	**0.01**	0.01
Total	99.81	99.51	99.74	99.58	99.34	99.38	**99.56**	0.19
				Ions per 8 Oxygen				
Si	2.993	2.994	2.997	2.994	3.000	3.000	**2.996**	0.003
Al	1.001	1.003	0.999	1.005	1.000	0.999	**1.001**	0.002
Fe	0.002	0.001	0.002	0.001	0.001	0.000	**0.001**	0.001
Ca	0.000	0.002	0.000	0.000	0.000	0.000	**0.000**	0.001
Sr	0.001	0.001	0.001	0.001	0.000	0.000	**0.001**	0.001
Ba	0.000	0.000	0.001	0.000	0.001	0.001	**0.001**	0.000
Na	0.026	0.034	0.024	0.024	0.023	0.029	**0.027**	0.004
K	0.990	0.974	0.979	0.976	0.972	0.973	**0.977**	0.007
P	0.000	0.000	0.001	0.001	0.000	0.000	**0.000**	0.000
Sum	5.014	5.008	5.004	5.002	4.996	5.001	**5.004**	0.006
An	0.01	0.16	0.00	0.00	0.00	0.00	**0.03**	0.06
Ab	2.57	3.36	2.38	2.44	2.28	2.87	**2.65**	0.40
Or	97.33	96.33	97.44	97.42	97.65	97.07	**97.21**	0.47
Cel	0.00	0.03	0.12	0.03	0.07	0.05	**0.05**	0.04
Slaw	0.09	0.12	0.06	0.11	0.00	0.01	**0.06**	0.05

Circle Seven - Alkali Feldspar 4 (Na Phase)

	Afs4-NF-1	Afs4-NF-2	Afs4-NF-3	Afs4-NF-4	Afs4-NF-5	**Average**	Std Dev
				Chemical Composition (Weight Percent)			
SiO_2	68.29	68.27	68.23	68.54	68.53	**68.37**	0.15
$Al2O_3$	19.44	19.41	19.25	19.38	19.36	**19.37**	0.07
Fe_2O_3	0.04	0.10	0.06	0.13	0.04	**0.07**	0.04
CaO	0.08	0.06	0.13	0.08	0.09	**0.09**	0.02
SrO	0.00	0.05	0.00	0.00	0.00	**0.01**	0.02
BaO	0.01	0.02	0.00	0.01	0.00	**0.01**	0.01
Na_2O	11.85	11.45	11.50	11.79	11.69	**11.66**	0.18
K_2O	0.08	0.14	0.12	0.10	0.09	**0.10**	0.02
P_2O_5	0.01	0.02	0.01	0.00	0.00	**0.01**	0.01
Total	99.80	99.51	99.29	100.04	99.81	**99.69**	0.29
				Ions per 8 Oxygen			
Si	2.991	2.996	3.000	2.995	2.999	**2.996**	0.003
Al	1.003	1.004	0.998	0.998	0.998	**1.000**	0.003
Fe	0.001	0.003	0.002	0.004	0.001	**0.002**	0.001
Ca	0.004	0.003	0.006	0.004	0.004	**0.004**	0.001
Sr	0.000	0.001	0.000	0.000	0.000	**0.000**	0.001
Ba	0.000	0.000	0.000	0.000	0.000	**0.000**	0.000
Na	1.007	0.975	0.980	0.999	0.992	**0.991**	0.013
K	0.004	0.008	0.007	0.006	0.005	**0.006**	0.001
P	0.000	0.001	0.001	0.000	0.000	**0.000**	0.000
Sum	5.011	4.991	4.993	5.006	5.000	**5.000**	0.009
An	0.36	0.29	0.59	0.39	0.43	**0.41**	0.11
Ab	99.18	98.77	98.75	99.03	99.08	**98.96**	0.19
Or	0.43	0.78	0.65	0.57	0.49	**0.59**	0.14
Cel	0.02	0.03	0.00	0.01	0.00	**0.01**	0.01
Slaw	0.00	0.12	0.00	0.00	0.00	**0.02**	0.05

Quantitative Electron Microprobe Analyses

Analyses of Alkali Feldspar

Circle Seven - Alkali Feldspar 5 (K Phase)

	Afs5-KF-1	Afs5-KF-2	Afs5-KF-3	Afs5-KF-4	Afs5-KF-5	Afs5-KF-6	**Average**	Std Dev
				Chemical Composition (Weight Percent)				
SiO_2	64.07	64.52	64.34	64.51	64.39	64.36	**64.36**	0.17
$Al2O_3$	18.16	18.27	18.21	18.19	18.18	18.23	**18.21**	0.04
Fe_2O_3	0.00	0.04	0.04	0.00	0.00	0.02	**0.02**	0.02
CaO	0.00	0.00	0.00	0.00	0.00	0.00	**0.00**	0.00
SrO	0.03	0.00	0.07	0.00	0.02	0.10	**0.04**	0.04
BaO	0.05	0.02	0.04	0.02	0.01	0.02	**0.03**	0.01
Na_2O	0.24	0.24	0.31	0.24	0.27	0.29	**0.26**	0.03
K_2O	16.66	16.63	16.29	16.59	16.45	16.48	**16.52**	0.14
P_2O_5	0.01	0.00	0.00	0.02	0.02	0.02	**0.01**	0.01
Total	99.21	99.72	99.31	99.58	99.34	99.50	**99.45**	0.19
				Ions per 8 Oxygen				
Si	2.995	2.997	2.998	3.000	3.000	2.996	**2.997**	0.002
Al	1.000	1.000	1.000	0.997	0.998	1.000	**0.999**	0.002
Fe	0.000	0.001	0.002	0.000	0.000	0.001	**0.001**	0.001
Ca	0.000	0.000	0.000	0.000	0.000	0.000	**0.000**	0.000
Sr	0.001	0.000	0.002	0.000	0.001	0.003	**0.001**	0.001
Ba	0.001	0.000	0.001	0.000	0.000	0.000	**0.001**	0.000
Na	0.022	0.022	0.028	0.021	0.025	0.026	**0.024**	0.003
K	0.993	0.985	0.968	0.984	0.977	0.979	**0.981**	0.008
P	0.000	0.000	0.000	0.001	0.001	0.001	**0.000**	0.000
Sum	5.013	5.006	4.999	5.003	5.001	5.005	**5.004**	0.005
An	0.00	0.00	0.00	0.00	0.00	0.00	**0.00**	0.00
Ab	2.17	2.14	2.79	2.13	2.44	2.59	**2.38**	0.28
Or	97.66	97.81	96.94	97.83	97.48	97.11	**97.47**	0.37
Cel	0.09	0.04	0.08	0.04	0.02	0.03	**0.05**	0.03
Slaw	0.08	0.01	0.19	0.00	0.06	0.27	**0.10**	0.11

Circle Seven - Alkali Feldspar 5 (Na Phase)

	Afs5-NF-1	Afs5-NF-2	Afs5-NF-3	Afs5-NF-4	Afs5-NF-5	Afs5-NF-6	Afs5-NF-7	**Average**	Std Dev
					Chemical Composition (Weight Percent)				
SiO_2	68.44	68.62	68.14	68.32	67.83	68.39	68.20	**68.28**	0.25
$Al2O_3$	19.45	19.42	19.37	19.45	19.31	19.45	19.40	**19.41**	0.05
Fe_2O_3	0.06	0.09	0.12	0.11	0.34	0.30	0.04	**0.15**	0.12
CaO	0.04	0.12	0.07	0.06	0.10	0.04	0.16	**0.09**	0.04
SrO	0.00	0.02	0.01	0.00	0.07	0.00	0.00	**0.01**	0.03
BaO	0.00	0.00	0.00	0.00	0.00	0.02	0.03	**0.01**	0.01
Na_2O	11.73	11.70	11.79	11.66	11.60	11.73	11.59	**11.68**	0.08
K_2O	0.07	0.12	0.11	0.12	0.15	0.08	0.11	**0.11**	0.03
P_2O_5	0.00	0.02	0.00	0.00	0.00	0.00	0.01	**0.00**	0.01
Total	99.81	100.10	99.63	99.72	99.41	100.00	99.53	**99.74**	0.25
					Ions per 8 Oxygen				
Si	2.995	2.995	2.991	2.993	2.987	2.990	2.994	**2.99**	0.00
Al	1.003	0.999	1.002	1.004	1.002	1.002	1.004	**1.00**	0.00
Fe	0.002	0.003	0.004	0.004	0.011	0.010	0.001	**0.01**	0.00
Ca	0.002	0.006	0.003	0.003	0.005	0.002	0.007	**0.00**	0.00
Sr	0.000	0.000	0.000	0.000	0.002	0.000	0.000	**0.00**	0.00
Ba	0.000	0.000	0.000	0.000	0.000	0.000	0.001	**0.00**	0.00
Na	0.996	0.990	1.004	0.990	0.990	0.994	0.986	**0.99**	0.01
K	0.004	0.007	0.006	0.007	0.009	0.004	0.006	**0.01**	0.00
P	0.000	0.001	0.000	0.000	0.000	0.000	0.000	**0.00**	0.00
Sum	5.002	5.001	5.011	5.001	5.006	5.003	4.999	**5.00**	0.00
An	0.20	0.57	0.34	0.28	0.46	0.21	0.74	**0.40**	0.20
Ab	99.41	98.73	99.04	99.05	98.50	99.33	98.59	**98.95**	0.36
Or	0.39	0.66	0.59	0.66	0.87	0.43	0.61	**0.60**	0.16
Cel	0.00	0.00	0.00	0.01	0.00	0.03	0.05	**0.01**	0.02
Slaw	0.00	0.04	0.03	0.00	0.18	0.00	0.01	**0.04**	0.06

Quantitative Electron Microprobe Analyses

Pre-run Standards for Analysis of Alkali Feldspar (Alkali Feldspar Run 2)

	AMAB-1	AMAB-2	AMAB-3	AMAB-4	SWAN-1	SWAN-2	SWAN-3	SWAN-4	SWAN-5	SGKF-1	SGKF-2	SGKF-3	SGKF-4	AUGI-1	AUGI-2	AUGI-3	BRT-1	BRT-2	BRT-3
	Chemical Composition (Weight Percent)																		
SiO_2	68.38	68.06	68.27	68.22	45.28	45.35	45.58	45.47	45.71	63.40	63.57	63.46	63.86	46.24	46.79	46.66	-0.36	-0.36	-0.37
$Al2O_3$	20.40	20.24	20.36	20.24	33.82	33.83	33.92	33.96	34.27	18.69	18.68	18.80	18.68	0.53	0.51	0.57	1.00	1.08	1.05
Fe_2O_3	0.02	0.00	0.00	0.01	0.42	0.41	0.41	0.38	0.40	0.00	0.00	0.01	0.02	33.23	33.53	33.55	0.00	0.00	0.00
CaO	0.24	0.21	0.22	0.26	17.17	17.49	17.21	17.08	17.34	0.02	0.01	0.01	0.02	19.35	19.19	19.17	0.01	0.00	0.00
BaO	0.02	0.00	0.00	0.00	0.01	0.04	0.00	0.00	0.00	0.30	0.33	0.34	0.31	0.01	0.03	0.02	65.21	64.97	64.50
Na_2O	11.44	11.52	11.47	11.38	1.61	1.62	1.64	1.67	1.59	1.29	1.30	1.27	1.26	0.19	0.19	0.22	0.13	0.12	0.14
K_2O	0.20	0.17	0.16	0.23	0.04	0.05	0.04	0.04	0.03	14.68	14.67	14.68	14.69	0.00	0.01	0.00	0.00	0.00	0.00
Total	100.70	100.20	100.48	100.34	98.36	98.80	98.80	98.61	99.34	98.39	98.56	98.58	98.83	99.53	100.25	100.18	65.99	65.82	65.33
	Ions per 8 Oxygen																		
Si	2.969	2.970	2.970	2.972	2.127	2.124	2.131	2.129	2.125	2.974	2.977	2.972	2.980	2.441	2.450	2.445	0.011	0.012	0.008
Al	1.044	1.040	1.043	1.039	1.862	1.857	1.858	1.864	1.868	1.033	1.031	1.037	1.027	0.039	0.038	0.042	0.378	0.405	0.399
Fe	0.001	0.000	0.000	0.000	0.015	0.014	0.014	0.013	0.014	0.000	0.000	0.000	0.001	1.309	1.310	1.312	0.000	0.000	0.000
Ca	0.011	0.010	0.010	0.012	0.857	0.870	0.854	0.850	0.856	0.001	0.000	0.001	0.001	1.085	1.068	1.067	0.003	0.000	0.001
Ba	0.000	0.000	0.000	0.000	0.000	0.001	0.000	0.000	0.000	0.006	0.006	0.006	0.006	0.000	0.001	0.000	7.372	7.335	7.345
Na	0.957	0.969	0.962	0.955	0.146	0.146	0.147	0.151	0.142	0.117	0.118	0.114	0.113	0.019	0.019	0.022	0.074	0.068	0.081
K	0.011	0.010	0.009	0.013	0.003	0.003	0.003	0.002	0.002	0.873	0.871	0.872	0.869	0.000	0.000	0.000	0.000	0.000	0.000
Sum	4.993	4.999	4.994	4.992	5.009	5.015	5.008	5.009	5.006	5.004	5.002	5.002	4.997	4.894	4.886	4.889	7.837	7.820	7.834

Standard abbreviations are as follows: AMAB - Amelia albite (Virginia: Na); SWAN - anorthite (Stillwater: An_{84}); SGKF - adularia (St. Goddard Switzerland: K); AUG - Augite (AMAX R&D Laboratory); BRT - Barite (Ba).

Quantitative Electron Microprobe Analyses

Analyses of Alkali Feldspar

Alkali Feldspar 1 (K Phase)

	JH292-Kf1	JH292-Kf2	JH292-Kf3	JH292-Kf4	JH292-Kf5	JH292-Kf6	JH292-Kf7	JH292-Kf8	JH292-Kf9	JH292-Kf10	**Average**	Std Dev
	Chemical Composition (Weight Percent)											
SiO_2	64.96	65.55	65.34	65.24	65.31	64.63	65.27	64.73	64.91	65.08	**65.10**	0.29
$Al2O_3$	18.89	18.94	18.87	18.87	19.02	18.83	18.91	18.95	18.75	18.99	**18.90**	0.08
Fe_2O_3	0.04	0.03	0.03	0.01	0.04	0.12	0.08	0.06	0.10	0.03	**0.05**	0.04
CaO	0.00	0.00	0.00	0.00	0.00	0.00	0.00	0.00	0.00	0.00	**0.00**	0.00
BaO	0.05	0.00	0.03	0.04	0.01	0.08	0.03	0.02	0.00	0.05	**0.03**	0.03
Na_2O	0.25	0.26	0.29	0.20	0.27	0.28	0.27	0.23	0.19	0.17	**0.24**	0.04
K_2O	16.15	16.25	16.16	16.24	16.24	16.26	16.14	16.17	16.35	16.23	**16.22**	0.06
Total	100.34	101.04	100.73	100.60	100.89	100.20	100.70	100.18	100.30	100.54	**100.55**	0.29
	Ions per 8 Oxygen											
Si	2.989	2.994	2.994	2.994	2.988	2.984	2.991	2.984	2.991	2.988	**2.990**	0.004
Al	1.024	1.019	1.019	1.020	1.025	1.024	1.021	1.030	1.018	1.027	**1.023**	0.004
Fe	0.001	0.001	0.001	0.000	0.001	0.004	0.003	0.002	0.004	0.001	**0.002**	0.001
Ca	0.000	0.000	0.000	0.000	0.000	0.000	0.000	0.000	0.000	0.000	**0.000**	0.000
Ba	0.001	0.000	0.001	0.001	0.000	0.002	0.001	0.000	0.000	0.001	**0.001**	0.000
Na	0.022	0.023	0.026	0.017	0.024	0.025	0.024	0.021	0.017	0.015	**0.021**	0.004
K	0.943	0.941	0.939	0.945	0.942	0.952	0.938	0.945	0.955	0.945	**0.945**	0.005
Sum	4.980	4.979	4.979	4.977	4.982	4.990	4.978	4.983	4.985	4.977	**4.981**	0.004
An	0.00	0.00	0.00	0.00	0.00	0.00	0.00	0.00	0.00	0.00	**0.00**	0.00
Ab	2.29	2.41	2.64	1.80	2.49	2.51	2.50	2.16	1.75	1.54	**2.21**	0.38
Or	97.62	97.58	97.31	98.12	97.49	97.34	97.44	97.81	98.25	98.38	**97.73**	0.39
Cel	0.09	0.01	0.05	0.08	0.02	0.15	0.05	0.03	0.00	0.08	**0.06**	0.05

Alkali Feldspar 1 (Na Phase)

	JH292-Ab1	JH292-Ab2	JH292-Ab3	JH292-Ab4	JH292-Ab5	**Average**	Std Dev
	Chemical Composition (Weight Percent)						
SiO_2	68.91	69.25	69.11	68.61	68.92	**68.96**	0.24
$Al2O_3$	20.14	20.32	20.00	20.11	20.08	**20.13**	0.12
Fe_2O_3	0.71	0.22	0.08	0.28	0.10	**0.28**	0.25
CaO	0.02	0.12	0.03	0.03	0.03	**0.04**	0.04
BaO	0.01	0.01	0.00	0.01	0.01	**0.01**	0.01
Na_2O	11.79	11.61	11.88	11.35	11.81	**11.69**	0.21
K_2O	0.11	0.11	0.10	0.71	0.11	**0.23**	0.27
Total	101.68	101.63	101.20	101.10	101.06	**101.33**	0.30
	Ions per 8 Oxygen						
Si	2.969	2.978	2.985	2.975	2.982	**2.978**	0.006
Al	1.022	1.029	1.018	1.027	1.023	**1.024**	0.004
Fe	0.023	0.007	0.003	0.009	0.003	**0.009**	0.008
Ca	0.001	0.005	0.001	0.001	0.001	**0.002**	0.002
Ba	0.000	0.000	0.000	0.000	0.000	**0.000**	0.000
Na	0.979	0.962	0.989	0.948	0.985	**0.973**	0.017
K	0.006	0.006	0.006	0.039	0.006	**0.013**	0.015
Sum	5.001	4.988	5.002	5.000	5.001	**4.998**	0.006
An	0.09	0.54	0.13	0.13	0.12	**0.20**	0.19
Ab	99.28	98.79	99.32	95.92	99.24	**98.51**	1.46
Or	0.62	0.65	0.55	3.92	0.62	**1.27**	1.48
Cel	0.01	0.02	0.00	0.02	0.01	**0.01**	0.01

Quantitative Electron Microprobe Analyses

Analyses of Alkali Feldspar

Alkali Feldspar 2 (K Phase)

	JH292-Kf1	JH292-Kf2	JH292-Kf3	JH292-Kf4	JH292-Kf5	JH292-Kf6	JH292-Kf7	JH292-Kf8	JH292-Kf9	JH292-Kf10	**Average**	Std Dev
	Chemical Composition (Weight Percent)											
SiO_2	64.76	64.89	65.17	64.30	64.70	64.63	64.69	64.87	64.87	65.16	**64.80**	0.25
$Al2O_3$	19.00	18.90	18.76	18.85	18.76	18.78	18.85	18.94	18.93	18.90	**18.87**	0.08
Fe_2O_3	0.04	0.12	0.00	0.05	0.04	0.05	0.01	0.03	0.02	0.01	**0.04**	0.03
CaO	0.00	0.00	0.00	0.00	0.00	0.00	0.00	0.00	0.00	0.00	**0.00**	0.00
BaO	0.00	0.06	0.04	0.05	0.01	0.08	0.04	0.02	0.01	0.02	**0.03**	0.03
Na_2O	0.20	0.21	0.16	0.14	0.17	0.18	0.19	0.27	0.26	0.19	**0.20**	0.04
K_2O	16.16	16.11	16.35	16.36	16.36	16.25	16.38	16.26	16.08	16.36	**16.27**	0.11
Total	100.15	100.30	100.48	99.74	100.04	99.98	100.16	100.38	100.16	100.63	**100.20**	0.26
	Ions per 8 Oxygen											
Si	2.985	2.988	2.996	2.982	2.989	2.988	2.987	2.986	2.988	2.991	**2.988**	0.004
Al	1.032	1.025	1.016	1.030	1.021	1.023	1.025	1.027	1.027	1.022	**1.025**	0.004
Fe	0.001	0.004	0.000	0.002	0.001	0.002	0.001	0.001	0.001	0.000	**0.001**	0.001
Ca	0.000	0.000	0.000	0.000	0.000	0.000	0.000	0.000	0.000	0.000	**0.000**	0.000
Ba	0.000	0.001	0.001	0.001	0.000	0.002	0.001	0.000	0.000	0.000	**0.001**	0.000
Na	0.017	0.019	0.014	0.013	0.015	0.016	0.017	0.024	0.023	0.017	**0.018**	0.004
K	0.944	0.940	0.953	0.962	0.959	0.953	0.958	0.949	0.939	0.952	**0.951**	0.008
Sum	4.980	4.978	4.980	4.989	4.986	4.984	4.988	4.987	4.979	4.982	**4.983**	0.004
An	0.00	0.02	0.00	0.00	0.00	0.00	0.00	0.00	0.00	0.00	**0.00**	0.01
Ab	1.80	1.98	1.49	1.29	1.57	1.68	1.69	2.45	2.42	1.73	**1.81**	0.38
Or	98.20	97.88	98.43	98.62	98.41	98.17	98.23	97.52	97.57	98.23	**98.12**	0.36
Cel	0.00	0.12	0.08	0.09	0.02	0.15	0.08	0.03	0.01	0.04	**0.06**	0.05

Alkali Feldspar 2 (Na Phase)

	JH292-Ab1	JH292-Ab2	JH292-Ab3	JH292-Ab4	JH292-Ab5	JH292-Ab6	**Average**	Std Dev
	Chemical Composition (Weight Percent)							
SiO_2	69.16	69.36	69.37	68.83	69.27	69.16	**69.19**	0.20
$Al2O_3$	20.33	19.91	19.85	19.93	20.17	20.23	**20.07**	0.20
Fe_2O_3	0.05	0.59	0.05	0.38	0.14	0.04	**0.21**	0.23
CaO	0.29	0.03	0.09	0.06	0.02	0.07	**0.09**	0.10
BaO	0.03	0.00	0.00	0.00	0.00	0.00	**0.01**	0.01
Na_2O	11.58	11.50	11.37	11.34	11.52	11.86	**11.53**	0.19
K_2O	0.13	0.07	0.12	0.19	0.08	0.09	**0.11**	0.04
Total	101.55	101.46	100.85	100.74	101.19	101.44	**101.21**	0.34
	Ions per 8 Oxygen							
Si	2.977	2.988	3.000	2.986	2.987	2.980	**2.986**	0.008
Al	1.031	1.010	1.012	1.019	1.025	1.027	**1.021**	0.008
Fe	0.002	0.019	0.002	0.012	0.005	0.001	**0.007**	0.007
Ca	0.013	0.002	0.004	0.003	0.001	0.003	**0.004**	0.005
Ba	0.000	0.000	0.000	0.000	0.000	0.000	**0.000**	0.000
Na	0.961	0.955	0.948	0.948	0.958	0.985	**0.959**	0.014
K	0.007	0.004	0.007	0.010	0.004	0.005	**0.006**	0.002
Sum	4.991	4.977	4.971	4.978	4.979	5.001	**4.983**	0.011
An	1.35	0.16	0.44	0.29	0.08	0.30	**0.44**	0.46
Ab	97.91	99.44	98.86	98.65	99.46	99.20	**98.92**	0.59
Or	0.70	0.41	0.69	1.06	0.46	0.49	**0.63**	0.24
Cel	0.04	0.00	0.01	0.00	0.00	0.00	**0.01**	0.02

Quantitative Electron Microprobe Analyses

Analyses of Alkali Feldspar

Alkali Feldspar 3 (K Phase)

	JH292-Kf1	JH292-Kf2	JH292-Kf3	JH292-Kf4	JH292-Kf5	JH292-Kf6	JH292-Kf7	JH292-Kf8	JH292-Kf9	JH292-Kf10	**Average**	Std Dev
	Chemical Composition (Weight Percent)											
SiO_2	65.21	65.00	65.13	65.38	64.77	65.10	65.31	65.02	64.68	65.03	**65.06**	0.22
$Al2O_3$	19.07	19.01	18.99	18.96	19.00	18.99	18.95	19.09	19.02	18.98	**19.01**	0.04
Fe_2O_3	0.04	0.03	0.00	0.00	0.02	0.06	0.04	0.02	0.04	0.05	**0.03**	0.02
CaO	0.00	0.00	0.00	0.00	0.00	0.01	0.00	0.00	0.00	0.00	**0.00**	0.00
BaO	0.02	0.06	0.02	0.00	0.00	0.00	0.00	0.00	0.01	0.02	**0.01**	0.02
Na_2O	0.19	0.22	0.16	0.21	0.30	0.26	0.19	0.24	0.13	0.19	**0.21**	0.05
K_2O	16.24	16.20	16.31	16.25	16.14	16.11	16.18	16.21	16.22	16.32	**16.22**	0.07
Total	100.78	100.53	100.61	100.81	100.23	100.53	100.67	100.58	100.11	100.59	**100.54**	0.22
	Ions per 8 Oxygen											
Si	2.987	2.986	2.989	2.993	2.984	2.988	2.993	2.984	2.984	2.987	**2.987**	0.003
Al	1.029	1.029	1.027	1.023	1.031	1.027	1.023	1.032	1.034	1.027	**1.028**	0.004
Fe	0.001	0.001	0.000	0.000	0.001	0.002	0.001	0.001	0.002	0.002	**0.001**	0.001
Ca	0.000	0.000	0.000	0.000	0.000	0.000	0.000	0.000	0.000	0.000	**0.000**	0.000
Ba	0.000	0.001	0.000	0.000	0.000	0.000	0.000	0.000	0.000	0.000	**0.000**	0.000
Na	0.017	0.019	0.014	0.019	0.027	0.023	0.017	0.021	0.012	0.017	**0.019**	0.004
K	0.943	0.944	0.949	0.943	0.943	0.937	0.940	0.943	0.948	0.950	**0.944**	0.004
Sum	4.978	4.980	4.979	4.977	4.985	4.978	4.974	4.982	4.979	4.983	**4.979**	0.003
An	0.00	0.00	0.00	0.00	0.00	0.03	0.00	0.00	0.00	0.00	**0.00**	0.01
Ab	1.79	1.99	1.47	1.92	2.73	2.43	1.79	2.22	1.23	1.74	**1.93**	0.44
Or	98.17	97.89	98.49	98.08	97.27	97.53	98.21	97.78	98.75	98.22	**98.04**	0.44
Cel	0.04	0.11	0.03	0.00	0.00	0.00	0.00	0.00	0.02	0.04	**0.02**	0.04

Alkali Feldspar 3 (Na Phase)

	JH292-Ab1	JH292-Ab2	JH292-Ab3	JH292-Ab4	JH292-Ab5	JH292-Ab6	JH292-Ab7	**Average**	Std Dev
	Chemical Composition (Weight Percent)								
SiO_2	69.43	68.42	68.89	68.43	69.10	68.70	68.99	**68.85**	0.37
$Al2O_3$	20.26	19.77	20.16	20.09	20.18	20.05	20.31	**20.12**	0.18
Fe_2O_3	0.22	0.12	0.27	1.01	0.08	0.05	0.06	**0.26**	0.34
CaO	0.15	0.02	0.03	0.04	0.04	0.04	0.09	**0.06**	0.05
BaO	0.03	0.01	0.03	0.00	0.02	0.02	0.00	**0.01**	0.01
Na_2O	11.74	11.65	11.73	11.80	11.66	11.70	11.44	**11.68**	0.12
K_2O	0.11	0.14	0.31	0.06	0.10	0.10	0.06	**0.13**	0.09
Total	101.94	100.13	101.43	101.43	101.18	100.65	100.94	**101.10**	0.59
	Ions per 8 Oxygen								
Si	2.979	2.987	2.975	2.960	2.983	2.983	2.982	**2.978**	0.009
Al	1.024	1.017	1.026	1.024	1.027	1.025	1.034	**1.025**	0.005
Fe	0.007	0.004	0.009	0.033	0.003	0.002	0.002	**0.008**	0.011
Ca	0.007	0.001	0.001	0.002	0.002	0.002	0.004	**0.003**	0.002
Ba	0.000	0.000	0.001	0.000	0.000	0.000	0.000	**0.000**	0.000
Na	0.971	0.981	0.976	0.984	0.970	0.979	0.953	**0.974**	0.010
K	0.006	0.008	0.017	0.003	0.006	0.005	0.004	**0.007**	0.005
Sum	4.995	4.997	5.005	5.006	4.990	4.996	4.979	**4.995**	0.009
An	0.71	0.08	0.14	0.17	0.20	0.18	0.44	**0.28**	0.23
Ab	98.63	99.13	98.09	99.49	99.19	99.24	99.20	**99.00**	0.51
Or	0.62	0.78	1.72	0.33	0.56	0.55	0.36	**0.70**	0.49
Cel	0.04	0.01	0.05	0.00	0.04	0.03	0.00	**0.02**	0.02

Quantitative Electron Microprobe Analyses

Analyses of Alkali Feldspar

Alkali Feldspar 4 (K Phase)

	JH292-Kf1	JH292-Kf2	JH292-Kf3	JH292-Kf4	JH292-Kf5	JH292-Kf6	JH292-Kf7	JH292-Kf8	JH292-Kf9	JH292-Kf10	**Average**	Std Dev
	Chemical Composition (Weight Percent)											
SiO_2	64.85	64.61	65.01	64.58	65.29	64.75	65.10	64.65	64.66	64.82	**64.83**	0.24
$Al2O_3$	18.97	18.95	18.94	19.01	19.06	18.61	18.95	18.93	18.84	19.01	**18.93**	0.13
Fe_2O_3	0.04	0.04	0.03	0.04	0.04	0.02	0.04	0.02	0.00	0.02	**0.03**	0.01
CaO	0.01	0.00	0.00	0.00	0.00	0.00	0.00	0.00	0.00	0.00	**0.00**	0.00
BaO	0.01	0.06	0.03	0.02	0.05	0.05	0.00	0.06	0.04	0.03	**0.03**	0.02
Na_2O	0.27	0.21	0.29	0.27	0.29	0.28	0.17	0.21	0.27	0.24	**0.25**	0.04
K_2O	16.20	16.34	16.14	16.16	16.23	16.15	16.33	16.21	16.23	16.13	**16.21**	0.07
Total	100.34	100.21	100.44	100.07	100.96	99.87	100.59	100.08	100.04	100.25	**100.29**	0.32
	Ions per 8 Oxygen											
Si	2.985	2.982	2.988	2.981	2.987	2.995	2.989	2.985	2.987	2.985	**2.986**	0.004
Al	1.029	1.031	1.026	1.034	1.027	1.014	1.025	1.030	1.025	1.031	**1.027**	0.005
Fe	0.001	0.001	0.001	0.002	0.001	0.001	0.001	0.001	0.000	0.001	**0.001**	0.000
Ca	0.001	0.000	0.000	0.000	0.000	0.000	0.000	0.000	0.000	0.000	**0.000**	0.000
Ba	0.000	0.001	0.001	0.000	0.001	0.001	0.000	0.001	0.001	0.001	**0.001**	0.000
Na	0.024	0.019	0.025	0.024	0.026	0.025	0.015	0.019	0.024	0.022	**0.022**	0.004
K	0.945	0.956	0.940	0.946	0.941	0.947	0.951	0.949	0.951	0.942	**0.947**	0.005
Sum	4.985	4.990	4.981	4.986	4.983	4.983	4.981	4.984	4.988	4.981	**4.984**	0.003
An	0.05	0.00	0.00	0.00	0.00	0.00	0.01	0.00	0.02	0.00	**0.01**	0.02
Ab	2.45	1.93	2.63	2.43	2.67	2.56	1.55	1.97	2.43	2.24	**2.29**	0.38
Or	97.47	97.97	97.32	97.53	97.25	97.36	98.44	97.93	97.47	97.71	**97.64**	0.39
Cel	0.02	0.10	0.05	0.03	0.08	0.08	0.00	0.10	0.08	0.05	**0.06**	0.04

Alkali Feldspar 4 (Na Phase)

	JH292-Ab1	JH292-Ab2	JH292-Ab3	JH292-Ab4	JH292-Ab5	JH292-Ab6	JH292-Ab7	JH292-Ab8	JH292-Ab9	**Average**	Std Dev
	Chemical Composition (Weight Percent)										
SiO_2	69.39	68.99	68.72	68.71	68.81	69.03	68.79	69.15	69.39	**69.00**	0.27
$Al2O_3$	20.30	20.17	20.14	20.18	20.01	20.09	20.24	20.11	20.14	**20.15**	0.08
Fe_2O_3	0.50	0.05	0.06	0.07	0.05	0.26	0.11	0.19	0.71	**0.22**	0.23
CaO	0.07	0.09	0.08	0.08	0.05	0.03	0.00	0.01	0.09	**0.06**	0.03
BaO	0.00	0.00	0.02	0.02	0.00	0.03	0.00	0.00	0.01	**0.01**	0.01
Na_2O	11.46	11.71	11.81	11.34	11.79	11.69	11.70	11.20	11.48	**11.57**	0.21
K_2O	0.56	0.11	0.09	1.16	0.08	0.06	0.12	0.12	0.09	**0.26**	0.37
Total	102.28	101.12	100.92	101.56	100.79	101.19	100.95	100.78	101.91	**101.28**	0.53
	Ions per 8 Oxygen										
Si	2.973	2.981	2.978	2.973	2.984	2.982	2.978	2.991	2.978	**2.980**	0.006
Al	1.025	1.027	1.028	1.029	1.022	1.022	1.032	1.025	1.019	**1.025**	0.004
Fe	0.016	0.002	0.002	0.002	0.002	0.008	0.004	0.006	0.023	**0.007**	0.007
Ca	0.003	0.004	0.004	0.004	0.002	0.002	0.000	0.001	0.004	**0.003**	0.002
Ba	0.000	0.000	0.000	0.000	0.000	0.001	0.000	0.000	0.000	**0.000**	0.000
Na	0.947	0.975	0.986	0.946	0.985	0.973	0.976	0.934	0.950	**0.964**	0.019
K	0.030	0.006	0.005	0.064	0.005	0.003	0.006	0.007	0.005	**0.014**	0.020
Sum	4.995	4.995	5.003	5.017	4.999	4.991	4.996	4.963	4.979	**4.993**	0.015
An	0.34	0.43	0.38	0.36	0.24	0.16	0.02	0.05	0.42	**0.27**	0.15
Ab	96.57	98.98	99.08	93.34	99.30	99.47	99.34	99.23	99.06	**98.26**	2.05
Or	3.09	0.59	0.51	6.27	0.45	0.32	0.64	0.71	0.51	**1.45**	2.00
Cel	0.00	0.00	0.03	0.04	0.00	0.05	0.00	0.00	0.01	**0.01**	0.02

Quantitative Electron Microprobe Analyses

Analyses of Alkali Feldspar

Alkali Feldspar 5 (K Phase)

	JH292-Kf1	JH292-Kf2	JH292-Kf3	JH292-Kf4	JH292-Kf5	JH292-Kf6	JH292-Kf7	JH292-Kf8	JH292-Kf9	JH292-Kf10	**Average**	Std Dev
	Chemical Composition (Weight Percent)											
SiO_2	65.09	65.05	64.68	64.26	64.59	64.71	64.65	64.68	63.88	64.73	**64.63**	0.35
$Al2O_3$	19.01	18.72	19.02	18.85	18.82	18.74	18.89	18.76	18.67	18.78	**18.83**	0.12
Fe_2O_3	0.06	0.07	0.04	0.02	0.04	0.02	0.04	0.05	0.08	0.02	**0.05**	0.02
CaO	0.02	0.00	0.00	0.00	0.00	0.00	0.00	0.00	0.00	0.01	**0.00**	0.01
BaO	0.00	0.03	0.03	0.00	0.04	0.02	0.06	0.06	0.02	0.01	**0.03**	0.02
Na_2O	0.25	0.20	0.17	0.26	0.22	0.25	0.24	0.17	0.23	0.31	**0.23**	0.04
K_2O	16.26	16.21	16.27	16.15	16.34	16.16	16.25	16.32	16.13	16.19	**16.23**	0.07
Total	100.69	100.28	100.21	99.54	100.05	99.91	100.13	100.05	99.01	100.05	**99.99**	0.45
	Ions per 8 Oxygen											
Si	2.986	2.995	2.982	2.983	2.986	2.991	2.985	2.989	2.983	2.989	**2.987**	0.004
Al	1.027	1.015	1.033	1.031	1.025	1.021	1.028	1.021	1.027	1.022	**1.025**	0.005
Fe	0.002	0.003	0.001	0.001	0.001	0.001	0.001	0.002	0.003	0.001	**0.002**	0.001
Ca	0.001	0.000	0.000	0.000	0.000	0.000	0.000	0.000	0.000	0.001	**0.000**	0.000
Ba	0.000	0.001	0.001	0.000	0.001	0.000	0.001	0.001	0.000	0.000	**0.000**	0.000
Na	0.022	0.018	0.015	0.024	0.020	0.022	0.022	0.015	0.021	0.027	**0.020**	0.004
K	0.946	0.947	0.951	0.951	0.958	0.947	0.951	0.956	0.955	0.948	**0.951**	0.004
Sum	4.983	4.978	4.984	4.988	4.990	4.983	4.987	4.985	4.989	4.987	**4.985**	0.004
An	0.09	0.00	0.00	0.01	0.00	0.00	0.00	0.00	0.00	0.06	**0.02**	0.03
Ab	2.24	1.82	1.55	2.41	2.01	2.30	2.21	1.54	2.10	2.79	**2.10**	0.39
Or	97.67	98.12	98.40	97.58	97.92	97.67	97.69	98.34	97.86	97.14	**97.84**	0.38
Cel	0.00	0.05	0.05	0.00	0.06	0.03	0.10	0.11	0.04	0.01	**0.05**	0.04

Alkali Feldspar 5 (Na Phase)

	JH292-Ab1	JH292-Ab2	JH292-Ab3	JH292-Ab4	JH292-Ab5	JH292-Ab6	JH292-Ab7	**Average**	Std Dev
	Chemical Composition (Weight Percent)								
SiO_2	68.61	68.45	68.57	68.55	67.79	68.50		**68.41**	0.31
$Al2O_3$	20.13	19.98	20.06	19.95	19.84	20.08		**20.01**	0.10
Fe_2O_3	0.20	0.07	0.29	0.32	0.13	0.43		**0.24**	0.13
CaO	0.06	0.10	0.05	0.04	0.02	0.04		**0.05**	0.03
BaO	0.01	0.00	0.00	0.00	0.00	0.00		**0.00**	0.01
Na_2O	11.73	11.48	11.49	11.48	11.43	11.72		**11.56**	0.13
K_2O	0.15	0.32	0.16	0.15	1.27	0.09		**0.36**	0.46
Total	100.90	100.40	100.62	100.51	100.49	100.86		**100.63**	0.21
	Ions per 8 Oxygen								
Si	2.975	2.982	2.979	2.982	2.969	2.973		**2.977**	0.005
Al	1.029	1.025	1.027	1.023	1.024	1.027		**1.026**	0.002
Fe	0.007	0.002	0.010	0.011	0.004	0.014		**0.008**	0.004
Ca	0.003	0.005	0.002	0.002	0.001	0.002		**0.002**	0.001
Ba	0.000	0.000	0.000	0.000	0.000	0.000		**0.000**	0.000
Na	0.980	0.964	0.962	0.963	0.965	0.980		**0.969**	0.009
K	0.008	0.018	0.009	0.009	0.071	0.005		**0.020**	0.025
Sum	5.002	4.995	4.989	4.988	5.034	5.000		**5.001**	0.017
An	0.28	0.46	0.23	0.18	0.08	0.19		**0.24**	0.13
Ab	98.88	97.76	98.87	98.94	93.09	99.32		**97.81**	2.37
Or	0.82	1.78	0.90	0.87	6.83	0.48		**1.95**	2.43
Cel	0.02	0.00	0.00	0.00	0.00	0.01		**0.01**	0.01

Quantitative Electron Microprobe Analyses

Analyses of Alkali Feldspar

Alkali Feldspar 6 (K Phase)

	JH292-Kf1	JH292-Kf2	JH292-Kf3	JH292-Kf4	JH292-Kf5	JH292-Kf6	JH292-Kf7	JH292-Kf8	JH292-Kf9	JH292-Kf10	JH292-Kf11	**Average**	Std Dev
	Chemical Composition (Weight Percent)												
SiO_2	64.75	64.78	64.40	64.19	64.92	64.53	64.78	64.87	64.99	64.76	64.86	**64.71**	0.24
Al2O_3	18.50	18.83	18.68	18.86	18.98	18.78	18.90	19.05	18.85	18.96	18.91	**18.84**	0.15
Fe_2O_3	0.01	0.02	0.03	0.03	0.03	0.04	0.03	0.02	0.00	0.01	0.03	**0.02**	0.01
CaO	0.00	0.00	0.00	0.00	0.00	0.00	0.00	0.00	0.00	0.00	0.00	**0.00**	0.00
BaO	0.05	0.00	0.04	0.01	0.00	0.02	0.01	0.03	0.02	0.05	0.00	**0.02**	0.02
Na_2O	0.18	0.19	0.19	0.16	0.17	0.19	0.16	0.29	0.19	0.18	0.17	**0.19**	0.04
K_2O	16.39	16.44	16.23	16.30	16.32	16.21	16.23	16.11	16.22	16.27	16.21	**16.27**	0.09
Total	99.88	100.26	99.56	99.55	100.42	99.77	100.11	100.38	100.28	100.22	100.18	**100.06**	0.31
	Ions per 8 Oxygen												
Si	2.998	2.988	2.990	2.982	2.986	2.988	2.988	2.984	2.992	2.985	2.989	**2.988**	0.004
Al	1.009	1.023	1.022	1.032	1.029	1.025	1.027	1.032	1.023	1.030	1.027	**1.025**	0.006
Fe	0.000	0.001	0.001	0.001	0.001	0.001	0.001	0.001	0.000	0.000	0.001	**0.001**	0.000
Ca	0.000	0.000	0.000	0.000	0.000	0.000	0.000	0.000	0.000	0.000	0.000	**0.000**	0.000
Ba	0.001	0.000	0.001	0.000	0.000	0.000	0.000	0.001	0.000	0.001	0.000	**0.000**	0.000
Na	0.016	0.017	0.017	0.015	0.015	0.017	0.015	0.026	0.017	0.016	0.015	**0.017**	0.003
K	0.962	0.962	0.955	0.960	0.952	0.952	0.949	0.940	0.947	0.951	0.947	**0.952**	0.007
Sum	4.987	4.990	4.985	4.989	4.983	4.984	4.980	4.983	4.979	4.983	4.978	**4.984**	0.004
An	0.00	0.00	0.00	0.00	0.00	0.00	0.00	0.00	0.00	0.00	0.00	**0.00**	0.00
Ab	1.65	1.77	1.76	1.49	1.58	1.78	1.50	2.70	1.78	1.67	1.57	**1.75**	0.33
Or	98.26	98.23	98.18	98.49	98.42	98.18	98.49	97.25	98.18	98.23	98.42	**98.21**	0.34
Cel	0.08	0.00	0.06	0.02	0.00	0.03	0.01	0.05	0.03	0.09	0.01	**0.04**	0.03

Alkali Feldspar 6 (Na Phase)

	JH292-Ab1	JH292-Ab2	JH292-Ab3	JH292-Ab4	JH292-Ab5	JH292-Ab6	JH292-Ab7	JH292-Ab8	JH292-Ab9	JH292-Ab10	JH292-Ab11	JH292-Ab12	JH292-Ab13	**Average**	Std Dev
	Chemical Composition (Weight Percent)														
SiO_2	68.28	68.87	67.91	69.40	68.63	67.85	68.16	68.58	68.68	68.70	68.88	68.24	68.66	**68.53**	0.43
Al2O_3	19.70	20.21	20.09	20.09	19.50	20.12	20.05	20.06	20.06	19.96	20.26	19.85	20.07	**20.00**	0.21
Fe_2O_3	0.18	0.05	0.07	0.05	0.16	0.17	0.78	0.07	0.04	0.03	0.04	0.97	0.26	**0.22**	0.30
CaO	0.13	0.07	0.03	0.04	0.00	0.10	0.06	0.07	0.03	0.06	0.13	0.02	0.10	**0.06**	0.04
BaO	0.00	0.00	0.00	0.00	0.00	0.04	0.00	0.00	0.02	0.00	0.00	0.00	0.00	**0.01**	0.01
Na_2O	11.64	11.65	11.67	11.76	11.63	11.66	11.86	11.79	11.84	11.66	11.71	11.34	11.78	**11.69**	0.13
K_2O	0.09	0.07	0.12	0.09	0.09	0.06	0.08	0.09	0.09	0.10	0.08	0.05	0.03	**0.08**	0.02
Total	100.02	100.91	99.90	101.42	100.02	99.99	100.99	100.67	100.77	100.51	101.10	100.46	100.90	**100.59**	0.49
	Ions per 8 Oxygen														
Si	2.985	2.981	2.973	2.988	2.997	2.969	2.961	2.979	2.980	2.986	2.977	2.973	2.976	**2.979**	0.009
Al	1.015	1.031	1.036	1.019	1.004	1.037	1.026	1.027	1.026	1.022	1.032	1.019	1.025	**1.024**	0.009
Fe	0.006	0.002	0.002	0.002	0.005	0.006	0.025	0.002	0.001	0.001	0.001	0.032	0.008	**0.007**	0.010
Ca	0.006	0.003	0.002	0.002	0.000	0.004	0.003	0.003	0.001	0.003	0.006	0.001	0.004	**0.003**	0.002
Ba	0.000	0.000	0.000	0.000	0.000	0.001	0.000	0.000	0.000	0.000	0.000	0.000	0.000	**0.000**	0.000
Na	0.981	0.972	0.985	0.976	0.979	0.983	0.993	0.987	0.990	0.977	0.976	0.952	0.985	**0.980**	0.010
K	0.005	0.004	0.007	0.005	0.005	0.003	0.004	0.005	0.005	0.006	0.004	0.003	0.002	**0.004**	0.001
Sum	4.998	4.991	5.004	4.992	4.991	5.003	5.012	5.003	5.004	4.994	4.997	4.979	5.000	**4.998**	0.008
An	0.59	0.32	0.16	0.20	0.01	0.44	0.26	0.34	0.12	0.30	0.61	0.10	0.44	**0.30**	0.18
Ab	98.89	99.29	99.15	99.31	99.47	99.14	99.31	99.16	99.34	99.12	98.96	99.63	99.38	**99.24**	0.20
Or	0.51	0.39	0.68	0.49	0.51	0.34	0.43	0.50	0.50	0.58	0.44	0.26	0.17	**0.45**	0.13
Cel	0.00	0.00	0.00	0.00	0.01	0.07	0.00	0.00	0.04	0.00	0.00	0.00	0.00	**0.01**	0.02

Quantitative Electron Microprobe Analyses

Analyses of Alkali Feldspar

Alkali Feldspar 7 (K Phase)

	JH292-Kf1	JH292-Kf2	JH292-Kf3	JH292-Kf4	JH292-Kf5	JH292-Kf6	JH292-Kf7	JH292-Kf8	JH292-Kf9	JH292-Kf10	**Average**	Std Dev
	Chemical Composition (Weight Percent)											
SiO_2	64.74	64.86	64.61	64.63	64.84	64.84	64.82	64.82	64.84	64.72	**64.77**	0.09
$Al2O_3$	19.04	18.94	18.87	19.00	18.88	18.92	18.75	18.79	19.07	18.86	**18.91**	0.10
Fe_2O_3	0.08	0.02	0.01	0.01	0.02	0.05	0.03	0.03	0.02	0.02	**0.03**	0.02
CaO	0.00	0.00	0.00	0.00	0.00	0.00	0.00	0.00	0.00	0.00	**0.00**	0.00
BaO	0.00	0.05	0.04	0.06	0.06	0.05	0.03	0.02	0.02	0.04	**0.04**	0.02
Na_2O	0.62	0.17	0.16	0.17	0.17	0.23	0.26	0.17	0.26	0.26	**0.25**	0.14
K_2O	14.73	16.16	16.20	16.36	16.23	16.18	16.02	16.24	16.18	16.28	**16.06**	0.48
Total	99.20	100.20	99.89	100.22	100.19	100.26	99.91	100.07	100.40	100.18	**100.05**	0.34
	Ions per 8 Oxygen											
Si	2.991	2.988	2.988	2.982	2.989	2.987	2.994	2.992	2.982	2.986	**2.988**	0.004
Al	1.036	1.028	1.028	1.033	1.025	1.027	1.020	1.022	1.034	1.025	**1.028**	0.005
Fe	0.003	0.001	0.000	0.000	0.001	0.002	0.001	0.001	0.001	0.001	**0.001**	0.001
Ca	0.000	0.000	0.000	0.000	0.000	0.000	0.000	0.000	0.000	0.000	**0.000**	0.000
Ba	0.000	0.001	0.001	0.001	0.001	0.001	0.001	0.000	0.000	0.001	**0.001**	0.000
Na	0.055	0.016	0.015	0.015	0.015	0.020	0.023	0.016	0.023	0.023	**0.022**	0.012
K	0.863	0.944	0.950	0.957	0.949	0.945	0.938	0.950	0.944	0.952	**0.939**	0.027
Sum	4.948	4.977	4.980	4.988	4.980	4.982	4.976	4.980	4.984	4.988	**4.978**	0.011
An	0.00	0.00	0.00	0.00	0.00	0.00	0.00	0.00	0.00	0.00	**0.00**	0.00
Ab	5.99	1.61	1.51	1.54	1.56	2.11	2.40	1.60	2.42	2.33	**2.31**	1.35
Or	94.01	98.29	98.41	98.35	98.34	97.80	97.54	98.35	97.55	97.59	**97.62**	1.32
Cel	0.00	0.09	0.07	0.11	0.10	0.09	0.05	0.04	0.03	0.08	**0.07**	0.04

Alkali Feldspar 7 (Na Phase)

	JH292-Ab1	*JH292-Ab2*	*JH292-Ab3*	*JH292-Ab4*	JH292-Ab5	JH292-Ab6	JH292-Ab7	JH292-Ab8	**Average**	Std Dev
	Chemical Composition (Weight Percent)									
SiO_2	68.31	*100.33*	*100.72*	*101.15*	68.22	69.14	68.28	68.45	**68.48**	0.38
$Al2O_3$	20.06	*-0.04*	*-0.03*	*-0.03*	20.14	20.14	19.83	20.06	**20.04**	0.13
Fe_2O_3	0.91	*0.03*	*0.02*	*0.04*	0.05	0.11	0.03	0.14	**0.25**	0.37
CaO	0.04	*0.00*	*0.02*	*0.00*	0.03	0.04	0.02	0.06	**0.04**	0.01
BaO	0.00	*0.02*	*0.00*	*0.03*	0.00	0.03	0.03	0.00	**0.01**	0.02
Na_2O	11.43	*0.00*	*0.02*	*0.00*	11.67	11.74	11.70	11.73	**11.65**	0.13
K_2O	0.09	*0.01*	*0.03*	*0.02*	0.51	0.06	0.09	0.12	**0.17**	0.19
Total	100.84	*100.36*	*100.77*	*101.20*	100.63	101.25	99.98	100.56	**100.65**	0.46
	Ions per 8 Oxygen									
Si	2.967	*3.997*	*3.996*	*3.996*	2.971	2.984	2.985	2.977	**2.98**	0.01
Al	1.026	*0.003*	*0.004*	*0.004*	1.033	1.024	1.021	1.028	**1.03**	0.00
Fe	0.030	*0.001*	*0.001*	*0.001*	0.002	0.003	0.001	0.004	**0.01**	0.01
Ca	0.002	*0.000*	*0.001*	*0.000*	0.002	0.002	0.001	0.003	**0.00**	0.00
Ba	0.000	*0.000*	*0.000*	*0.000*	0.000	0.001	0.001	0.000	**0.00**	0.00
Na	0.957	*0.000*	*0.001*	*0.000*	0.979	0.976	0.986	0.984	**0.98**	0.01
K	0.005	*0.001*	*0.001*	*0.001*	0.028	0.003	0.005	0.007	**0.01**	0.01
Sum	4.986	*4.002*	*4.004*	*4.002*	5.015	4.993	5.000	5.002	**5.00**	0.01
An	0.22	*0.00*	*20.59*	*0.00*	0.16	0.19	0.10	0.27	**0.19**	0.06
Ab	99.27	*0.00*	*41.18*	*20.00*	97.04	99.43	99.34	99.05	**98.83**	1.01
Or	0.51	*70.00*	*38.24*	*53.33*	2.80	0.32	0.51	0.67	**0.96**	1.04
Cel	0.00	*30.00*	*0.00*	*26.67*	0.00	0.06	0.05	0.00	**0.02**	0.03

Bad analyses have been omitted from the averages.

Quantitative Electron Microprobe Analyses
Alkali Feldspar Averages

	Run 1 (5 Feldspars)				Run 2 (7 Feldspars)			
	K Phase		Na Phase		K Phase		Na Phase	
	Avg	Std Dev	Avg	Std Dev	Avg	Std Dev	Avg	Std Dev
	Chemical Composition (Weight Percent)							
SiO_2	64.28	0.13	68.27	0.10	64.84	0.17	68.77	0.30
Al2O_3	18.20	0.06	19.35	0.09	18.90	0.06	20.07	0.06
Fe_2O_3	0.03	0.01	0.14	0.05	0.03	0.01	0.24	0.02
CaO	0.00	0.00	0.07	0.02	0.00	0.00	0.06	0.02
SrO	0.02	0.01	0.01	0.00				
BaO	0.03	0.01	0.01	0.01	0.03	0.01	0.01	0.00
Na_2O	0.26	0.04	11.66	0.03	0.22	0.02	11.62	0.07
K_2O	16.48	0.03	0.10	0.02	16.21	0.07	0.19	0.10
P_2O_5	0.01	0.00	0.01	0.01				
Total	99.32	0.21	99.62	0.19	100.24	0.23	100.97	0.33
	Ions per 8 Oxygen							
Si	3.00	0.00	2.99	0.00	2.99	0.00	2.98	0.00
Al	1.00	0.00	1.00	0.00	1.03	0.00	1.02	0.00
Fe	0.00	0.00	0.00	0.00	0.00	0.00	0.01	0.00
Ca	0.00	0.00	0.00	0.00	0.00	0.00	0.00	0.00
Sr	0.00	0.00	0.00	0.00				
Ba	0.00	0.00	0.00	0.00	0.00	0.00	0.00	0.00
Na	0.02	0.00	0.99	0.00	0.02	0.00	0.97	0.01
K	0.98	0.00	0.01	0.00	0.95	0.00	0.01	0.01
P	0.00	0.00	0.00	0.00				
Sum	5.00	0.00	5.00	0.00	4.98	0.00	5.00	0.01
An	0.01	0.01	0.32	0.08	0.00	0.01	0.27	0.08
Ab	2.32	0.31	99.08	0.16	2.06	0.23	98.65	0.49
Or	97.54	0.31	0.56	0.10	97.89	0.24	1.06	0.53
Cel	0.06	0.01	0.02	0.01	0.05	0.02	0.01	0.01
Slaw	0.06	0.02	0.03	0.01				

Quantitative Electron Microprobe Analyses

Pre-run Standards for Analysis of the Dike Matrix

	PHLSY-test	AMAB-1	AMAB-2	AMAB-3	SWAN-1	SWAN-2	SWAN-3	SGKF-1	SGKF-2	SGKF-3	AUGI-1	AUGI-2
	Chemical Composition (Weight Percent)											
SiO_2	41.83	68.30	67.91	67.71	45.86	45.67	46.32	64.27	63.34	63.51	46.80	46.51
TiO_2	0.00	0.00	0.01	0.00	0.00	0.00	0.00	0.00	0.00	0.01	0.29	0.34
$Al2O_3$	12.40	19.48	19.44	19.45	33.77	33.86	34.12	18.35	18.24	18.34	0.61	0.61
Fe_2O_3	0.01	0.00	0.00	0.02	0.42	0.39	0.38	0.02	0.00	0.00	33.60	33.52
MnO	0.00	0.00	0.00	0.00	0.00	0.01	0.00	0.00	0.00	0.00	0.68	0.74
MgO	28.52	0.00	0.02	0.01	0.05	0.06	0.04	0.00	0.00	0.00	1.19	1.26
CaO	0.01	0.25	0.27	0.26	17.48	17.54	17.42	0.02	0.00	0.02	19.47	19.56
SrO	0.00	0.00	0.03	0.01	0.00	0.00	0.00	0.00	0.11	0.15	0.00	0.00
BaO	0.02	0.00	0.01	0.02	0.00	0.01	0.00	0.37	0.35	0.33	0.00	0.00
Na_2O	0.00	11.37	11.45	11.49	1.68	1.67	1.61	1.26	1.27	1.24	0.17	0.15
K_2O	11.22	0.22	0.21	0.19	0.04	0.03	0.05	14.78	14.82	14.84	0.00	0.00
P_2O_5	0.05	0.06	0.01	0.01	0.00	0.03	0.03	0.01	0.00	0.00	0.00	0.04
F	8.85	0.11	0.00	0.04	0.00	0.15	0.00	0.11	0.13	0.00	0.00	0.00
Cl	0.02	0.01	0.02	0.00	0.02	0.02	0.00	0.01	0.00	0.00	0.00	0.00
O=F	-3.72	-0.05	0.00	-0.02	0.00	-0.06	0.00	-0.04	-0.05	0.00	0.00	0.00
O=Cl	0.00	0.00	0.00	0.00	0.00	0.00	0.00	0.00	0.00	0.00	0.00	0.00
Total	99.19	99.75	99.37	99.20	99.31	99.37	99.99	99.16	98.23	98.45	102.82	102.74
	Ions per 8 Oxygen (sum excludes F & Cl)											
Si	2.367	2.995	2.989	2.987	2.129	2.125	2.132	2.995	2.987	2.982	2.394	2.383
Ti	0.000	0.000	0.000	0.000	0.000	0.000	0.000	0.000	0.000	0.001	0.011	0.013
Al	0.827	1.007	1.008	1.011	1.848	1.856	1.851	1.008	1.014	1.015	0.037	0.037
Fe	0.000	0.000	0.000	0.001	0.015	0.014	0.013	0.001	0.000	0.000	1.293	1.292
Mn	0.000	0.000	0.000	0.000	0.000	0.000	0.000	0.000	0.000	0.000	0.030	0.032
Mg	2.406	0.000	0.001	0.000	0.004	0.004	0.003	0.000	0.000	0.000	0.091	0.096
Ca	0.001	0.012	0.013	0.012	0.869	0.874	0.859	0.001	0.000	0.001	1.067	1.074
Sr	0.000	0.000	0.001	0.000	0.000	0.000	0.000	0.000	0.003	0.004	0.000	0.000
Ba	0.000	0.000	0.000	0.000	0.000	0.000	0.000	0.007	0.007	0.006	0.000	0.000
Na	0.000	0.967	0.977	0.983	0.151	0.151	0.144	0.114	0.116	0.113	0.017	0.015
K	0.810	0.013	0.012	0.011	0.002	0.002	0.003	0.879	0.892	0.889	0.000	0.000
P	0.002	0.002	0.001	0.000	0.000	0.001	0.001	0.000	0.000	0.000	0.000	0.002
F	1.583	0.015	0.000	0.006	0.000	0.022	0.000	0.016	0.019	0.000	0.000	0.000
Cl	0.002	0.001	0.001	0.000	0.001	0.002	0.000	0.001	0.000	0.000	0.000	0.000
Sum	6.413	4.995	5.001	5.006	5.018	5.027	5.007	5.005	5.019	5.011	4.939	4.944

Standard abbreviations are as follows: PHLSY - phlogopite (synthetic: Mg and Fe); AMAB - Amelia albite (Virginia: Na); SWAN - anorthite (Stillwater: An84); SGKF - adularia (St. Goddard Switzerland: K); AUG - Augite (AMAX R&D Laboratory).

Quantitative Electron Microprobe Analyses

Rhyolite Dike Matrix: Circle One (Analyzed using a 30 µm wide bean and taking 100 points on a 10 x 10 grid)

	C1-Mat1-1	C1-Mat1-2	C1-Mat1-3	C1-Mat1-4	C1-Mat1-5	C1-Mat1-6	C1-Mat1-7	C1-Mat1-8	C1-Mat1-9	C1-Mat1-10	C1-Mat1-11	C1-Mat1-12	C1-Mat1-13	C1-Mat1-14	C1-Mat1-15
							Chemical Composition (Weight Percent)								
SiO_2	84.99	77.36	71.15	74.78	71.86	81.66	94.02	78.52	70.13	83.82	71.19	71.92	76.79	97.64	61.13
TiO_2	0.01	0.00	0.00	0.00	0.00	0.00	0.00	0.03	0.04	0.00	0.04	0.00	0.00	0.00	0.05
$Al2O_3$	8.07	12.27	17.32	14.50	15.40	9.35	3.31	12.63	16.92	9.02	14.51	15.63	12.70	1.10	19.30
Fe_2O_3	0.30	0.61	0.66	0.33	0.46	0.56	0.17	0.31	0.57	0.34	3.23	0.32	0.23	0.29	7.36
MnO	0.00	0.02	0.00	0.00	0.00	0.00	0.00	0.02	0.01	0.00	0.01	0.01	0.00	0.00	0.01
MgO	0.00	0.03	0.02	0.00	0.01	0.00	0.01	0.01	0.01	0.00	0.01	0.01	0.01	0.01	0.01
CaO	0.02	0.02	0.05	0.04	0.04	0.03	0.01	0.05	0.06	0.02	0.03	0.04	0.03	0.02	0.10
SrO	0.00	0.00	0.05	0.00	0.00	0.06	0.03	0.02	0.01	0.05	0.00	0.08	0.00	0.08	0.00
BaO	0.04	0.01	0.00	0.02	0.00	0.04	0.00	0.00	0.00	0.01	0.00	0.00	0.01	0.02	0.03
Na_2O	1.69	2.89	5.87	6.82	3.77	0.83	1.70	7.37	6.94	4.27	4.75	5.04	3.18	0.14	5.69
K_2O	4.88	6.75	4.82	3.47	8.36	7.46	0.72	0.94	5.28	2.28	5.99	6.88	7.05	0.69	6.16
P_2O_5	0.00	0.00	0.03	0.01	0.01	0.01	0.03	0.07	0.00	0.01	0.05	0.00	0.00	0.00	0.03
F	0.00	0.00	0.00	0.03	0.07	0.00	0.00	0.03	0.02	0.16	0.18	0.04	0.00	0.00	0.12
Cl	0.00	0.04	0.03	0.00	0.01	0.01	0.01	0.01	0.00	0.00	0.01	0.02	0.00	0.00	0.01
O=F	0.00	0.00	0.00	-0.01	-0.03	0.00	0.00	-0.01	-0.01	-0.07	-0.08	-0.02	0.00	0.00	-0.05
O=Cl	0.00	0.01	0.01	0.00	0.00	0.00	0.00	0.00	0.00	0.00	0.00	0.00	0.00	0.00	0.00
Total	100.00	100.01	100.01	99.99	99.97	100.00	100.00	99.99	99.99	99.93	99.93	99.99	100.00	100.00	99.95
							Ions per 8 Oxygen (sum excludes F & Cl)								
Si	3.590	3.359	3.118	3.244	3.187	3.510	3.832	3.347	3.099	3.540	3.164	3.176	3.340	3.941	2.807
Ti	0.000	0.000	0.000	0.000	0.000	0.000	0.000	0.001	0.001	0.000	0.001	0.000	0.000	0.000	0.002
Al	0.402	0.628	0.895	0.741	0.805	0.474	0.159	0.635	0.881	0.449	0.760	0.814	0.651	0.052	1.045
Fe	0.009	0.020	0.022	0.011	0.015	0.018	0.005	0.010	0.019	0.011	0.108	0.011	0.008	0.009	0.254
Mn	0.000	0.001	0.000	0.000	0.000	0.000	0.000	0.001	0.000	0.000	0.000	0.000	0.000	0.000	0.001
Mg	0.000	0.002	0.001	0.000	0.000	0.000	0.001	0.000	0.001	0.000	0.000	0.001	0.001	0.001	0.001
Ca	0.001	0.001	0.002	0.002	0.002	0.001	0.000	0.002	0.003	0.001	0.002	0.002	0.001	0.001	0.005
Sr	0.000	0.000	0.001	0.000	0.000	0.002	0.001	0.000	0.000	0.001	0.000	0.002	0.000	0.002	0.000
Ba	0.001	0.000	0.000	0.000	0.000	0.001	0.000	0.000	0.000	0.000	0.000	0.000	0.000	0.000	0.001
Na	0.138	0.243	0.499	0.574	0.324	0.069	0.134	0.610	0.595	0.350	0.409	0.432	0.268	0.011	0.507
K	0.263	0.374	0.269	0.192	0.473	0.409	0.038	0.051	0.298	0.123	0.340	0.387	0.391	0.035	0.361
P	0.000	0.000	0.001	0.000	0.000	0.000	0.001	0.003	0.000	0.001	0.002	0.000	0.000	0.000	0.001
F	0.000	0.000	0.000	0.004	0.010	0.000	0.000	0.004	0.003	0.021	0.026	0.006	0.000	0.000	0.018
Cl	0.000	0.003	0.002	0.000	0.001	0.001	0.001	0.001	0.000	0.000	0.001	0.001	0.000	0.000	0.001
Sum	4.404	4.627	4.808	4.765	4.807	4.483	4.171	4.659	4.897	4.476	4.786	4.825	4.660	4.052	4.983

Quantitative Electron Microprobe Analyses

Rhyolite Dike Matrix: Circle One cont.

	C1-Mat1-16	C1-Mat1-17	C1-Mat1-18	C1-Mat1-19	C1-Mat1-20	C1-Mat1-21	C1-Mat1-22	C1-Mat1-23	C1-Mat1-24	C1-Mat1-25	C1-Mat1-26	C1-Mat1-27	C1-Mat1-28	C1-Mat1-29	C1-Mat1-30
							Chemical Composition (Weight Percent)								
SiO_2	83.67	81.03	68.19	84.76	91.32	79.56	82.83	80.83	81.29	67.37	72.95	77.25	77.25	69.66	75.76
TiO_2	0.00	0.00	0.05	0.02	0.04	0.04	0.03	0.01	0.00	0.00	0.10	0.02	0.00	0.00	0.01
$Al2O_3$	9.40	10.60	18.31	8.57	4.55	10.98	9.18	10.57	10.18	17.55	13.92	12.25	11.95	16.94	13.87
Fe_2O_3	0.24	0.51	0.96	0.46	0.65	0.83	0.50	0.32	0.40	0.68	2.30	0.66	0.32	0.47	0.58
MnO	0.00	0.01	0.01	0.00	0.00	0.02	0.00	0.00	0.00	0.00	0.01	0.01	0.00	0.00	0.01
MgO	0.00	0.00	0.01	0.04	0.00	0.00	0.06	0.01	0.01	0.00	0.02	0.00	0.00	0.02	0.00
CaO	0.02	0.04	0.06	0.02	0.03	0.05	0.03	0.03	0.01	0.03	0.03	0.03	0.02	0.02	0.03
SrO	0.00	0.07	0.06	0.06	0.01	0.05	0.01	0.03	0.00	0.11	0.00	0.07	0.04	0.04	0.06
BaO	0.00	0.00	0.00	0.02	0.00	0.00	0.02	0.00	0.00	0.02	0.03	0.02	0.04	0.03	0.00
Na_2O	4.00	4.64	8.50	3.87	2.57	3.82	2.89	3.37	3.39	3.76	3.91	3.61	1.45	5.43	7.04
K_2O	2.67	3.09	3.71	2.18	0.71	4.65	4.44	4.82	4.71	10.29	6.70	5.90	8.90	7.21	2.64
P_2O_5	0.00	0.01	0.00	0.00	0.00	0.00	0.00	0.00	0.02	0.02	0.02	0.02	0.03	0.02	0.01
F	0.00	0.00	0.14	0.00	0.12	0.00	0.00	0.00	0.00	0.17	0.00	0.16	0.00	0.16	0.00
Cl	0.00	0.01	0.00	0.00	0.01	0.00	0.01	0.02	0.00	0.01	0.02	0.00	0.00	0.01	0.00
O=F	0.00	0.00	-0.06	0.00	-0.05	0.00	0.00	0.00	0.00	-0.07	0.00	-0.07	0.00	-0.07	0.00
O=Cl	0.00	0.00	0.00	0.00	0.00	0.00	0.00	0.00	0.00	0.00	0.01	0.00	0.00	0.00	0.00
Total	100.00	100.00	99.94	100.00	99.95	100.00	100.00	100.00	100.00	99.93	100.00	99.93	100.00	99.94	100.00
							Ions per 8 Oxygen (sum excludes F & Cl)								
Si	3.526	3.449	3.024	3.560	3.761	3.417	3.520	3.456	3.471	3.052	3.217	3.357	3.373	3.104	3.271
Ti	0.000	0.000	0.002	0.001	0.001	0.001	0.001	0.000	0.000	0.000	0.003	0.001	0.000	0.000	0.000
Al	0.467	0.532	0.957	0.424	0.221	0.556	0.460	0.533	0.512	0.937	0.723	0.627	0.615	0.890	0.706
Fe	0.008	0.016	0.032	0.015	0.020	0.027	0.016	0.010	0.013	0.023	0.077	0.022	0.010	0.016	0.019
Mn	0.000	0.000	0.000	0.000	0.000	0.001	0.000	0.000	0.000	0.000	0.000	0.000	0.000	0.000	0.000
Mg	0.000	0.000	0.001	0.003	0.000	0.000	0.004	0.000	0.000	0.000	0.001	0.000	0.000	0.001	0.000
Ca	0.001	0.002	0.003	0.001	0.001	0.002	0.002	0.002	0.000	0.002	0.002	0.001	0.001	0.001	0.002
Sr	0.000	0.002	0.002	0.001	0.000	0.001	0.000	0.001	0.000	0.003	0.000	0.002	0.001	0.001	0.001
Ba	0.000	0.000	0.000	0.000	0.000	0.000	0.000	0.000	0.000	0.000	0.001	0.000	0.001	0.001	0.000
Na	0.327	0.383	0.731	0.315	0.205	0.318	0.238	0.279	0.280	0.330	0.334	0.304	0.123	0.469	0.589
K	0.143	0.168	0.210	0.117	0.038	0.255	0.241	0.263	0.257	0.595	0.377	0.327	0.496	0.410	0.145
P	0.000	0.001	0.000	0.000	0.000	0.000	0.000	0.000	0.001	0.001	0.001	0.001	0.001	0.001	0.000
F	0.000	0.000	0.020	0.000	0.015	0.000	0.000	0.000	0.000	0.024	0.000	0.022	0.000	0.022	0.000
Cl	0.000	0.001	0.000	0.000	0.001	0.000	0.001	0.001	0.000	0.001	0.002	0.000	0.000	0.001	0.000
Sum	4.472	4.552	4.960	4.436	4.247	4.577	4.481	4.544	4.534	4.942	4.735	4.643	4.621	4.893	4.734

Quantitative Electron Microprobe Analyses

Rhyolite Dike Matrix: Circle One cont.

	C1-Mat1-31	C1-Mat1-32	C1-Mat1-33	C1-Mat1-34	C1-Mat1-35	C1-Mat1-36	C1-Mat1-37	C1-Mat1-38	C1-Mat1-39	C1-Mat1-40	C1-Mat1-41	C1-Mat1-42	C1-Mat1-43	C1-Mat1-44	C1-Mat1-45
							Chemical Composition (Weight Percent)								
SiO_2	97.09	87.74	83.99	98.91	72.15	70.43	86.34	92.23	74.36	86.02	77.99	91.47	89.98	78.38	70.58
TiO_2	0.00	0.00	0.00	0.04	0.06	0.09	0.00	0.05	0.03	0.48	0.01	0.02	0.03	0.00	0.07
$Al2O_3$	1.52	6.50	8.60	0.50	15.16	14.30	7.30	4.17	14.31	7.69	12.00	4.95	4.98	11.71	15.47
Fe_2O_3	0.08	0.35	0.34	0.14	0.89	3.98	0.33	0.17	0.87	0.33	0.47	0.17	0.37	0.77	2.00
MnO	0.00	0.01	0.00	0.01	0.00	0.00	0.00	0.00	0.01	0.00	0.00	0.01	0.00	0.00	0.01
MgO	0.02	0.00	0.00	0.00	0.01	0.02	0.01	0.01	0.00	0.00	0.00	0.00	0.01	0.01	0.01
CaO	0.01	0.04	0.03	0.02	0.04	0.04	0.03	0.02	0.03	0.04	0.02	0.02	0.00	0.03	0.04
SrO	0.05	0.07	0.02	0.06	0.00	0.00	0.00	0.00	0.00	0.04	0.03	0.06	0.07	0.08	0.01
BaO	0.00	0.00	0.00	0.03	0.04	0.00	0.00	0.03	0.00	0.03	0.01	0.00	0.05	0.00	0.02
Na_2O	0.66	2.30	2.10	0.18	5.73	4.84	0.79	1.32	3.49	3.03	3.65	3.06	1.32	1.58	5.54
K_2O	0.55	2.98	4.91	0.11	5.72	6.24	5.10	1.98	6.60	2.20	5.78	0.12	3.02	7.36	6.25
P_2O_5	0.01	0.00	0.01	0.00	0.00	0.00	0.00	0.00	0.00	0.04	0.02	0.00	0.00	0.01	0.00
F	0.00	0.00	0.00	0.00	0.19	0.05	0.07	0.00	0.28	0.08	0.02	0.12	0.14	0.06	0.00
Cl	0.00	0.00	0.00	0.00	0.01	0.01	0.02	0.01	0.02	0.00	0.01	0.01	0.02	0.00	0.00
O=F	0.00	0.00	0.00	0.00	-0.08	-0.02	-0.03	0.00	-0.12	-0.04	-0.01	-0.05	-0.06	-0.03	0.00
O=Cl	0.00	0.00	0.00	0.00	0.00	0.00	0.00	0.00	0.00	0.00	0.00	0.00	0.01	0.00	0.00
Total	100.00	100.00	100.00	100.00	99.92	99.98	99.97	100.00	99.88	99.97	99.99	99.95	99.95	99.97	100.00
							Ions per 8 Oxygen (sum excludes F & Cl)								
Si	3.922	3.663	3.559	3.972	3.186	3.140	3.637	3.790	3.265	3.601	3.373	3.756	3.744	3.397	3.132
Ti	0.000	0.000	0.000	0.001	0.002	0.003	0.000	0.002	0.001	0.015	0.000	0.001	0.001	0.000	0.002
Al	0.072	0.320	0.429	0.024	0.789	0.752	0.362	0.202	0.740	0.379	0.611	0.239	0.244	0.598	0.809
Fe	0.003	0.011	0.011	0.004	0.030	0.133	0.011	0.005	0.029	0.010	0.015	0.005	0.012	0.025	0.067
Mn	0.000	0.000	0.000	0.000	0.000	0.000	0.000	0.000	0.000	0.000	0.000	0.000	0.000	0.000	0.000
Mg	0.001	0.000	0.000	0.000	0.000	0.001	0.001	0.000	0.000	0.000	0.000	0.000	0.000	0.001	0.001
Ca	0.000	0.002	0.001	0.001	0.002	0.002	0.002	0.001	0.002	0.002	0.001	0.001	0.000	0.001	0.002
Sr	0.001	0.002	0.001	0.001	0.000	0.000	0.000	0.000	0.000	0.001	0.001	0.002	0.002	0.002	0.000
Ba	0.000	0.000	0.000	0.001	0.001	0.000	0.000	0.001	0.000	0.001	0.000	0.000	0.001	0.000	0.000
Na	0.052	0.186	0.172	0.014	0.491	0.418	0.064	0.105	0.297	0.246	0.306	0.244	0.106	0.133	0.477
K	0.029	0.159	0.265	0.006	0.322	0.355	0.274	0.104	0.370	0.118	0.319	0.006	0.160	0.407	0.354
P	0.001	0.000	0.001	0.000	0.000	0.000	0.000	0.000	0.000	0.002	0.001	0.000	0.000	0.000	0.000
F	0.000	0.000	0.000	0.000	0.026	0.007	0.010	0.000	0.039	0.011	0.003	0.015	0.018	0.009	0.000
Cl	0.000	0.000	0.000	0.000	0.001	0.001	0.001	0.001	0.001	0.000	0.001	0.001	0.002	0.000	0.000
Sum	4.080	4.343	4.439	4.023	4.822	4.805	4.351	4.210	4.704	4.374	4.627	4.254	4.271	4.565	4.844

Quantitative Electron Microprobe Analyses

Rhyolite Dike Matrix: Circle One cont.

	C1-Mat1-46	C1-Mat1-47	C1-Mat1-48	C1-Mat1-49	C1-Mat1-50	C1-Mat1-51	C1-Mat1-52	C1-Mat1-53	C1-Mat1-54	C1-Mat1-55	C1-Mat1-56	C1-Mat1-57	C1-Mat1-58	C1-Mat1-59	C1-Mat1-60
Chemical Composition (Weight Percent)															
SiO_2	78.62	76.57	79.47	72.26	84.16	90.69	88.51	82.37	65.90	69.53	90.29	91.91	92.39	70.78	86.80
TiO_2	0.00	0.00	0.00	0.00	0.04	0.01	0.00	0.05	0.32	0.00	0.01	0.01	0.03	0.02	0.00
$Al2O_3$	11.98	12.59	10.98	15.21	8.77	4.72	6.55	10.46	13.69	17.79	4.46	5.61	4.33	16.25	7.19
Fe_2O_3	0.34	0.71	0.70	0.55	0.30	0.14	0.39	0.28	10.24	0.87	1.92	0.10	0.21	0.85	0.17
MnO	0.02	0.01	0.01	0.00	0.00	0.00	0.02	0.00	0.08	0.02	0.01	0.00	0.00	0.00	0.00
MgO	0.00	0.00	0.01	0.00	0.00	0.00	0.01	0.01	0.00	0.01	0.00	0.01	0.00	0.00	0.01
CaO	0.05	0.01	0.01	0.03	0.02	0.00	0.04	0.02	0.04	0.06	0.03	0.04	0.01	0.03	0.02
SrO	0.08	0.01	0.00	0.03	0.01	0.09	0.09	0.01	0.06	0.00	0.11	0.00	0.04	0.03	0.04
BaO	0.02	0.04	0.02	0.00	0.01	0.00	0.00	0.00	0.00	0.02	0.02	0.01	0.00	0.01	0.01
Na_2O	5.86	0.95	2.82	4.17	3.61	0.45	4.08	5.54	1.58	9.03	2.70	2.19	2.69	6.20	1.92
K_2O	2.98	9.10	5.81	7.70	2.95	3.83	0.28	1.26	8.07	2.66	0.38	0.11	0.20	5.83	3.73
P_2O_5	0.04	0.00	0.00	0.00	0.00	0.06	0.01	0.00	0.00	0.00	0.00	0.01	0.02	0.00	0.03
F	0.00	0.00	0.16	0.04	0.11	0.02	0.02	0.00	0.01	0.00	0.06	0.00	0.07	0.00	0.07
Cl	0.02	0.01	0.01	0.01	0.01	0.00	0.00	0.00	0.00	0.00	0.00	0.00	0.01	0.00	0.00
O=F	0.00	0.00	-0.07	-0.02	-0.04	-0.01	-0.01	0.00	0.00	0.00	-0.03	0.00	-0.03	0.00	-0.03
O=Cl	0.00	0.00	0.00	0.00	0.00	0.00	0.00	0.00	0.00	0.00	0.00	0.00	0.00	0.00	0.00
Total	100.00	100.00	99.94	99.98	99.96	99.99	99.99	100.00	100.00	100.00	99.97	100.00	99.97	100.00	99.97
Ions per 8 Oxygen (sum excludes F & Cl)															
Si	3.371	3.348	3.430	3.194	3.553	3.761	3.664	3.471	3.015	3.055	3.732	3.749	3.783	3.128	3.640
Ti	0.000	0.000	0.000	0.000	0.001	0.000	0.000	0.002	0.011	0.000	0.000	0.000	0.001	0.001	0.000
Al	0.606	0.649	0.559	0.792	0.437	0.231	0.319	0.519	0.738	0.921	0.218	0.270	0.209	0.846	0.356
Fe	0.011	0.023	0.023	0.018	0.010	0.004	0.012	0.009	0.353	0.029	0.060	0.003	0.006	0.028	0.005
Mn	0.001	0.000	0.000	0.000	0.000	0.000	0.001	0.000	0.003	0.001	0.000	0.000	0.000	0.000	0.000
Mg	0.000	0.000	0.001	0.000	0.000	0.000	0.001	0.001	0.000	0.001	0.000	0.000	0.000	0.000	0.000
Ca	0.002	0.001	0.001	0.001	0.001	0.000	0.002	0.001	0.002	0.003	0.002	0.002	0.000	0.002	0.001
Sr	0.002	0.000	0.000	0.001	0.000	0.002	0.002	0.000	0.002	0.000	0.003	0.000	0.001	0.001	0.001
Ba	0.000	0.001	0.000	0.000	0.000	0.000	0.000	0.000	0.000	0.000	0.000	0.000	0.000	0.000	0.000
Na	0.487	0.080	0.236	0.358	0.296	0.036	0.328	0.453	0.140	0.770	0.216	0.173	0.214	0.531	0.156
K	0.163	0.508	0.320	0.434	0.159	0.203	0.015	0.068	0.471	0.149	0.020	0.006	0.011	0.329	0.199
P	0.001	0.000	0.000	0.000	0.000	0.002	0.000	0.000	0.000	0.000	0.000	0.001	0.001	0.000	0.001
F	0.000	0.000	0.022	0.006	0.014	0.003	0.003	0.000	0.001	0.000	0.008	0.000	0.010	0.000	0.010
Cl	0.001	0.001	0.001	0.001	0.001	0.000	0.000	0.000	0.000	0.000	0.000	0.000	0.001	0.000	0.000
Sum	4.644	4.610	4.569	4.800	4.457	4.239	4.343	4.523	4.735	4.929	4.251	4.203	4.225	4.864	4.360

Quantitative Electron Microprobe Analyses

Rhyolite Dike Matrix: Circle One cont.

	C1-Mat1-61	C1-Mat1-62	C1-Mat1-63	C1-Mat1-64	C1-Mat1-65	C1-Mat1-66	C1-Mat1-67	C1-Mat1-68	C1-Mat1-69	C1-Mat1-70	C1-Mat1-71	C1-Mat1-72	C1-Mat1-73	C1-Mat1-74	C1-Mat1-75
	Chemical Composition (Weight Percent)														
SiO_2	78.36	75.20	66.56	81.68	72.05	70.31	67.27	73.63	71.93	77.13	79.88	92.96	53.80	70.95	77.84
TiO_2	0.04	0.03	0.05	0.07	0.00	0.02	0.00	0.02	0.06	0.02	0.03	0.00	0.58	0.00	0.00
$Al2O_3$	11.81	13.37	19.19	10.05	15.24	17.74	18.30	16.09	15.44	12.64	11.42	3.63	15.84	15.89	11.57
Fe_2O_3	0.68	0.60	0.68	0.58	0.63	0.35	2.13	0.59	1.15	0.32	0.55	0.14	17.90	0.24	0.26
MnO	0.00	0.00	0.00	0.00	0.00	0.00	0.00	0.00	0.01	0.00	0.01	0.00	0.12	0.01	0.02
MgO	0.00	0.01	0.01	0.02	0.00	0.00	0.00	0.01	0.01	0.02	0.00	0.00	0.00	0.00	0.00
CaO	0.04	0.01	0.05	0.04	0.01	0.06	0.08	0.06	0.05	0.02	0.02	0.02	0.06	0.03	0.04
SrO	0.03	0.00	0.00	0.00	0.00	0.01	0.00	0.07	0.09	0.02	0.00	0.09	0.00	0.00	0.01
BaO	0.01	0.05	0.00	0.06	0.02	0.02	0.00	0.00	0.00	0.00	0.05	0.02	0.03	0.00	0.03
Na_2O	4.43	2.78	7.49	4.38	3.90	7.86	8.84	8.98	6.29	4.12	4.98	0.92	7.51	3.51	1.75
K_2O	4.62	7.94	5.91	3.09	8.16	3.49	3.38	0.44	4.95	5.71	3.04	2.20	4.03	9.33	8.43
P_2O_5	0.00	0.00	0.01	0.01	0.00	0.00	0.00	0.01	0.01	0.00	0.00	0.01	0.04	0.00	0.04
F	0.00	0.00	0.05	0.02	0.00	0.11	0.00	0.08	0.00	0.00	0.01	0.00	0.08	0.00	0.00
Cl	0.00	0.01	0.00	0.00	0.00	0.02	0.00	0.00	0.01	0.00	0.01	0.00	0.01	0.03	0.02
O=F	0.00	0.00	-0.02	-0.01	0.00	-0.05	0.00	-0.03	0.00	0.00	0.00	0.00	-0.03	0.00	0.00
O=Cl	0.00	0.00	0.00	0.00	0.00	0.01	0.00	0.00	0.00	0.00	0.00	0.00	0.00	0.01	0.00
Total	100.00	100.00	99.98	99.99	100.00	99.96	100.00	99.97	100.00	100.00	100.00	100.00	99.97	100.01	100.00
	Ions per 8 Oxygen (sum excludes F & Cl)														
Si	3.376	3.296	2.976	3.472	3.189	3.088	2.988	3.177	3.163	3.341	3.410	3.816	2.583	3.160	3.391
Ti	0.001	0.001	0.002	0.002	0.000	0.001	0.000	0.001	0.002	0.001	0.001	0.000	0.021	0.000	0.000
Al	0.600	0.691	1.011	0.504	0.795	0.918	0.958	0.818	0.800	0.645	0.575	0.176	0.896	0.834	0.594
Fe	0.022	0.020	0.023	0.019	0.021	0.011	0.071	0.019	0.038	0.010	0.018	0.005	0.647	0.008	0.008
Mn	0.000	0.000	0.000	0.000	0.000	0.000	0.000	0.000	0.000	0.000	0.000	0.000	0.005	0.000	0.001
Mg	0.000	0.001	0.001	0.001	0.000	0.000	0.000	0.001	0.001	0.001	0.000	0.000	0.000	0.000	0.000
Ca	0.002	0.000	0.002	0.002	0.000	0.003	0.004	0.003	0.002	0.001	0.001	0.001	0.003	0.001	0.002
Sr	0.001	0.000	0.000	0.000	0.000	0.000	0.000	0.002	0.002	0.001	0.000	0.002	0.000	0.000	0.000
Ba	0.000	0.001	0.000	0.001	0.000	0.000	0.000	0.000	0.000	0.000	0.001	0.000	0.001	0.000	0.001
Na	0.370	0.236	0.649	0.361	0.334	0.670	0.761	0.752	0.537	0.346	0.412	0.074	0.699	0.303	0.148
K	0.254	0.444	0.337	0.168	0.461	0.195	0.191	0.024	0.278	0.316	0.166	0.115	0.247	0.530	0.468
P	0.000	0.000	0.000	0.000	0.000	0.000	0.000	0.000	0.000	0.000	0.000	0.001	0.002	0.000	0.002
F	0.000	0.000	0.007	0.003	0.000	0.016	0.000	0.011	0.000	0.000	0.001	0.000	0.012	0.000	0.000
Cl	0.000	0.001	0.000	0.000	0.000	0.002	0.000	0.000	0.001	0.000	0.001	0.000	0.001	0.003	0.001
Sum	4.624	4.689	5.002	4.530	4.801	4.887	4.974	4.797	4.823	4.662	4.583	4.188	5.102	4.837	4.615

Quantitative Electron Microprobe Analyses

Rhyolite Dike Matrix: Circle One cont.

	C1-Mat1-76	C1-Mat1-77	C1-Mat1-78	C1-Mat1-79	C1-Mat1-80	C1-Mat1-81	C1-Mat1-82	C1-Mat1-83	C1-Mat1-84	C1-Mat1-85	C1-Mat1-86	C1-Mat1-87	C1-Mat1-88	C1-Mat1-89	C1-Mat1-90
Chemical Composition (Weight Percent)															
SiO_2	92.18	81.33	70.01	64.00	68.60	67.61	77.60	67.63	73.54	82.42	86.76	67.79	65.35	55.99	71.46
TiO_2	0.00	0.00	0.03	0.01	0.06	0.03	0.04	0.03	0.72	0.03	0.01	0.00	0.00	0.11	0.01
Al2O_3	4.23	9.94	17.04	17.93	18.70	19.27	12.63	18.66	14.97	9.58	7.50	17.97	18.95	18.15	16.42
Fe_2O_3	0.30	0.56	1.67	3.60	0.41	0.47	1.05	0.44	0.70	0.25	0.20	0.89	0.24	14.11	0.55
MnO	0.00	0.00	0.01	0.02	0.00	0.00	0.00	0.00	0.00	0.01	0.01	0.00	0.02	0.02	0.00
MgO	0.00	0.00	0.01	0.00	0.00	0.00	0.00	0.00	0.01	0.00	0.01	0.00	0.00	0.00	0.01
CaO	0.03	0.03	0.05	0.04	0.07	0.05	0.05	0.05	0.06	0.03	0.01	0.05	0.02	0.10	0.08
SrO	0.00	0.10	0.02	0.00	0.08	0.04	0.06	0.02	0.02	0.03	0.05	0.00	0.00	0.00	0.00
BaO	0.00	0.01	0.06	0.00	0.03	0.04	0.04	0.01	0.00	0.00	0.01	0.00	0.00	0.00	0.00
Na_2O	2.14	2.07	9.31	5.10	9.12	10.89	4.72	8.55	7.60	2.92	4.23	5.82	5.60	8.46	7.85
K_2O	1.03	5.94	1.68	9.31	2.83	1.52	3.81	4.44	2.23	4.72	1.17	7.47	9.62	3.00	3.51
P_2O_5	0.00	0.00	0.01	0.00	0.01	0.00	0.00	0.00	0.00	0.00	0.00	0.00	0.00	0.04	0.04
F	0.07	0.00	0.12	0.00	0.08	0.07	0.00	0.17	0.14	0.00	0.03	0.00	0.18	0.00	0.06
Cl	0.00	0.02	0.00	0.01	0.02	0.01	0.00	0.01	0.01	0.00	0.02	0.01	0.01	0.01	0.02
O=F	-0.03	0.00	-0.05	0.00	-0.03	-0.03	0.00	-0.07	-0.06	0.00	-0.01	0.00	-0.07	0.00	-0.03
O=Cl	0.00	0.00	0.00	0.00	0.00	0.00	0.00	0.00	0.00	0.00	0.00	0.00	0.00	0.00	0.01
Total	99.97	100.00	99.95	100.00	99.97	99.97	100.00	99.93	99.94	100.00	99.99	100.00	99.93	100.00	99.98
Ions per 8 Oxygen (sum excludes F & Cl)															
Si	3.785	3.484	3.076	2.931	3.024	2.982	3.340	3.011	3.196	3.507	3.618	3.033	2.974	2.627	3.133
Ti	0.000	0.000	0.001	0.000	0.002	0.001	0.001	0.001	0.023	0.001	0.000	0.000	0.000	0.004	0.000
Al	0.205	0.502	0.882	0.968	0.972	1.002	0.641	0.979	0.767	0.481	0.369	0.947	1.016	1.004	0.848
Fe	0.009	0.018	0.055	0.124	0.014	0.016	0.034	0.015	0.023	0.008	0.006	0.030	0.008	0.498	0.018
Mn	0.000	0.000	0.000	0.001	0.000	0.000	0.000	0.000	0.000	0.000	0.000	0.000	0.001	0.001	0.000
Mg	0.000	0.000	0.001	0.000	0.000	0.000	0.000	0.000	0.000	0.000	0.001	0.000	0.000	0.000	0.000
Ca	0.001	0.001	0.003	0.002	0.003	0.002	0.002	0.002	0.003	0.002	0.001	0.002	0.001	0.005	0.004
Sr	0.000	0.003	0.000	0.000	0.002	0.001	0.002	0.001	0.000	0.001	0.001	0.000	0.000	0.000	0.000
Ba	0.000	0.000	0.001	0.000	0.001	0.001	0.001	0.000	0.000	0.000	0.000	0.000	0.000	0.000	0.000
Na	0.170	0.172	0.793	0.452	0.779	0.931	0.394	0.738	0.641	0.241	0.342	0.505	0.494	0.770	0.667
K	0.054	0.325	0.094	0.544	0.159	0.086	0.209	0.252	0.123	0.256	0.062	0.427	0.559	0.180	0.196
P	0.000	0.000	0.000	0.000	0.000	0.000	0.000	0.000	0.000	0.000	0.000	0.000	0.000	0.002	0.001
F	0.010	0.000	0.017	0.000	0.011	0.010	0.000	0.024	0.020	0.000	0.004	0.000	0.026	0.000	0.009
Cl	0.000	0.002	0.000	0.001	0.001	0.001	0.000	0.001	0.001	0.000	0.001	0.001	0.000	0.001	0.002
Sum	4.225	4.505	4.906	5.022	4.956	5.022	4.623	4.999	4.778	4.496	4.400	4.944	5.053	5.090	4.868

Quantitative Electron Microprobe Analyses

Rhyolite Dike Matrix: Circle One cont.

	C1-Mat1-91	C1-Mat1-92	C1-Mat1-93	C1-Mat1-94	C1-Mat1-95	C1-Mat1-96	C1-Mat1-97	C1-Mat1-98	C1-Mat1-99	C1-Mat1-100
	Chemical Composition (Weight Percent)									
SiO_2	82.41	89.90	75.37	72.77	66.58	84.95	65.10	68.90	68.75	75.77
TiO_2	0.00	0.01	0.00	0.02	0.02	0.00	0.00	0.00	0.08	0.03
Al2O_3	9.59	5.42	14.15	14.29	19.28	8.14	19.29	17.88	16.90	13.58
Fe_2O_3	0.60	0.44	0.48	1.66	1.55	0.29	0.44	0.76	1.53	0.34
MnO	0.00	0.00	0.00	0.01	0.00	0.00	0.02	0.00	0.01	0.01
MgO	0.00	0.00	0.00	0.01	0.02	0.00	0.01	0.01	0.00	0.00
CaO	0.03	0.02	0.01	0.02	0.06	0.02	0.03	0.05	0.25	0.04
SrO	0.06	0.06	0.01	0.00	0.01	0.06	0.00	0.00	0.00	0.04
BaO	0.00	0.03	0.02	0.05	0.04	0.02	0.01	0.02	0.00	0.04
Na_2O	3.41	2.23	5.65	5.11	8.22	2.10	0.75	7.84	5.92	5.56
K_2O	3.74	1.85	4.20	5.94	4.12	4.30	14.16	4.47	6.32	4.56
P_2O_5	0.00	0.00	0.06	0.02	0.01	0.01	0.06	0.00	0.00	0.00
F	0.15	0.02	0.05	0.09	0.11	0.11	0.12	0.05	0.22	0.02
Cl	0.00	0.01	0.00	0.01	0.00	0.00	0.01	0.02	0.01	0.02
O=F	-0.06	-0.01	-0.02	-0.04	-0.05	-0.04	-0.05	-0.02	-0.09	-0.01
O=Cl	0.00	0.00	0.00	0.00	0.00	0.00	0.00	0.00	0.00	0.00
Total	99.94	99.99	99.98	99.96	99.95	99.96	99.95	99.98	99.91	99.99
	Ions per 8 Oxygen (sum excludes F & Cl)									
Si	3.507	3.721	3.268	3.209	2.966	3.590	2.984	3.050	3.074	3.289
Ti	0.000	0.000	0.000	0.001	0.001	0.000	0.000	0.000	0.003	0.001
Al	0.481	0.264	0.723	0.743	1.013	0.405	1.042	0.933	0.891	0.695
Fe	0.019	0.014	0.016	0.055	0.052	0.009	0.015	0.025	0.051	0.011
Mn	0.000	0.000	0.000	0.001	0.000	0.000	0.001	0.000	0.001	0.000
Mg	0.000	0.000	0.000	0.000	0.002	0.000	0.001	0.001	0.000	0.000
Ca	0.002	0.001	0.001	0.001	0.003	0.001	0.002	0.002	0.012	0.002
Sr	0.001	0.002	0.000	0.000	0.000	0.002	0.000	0.000	0.000	0.001
Ba	0.000	0.001	0.000	0.001	0.001	0.000	0.000	0.000	0.000	0.001
Na	0.282	0.179	0.475	0.437	0.710	0.172	0.067	0.673	0.514	0.468
K	0.203	0.098	0.232	0.334	0.234	0.232	0.828	0.253	0.361	0.252
P	0.000	0.000	0.002	0.001	0.000	0.000	0.002	0.000	0.000	0.000
F	0.020	0.003	0.007	0.013	0.016	0.014	0.017	0.007	0.031	0.003
Cl	0.000	0.001	0.000	0.001	0.000	0.000	0.001	0.001	0.001	0.001
Sum	4.495	4.279	4.717	4.783	4.980	4.412	4.941	4.938	4.905	4.720

Quantitative Electron Microprobe Analyses

Rhyolite Dike Matrix: Circle Two (Analyzed using a 30 µm wide bean and taking 100 points on a 10 x 10 grid)

	C2-Mat2-1	C2-Mat2-2	C2-Mat2-3	C2-Mat2-4	C2-Mat2-5	C2-Mat2-6	C2-Mat2-7	C2-Mat2-8	C2-Mat2-9	C2-Mat2-10	C2-Mat2-11	C2-Mat2-12	C2-Mat2-13	C2-Mat2-14	C2-Mat2-15
							Chemical Composition (Weight Percent)								
SiO_2	81.43	75.47	76.87	80.74	84.13	83.85	87.02	73.49	81.75	91.54	90.67	87.28	92.43	78.36	75.84
TiO_2	0.00	0.01	0.00	0.00	0.04	0.00	0.00	0.00	0.02	0.00	0.02	0.03	0.00	0.00	0.02
$Al2O_3$	10.69	13.78	13.69	10.46	9.33	9.29	7.61	15.54	10.96	4.68	5.30	7.12	4.26	11.95	13.49
Fe_2O_3	0.45	0.85	0.38	0.58	0.35	0.59	0.17	0.59	0.49	0.16	0.20	0.23	0.18	0.53	0.50
MnO	0.00	0.01	0.00	0.00	0.00	0.02	0.00	0.01	0.00	0.00	0.02	0.00	0.00	0.00	0.00
MgO	0.00	0.00	0.00	0.01	0.01	0.00	0.00	0.00	0.01	0.00	0.01	0.00	0.01	0.01	0.00
CaO	0.03	0.03	0.03	0.03	0.03	0.05	0.02	0.04	0.04	0.01	0.02	0.05	0.02	0.03	0.04
SrO	0.02	0.00	0.03	0.06	0.06	0.01	0.01	0.05	0.00	0.06	0.05	0.03	0.02	0.01	0.00
BaO	0.00	0.02	0.03	0.03	0.05	0.02	0.03	0.00	0.00	0.03	0.00	0.00	0.00	0.00	0.00
Na_2O	4.91	6.49	7.56	4.37	2.91	4.26	4.52	8.50	4.28	1.21	2.80	3.51	2.64	5.21	5.32
K_2O	2.44	3.29	1.41	3.60	3.03	1.89	0.55	1.73	2.43	2.30	0.83	1.64	0.13	3.70	4.76
P_2O_5	0.02	0.01	0.00	0.03	0.00	0.00	0.01	0.03	0.02	0.00	0.07	0.02	0.00	0.00	0.02
F	0.00	0.04	0.00	0.09	0.06	0.00	0.04	0.00	0.00	0.00	0.01	0.09	0.29	0.22	0.00
Cl	0.00	0.01	0.00	0.00	0.01	0.00	0.00	0.00	0.00	0.01	0.00	0.00	0.00	0.00	0.01
O=F	0.00	-0.02	0.00	-0.04	-0.03	0.00	-0.02	0.00	0.00	0.00	0.00	-0.04	-0.12	-0.09	0.00
O=Cl	0.00	0.00	0.00	0.00	0.00	0.00	0.00	0.00	0.00	0.00	0.00	0.00	0.00	0.00	0.00
Total	100.00	99.99	100.00	99.96	99.98	100.00	99.98	100.00	100.00	100.00	100.00	99.96	99.88	99.91	100.00
							Ions per 8 Oxygen (sum excludes F & Cl)								
Si	3.453	3.270	3.295	3.451	3.543	3.526	3.618	3.185	3.456	3.770	3.731	3.639	3.795	3.379	3.291
Ti	0.000	0.000	0.000	0.000	0.001	0.000	0.000	0.000	0.001	0.000	0.001	0.001	0.000	0.000	0.001
Al	0.534	0.704	0.691	0.527	0.463	0.461	0.373	0.794	0.546	0.227	0.257	0.350	0.206	0.607	0.690
Fe	0.014	0.028	0.012	0.019	0.011	0.019	0.005	0.019	0.016	0.005	0.006	0.007	0.006	0.017	0.016
Mn	0.000	0.000	0.000	0.000	0.000	0.001	0.000	0.001	0.000	0.000	0.001	0.000	0.000	0.000	0.000
Mg	0.000	0.000	0.000	0.000	0.001	0.000	0.000	0.000	0.001	0.000	0.000	0.000	0.001	0.000	0.000
Ca	0.002	0.001	0.002	0.001	0.002	0.002	0.001	0.002	0.002	0.000	0.001	0.002	0.001	0.001	0.002
Sr	0.001	0.000	0.001	0.002	0.001	0.000	0.000	0.001	0.000	0.001	0.001	0.001	0.001	0.000	0.000
Ba	0.000	0.000	0.001	0.001	0.001	0.000	0.001	0.000	0.000	0.000	0.000	0.000	0.000	0.000	0.000
Na	0.404	0.545	0.628	0.362	0.238	0.348	0.364	0.714	0.351	0.097	0.224	0.284	0.210	0.435	0.448
K	0.132	0.182	0.077	0.196	0.163	0.101	0.029	0.096	0.131	0.121	0.043	0.087	0.007	0.204	0.263
P	0.001	0.000	0.000	0.001	0.000	0.000	0.000	0.001	0.001	0.000	0.003	0.001	0.000	0.000	0.001
F	0.000	0.006	0.000	0.013	0.008	0.000	0.006	0.000	0.000	0.000	0.001	0.013	0.038	0.030	0.000
Cl	0.000	0.001	0.000	0.000	0.001	0.000	0.000	0.000	0.000	0.000	0.000	0.000	0.000	0.000	0.001
Sum	4.540	4.730	4.706	4.560	4.423	4.458	4.392	4.812	4.503	4.223	4.267	4.372	4.227	4.644	4.711

Quantitative Electron Microprobe Analyses

Rhyolite Dike Matrix: Circle Two cont.

	C2-Mat2-16	C2-Mat2-17	C2-Mat2-18	C2-Mat2-19	C2-Mat2-20	C2-Mat2-21	C2-Mat2-22	C2-Mat2-23	C2-Mat2-24	C2-Mat2-25	C2-Mat2-26	C2-Mat2-27	C2-Mat2-28	C2-Mat2-29	C2-Mat2-30
	Chemical Composition (Weight Percent)														
SiO_2	79.88	93.08	73.43	75.75	81.23	89.59	76.94	68.62	94.50	89.00	89.09	76.27	78.80	86.37	80.35
TiO_2	0.01	0.05	0.00	0.00	0.03	0.00	0.04	0.00	0.00	0.01	0.05	0.01	0.00	0.08	0.14
$Al2O_3$	11.48	3.74	14.75	12.05	10.29	5.89	12.79	16.69	2.73	5.85	5.88	13.29	12.68	6.59	9.47
Fe_2O_3	0.63	0.23	1.79	3.72	0.24	0.24	1.78	3.34	0.76	0.27	0.19	0.73	0.26	2.27	2.85
MnO	0.00	0.00	0.00	0.00	0.01	0.00	0.00	0.03	0.00	0.02	0.00	0.02	0.01	0.00	0.03
MgO	0.00	0.00	0.00	0.00	0.00	0.00	0.00	0.01	0.00	0.00	0.00	0.01	0.00	0.01	0.01
CaO	0.04	0.02	0.07	0.06	0.03	0.03	0.05	0.28	0.02	0.02	0.01	0.16	0.03	0.03	0.06
SrO	0.00	0.10	0.01	0.00	0.03	0.00	0.00	0.09	0.05	0.02	0.04	0.00	0.04	0.00	0.00
BaO	0.00	0.05	0.00	0.00	0.01	0.00	0.04	0.04	0.02	0.01	0.00	0.00	0.00	0.00	0.00
Na_2O	5.64	1.85	8.78	5.25	2.65	3.81	7.30	9.08	1.41	1.45	1.70	2.94	7.23	2.01	3.90
K_2O	2.15	0.84	0.91	3.14	5.30	0.21	1.00	1.75	0.52	3.31	3.01	6.55	0.77	2.61	3.20
P_2O_5	0.07	0.02	0.00	0.03	0.03	0.04	0.00	0.01	0.00	0.03	0.01	0.00	0.00	0.00	0.00
F	0.10	0.02	0.26	0.00	0.15	0.19	0.04	0.05	0.00	0.00	0.00	0.00	0.17	0.00	0.00
Cl	0.00	0.01	0.00	0.00	0.00	0.00	0.01	0.00	0.00	0.01	0.00	0.00	0.00	0.02	0.00
O=F	-0.04	-0.01	-0.11	0.00	-0.06	-0.08	-0.02	-0.02	0.00	0.00	0.00	0.00	-0.07	0.00	0.00
O=Cl	0.00	0.00	0.00	0.00	0.00	0.00	0.00	0.00	0.00	0.00	0.00	0.00	0.00	0.00	0.00
Total	99.96	99.99	99.89	100.00	99.94	99.92	99.99	99.98	100.00	100.00	100.00	100.00	99.93	100.00	100.00
	Ions per 8 Oxygen (sum excludes F & Cl)														
Si	3.406	3.808	3.198	3.290	3.479	3.704	3.304	3.037	3.849	3.703	3.702	3.314	3.360	3.623	3.441
Ti	0.000	0.002	0.000	0.000	0.001	0.000	0.001	0.000	0.000	0.000	0.002	0.001	0.000	0.003	0.005
Al	0.577	0.180	0.757	0.617	0.520	0.287	0.647	0.870	0.131	0.287	0.288	0.681	0.637	0.326	0.478
Fe	0.020	0.007	0.059	0.122	0.008	0.008	0.058	0.111	0.023	0.008	0.006	0.024	0.009	0.072	0.092
Mn	0.000	0.000	0.000	0.000	0.000	0.000	0.000	0.001	0.000	0.001	0.000	0.001	0.000	0.000	0.001
Mg	0.000	0.000	0.000	0.000	0.000	0.000	0.000	0.001	0.000	0.000	0.000	0.001	0.000	0.001	0.001
Ca	0.002	0.001	0.003	0.003	0.002	0.001	0.002	0.013	0.001	0.001	0.001	0.007	0.002	0.001	0.003
Sr	0.000	0.002	0.000	0.000	0.001	0.000	0.000	0.002	0.001	0.001	0.001	0.000	0.001	0.000	0.000
Ba	0.000	0.001	0.000	0.000	0.000	0.000	0.001	0.001	0.000	0.000	0.000	0.000	0.000	0.000	0.000
Na	0.466	0.147	0.741	0.442	0.220	0.306	0.608	0.779	0.111	0.117	0.137	0.248	0.597	0.164	0.324
K	0.117	0.044	0.051	0.174	0.289	0.011	0.055	0.099	0.027	0.176	0.160	0.363	0.042	0.140	0.175
P	0.002	0.001	0.000	0.001	0.001	0.001	0.000	0.001	0.000	0.001	0.001	0.000	0.000	0.000	0.000
F	0.014	0.003	0.036	0.000	0.020	0.025	0.005	0.007	0.000	0.000	0.000	0.000	0.023	0.000	0.000
Cl	0.000	0.001	0.000	0.000	0.000	0.000	0.001	0.000	0.000	0.001	0.000	0.000	0.000	0.001	0.000
Sum	4.590	4.193	4.808	4.648	4.520	4.318	4.676	4.915	4.143	4.294	4.297	4.639	4.648	4.328	4.518

Quantitative Electron Microprobe Analyses

Rhyolite Dike Matrix: Circle Two cont.

	C2-Mat2-31	C2-Mat2-32	C2-Mat2-33	C2-Mat2-34	C2-Mat2-35	C2-Mat2-36	C2-Mat2-37	C2-Mat2-38	C2-Mat2-39	C2-Mat2-40	C2-Mat2-41	C2-Mat2-42	C2-Mat2-43	C2-Mat2-44	C2-Mat2-45
	Chemical Composition (Weight Percent)														
SiO_2	87.89	72.42	79.62	94.31	85.60	78.40	86.36	81.50	85.07	99.66	67.87	94.84	71.77	65.87	81.27
TiO_2	0.03	0.00	0.03	0.00	0.00	0.00	0.02	0.02	0.10	0.04	0.00	0.02	0.01	0.00	0.09
$Al2O_3$	6.65	15.60	12.09	3.11	8.27	11.60	7.40	11.03	4.20	0.12	19.65	3.10	16.47	19.23	7.43
Fe_2O_3	0.26	0.36	0.28	0.34	0.11	0.66	0.34	0.63	7.68	0.05	0.67	0.14	0.91	1.05	6.10
MnO	0.00	0.00	0.01	0.02	0.00	0.01	0.02	0.00	0.00	0.00	0.00	0.00	0.00	0.00	0.03
MgO	0.00	0.00	0.00	0.00	0.01	0.00	0.01	0.00	0.00	0.00	0.00	0.01	0.00	0.01	0.00
CaO	0.03	0.03	0.05	0.02	0.03	0.02	0.04	0.04	0.03	0.00	0.06	0.02	0.04	0.06	0.03
SrO	0.05	0.01	0.07	0.05	0.03	0.01	0.08	0.04	0.03	0.08	0.00	0.09	0.05	0.00	0.00
BaO	0.04	0.02	0.03	0.02	0.00	0.02	0.00	0.00	0.03	0.00	0.02	0.01	0.03	0.00	0.04
Na_2O	2.17	6.27	7.37	1.96	3.55	3.90	2.45	6.01	2.03	0.02	9.04	1.37	9.10	8.40	3.93
K_2O	2.87	5.17	0.34	0.14	2.36	5.36	3.27	0.72	0.80	0.00	2.69	0.34	1.62	5.28	1.03
P_2O_5	0.00	0.00	0.04	0.00	0.00	0.00	0.00	0.01	0.00	0.00	0.00	0.00	0.00	0.02	0.00
F	0.00	0.10	0.06	0.00	0.02	0.00	0.00	0.00	0.02	0.00	0.00	0.05	0.00	0.08	0.06
Cl	0.00	0.02	0.02	0.04	0.01	0.00	0.02	0.00	0.01	0.02	0.01	0.01	0.00	0.00	0.01
O=F	0.00	-0.04	-0.03	0.00	-0.01	0.00	0.00	0.00	-0.01	0.00	0.00	-0.02	0.00	-0.03	-0.02
O=Cl	0.00	0.00	0.00	0.01	0.00	0.00	0.00	0.00	0.00	0.01	0.00	0.00	0.00	0.00	0.00
Total	100.00	99.96	99.98	100.01	99.99	100.00	100.00	100.00	99.99	100.01	100.00	99.98	100.00	99.97	99.98
	Ions per 8 Oxygen (sum excludes F & Cl)														
Si	3.664	3.182	3.381	3.839	3.587	3.385	3.622	3.439	3.603	3.992	2.987	3.854	3.127	2.954	3.475
Ti	0.001	0.000	0.001	0.000	0.000	0.000	0.001	0.001	0.003	0.001	0.000	0.001	0.000	0.000	0.003
Al	0.327	0.808	0.605	0.149	0.408	0.590	0.366	0.549	0.210	0.006	1.019	0.149	0.846	1.016	0.374
Fe	0.008	0.012	0.009	0.011	0.004	0.022	0.011	0.020	0.245	0.001	0.022	0.004	0.030	0.035	0.196
Mn	0.000	0.000	0.001	0.001	0.000	0.000	0.001	0.000	0.000	0.000	0.000	0.000	0.000	0.000	0.001
Mg	0.000	0.000	0.000	0.000	0.001	0.000	0.001	0.000	0.000	0.000	0.000	0.001	0.000	0.001	0.000
Ca	0.002	0.002	0.002	0.001	0.001	0.001	0.002	0.002	0.001	0.000	0.003	0.001	0.002	0.003	0.001
Sr	0.001	0.000	0.002	0.001	0.001	0.000	0.002	0.001	0.001	0.002	0.000	0.002	0.001	0.000	0.000
Ba	0.001	0.000	0.001	0.000	0.000	0.000	0.000	0.000	0.000	0.000	0.000	0.000	0.000	0.000	0.001
Na	0.175	0.534	0.607	0.154	0.289	0.327	0.199	0.491	0.167	0.001	0.772	0.108	0.768	0.730	0.326
K	0.153	0.290	0.018	0.007	0.126	0.295	0.175	0.039	0.043	0.000	0.151	0.018	0.090	0.302	0.056
P	0.000	0.000	0.001	0.000	0.000	0.000	0.000	0.001	0.000	0.000	0.000	0.000	0.000	0.001	0.000
F	0.000	0.014	0.008	0.000	0.003	0.000	0.000	0.000	0.003	0.000	0.000	0.007	0.000	0.012	0.008
Cl	0.000	0.001	0.001	0.003	0.001	0.000	0.001	0.000	0.001	0.002	0.001	0.001	0.000	0.000	0.000
Sum	4.332	4.827	4.627	4.163	4.416	4.621	4.377	4.541	4.273	4.004	4.954	4.136	4.865	5.041	4.432

Quantitative Electron Microprobe Analyses

Rhyolite Dike Matrix: Circle Two cont.

	C2-Mat2-46	C2-Mat2-47	C2-Mat2-48	C2-Mat2-49	C2-Mat2-50	C2-Mat2-51	C2-Mat2-52	C2-Mat2-53	C2-Mat2-54	C2-Mat2-55	C2-Mat2-56	C2-Mat2-57	C2-Mat2-58	C2-Mat2-59	C2-Mat2-60
Chemical Composition (Weight Percent)															
SiO_2	79.70	90.69	80.46	84.87	81.72	99.58	79.32	77.73	74.42	96.85	73.49	81.28	70.15	66.76	86.05
TiO_2	0.03	0.01	0.00	0.05	0.06	0.03	0.01	0.00	0.03	0.00	0.01	0.03	0.01	0.00	0.05
$Al2O_3$	11.77	5.70	11.26	8.74	10.51	0.12	11.00	12.48	12.39	1.59	14.61	9.80	16.77	19.06	7.65
Fe_2O_3	0.32	0.23	0.19	0.34	0.35	0.03	0.22	0.28	4.72	0.08	0.33	1.15	0.72	0.46	0.16
MnO	0.00	0.04	0.00	0.02	0.03	0.01	0.00	0.00	0.05	0.02	0.00	0.00	0.00	0.01	0.00
MgO	0.00	0.01	0.00	0.00	0.01	0.00	0.00	0.00	0.01	0.00	0.01	0.01	0.00	0.00	0.00
CaO	0.04	0.04	0.05	0.04	0.03	0.01	0.01	0.03	0.05	0.00	0.04	0.04	0.05	0.05	0.03
SrO	0.01	0.07	0.07	0.02	0.00	0.00	0.06	0.10	0.00	0.04	0.04	0.03	0.00	0.00	0.00
BaO	0.00	0.00	0.00	0.00	0.04	0.00	0.01	0.02	0.01	0.01	0.03	0.00	0.00	0.00	0.00
Na_2O	5.66	3.01	4.44	4.79	4.36	0.05	1.01	4.58	6.42	0.60	4.20	3.42	6.11	7.77	1.85
K_2O	2.42	0.20	3.47	1.03	2.84	0.01	8.35	4.63	1.82	0.65	7.17	4.21	6.04	5.85	4.12
P_2O_5	0.02	0.00	0.00	0.01	0.01	0.00	0.00	0.00	0.01	0.00	0.00	0.00	0.03	0.00	0.00
F	0.02	0.00	0.06	0.09	0.04	0.16	0.00	0.14	0.06	0.14	0.06	0.02	0.11	0.05	0.10
Cl	0.00	0.01	0.00	0.00	0.00	0.00	0.00	0.01	0.01	0.01	0.00	0.00	0.01	0.01	0.00
O=F	-0.01	0.00	-0.03	-0.04	-0.02	-0.07	0.00	-0.06	-0.02	-0.06	-0.03	-0.01	-0.05	-0.02	-0.04
O=Cl	0.00	0.00	0.00	0.00	0.00	0.00	0.00	0.00	0.00	0.00	0.00	0.00	0.00	0.00	0.00
Total	99.99	100.00	99.97	99.96	99.98	99.93	100.00	99.94	99.98	99.94	99.97	99.99	99.96	99.98	99.96
Ions per 8 Oxygen (sum excludes F & Cl)															
Si	3.397	3.723	3.432	3.557	3.467	3.998	3.435	3.359	3.244	3.925	3.233	3.472	3.110	2.985	3.620
Ti	0.001	0.000	0.000	0.002	0.002	0.001	0.000	0.000	0.001	0.000	0.000	0.001	0.001	0.000	0.001
Al	0.591	0.276	0.566	0.432	0.526	0.006	0.562	0.636	0.636	0.076	0.757	0.494	0.876	1.004	0.379
Fe	0.010	0.007	0.006	0.011	0.011	0.001	0.007	0.009	0.155	0.003	0.011	0.037	0.024	0.015	0.005
Mn	0.000	0.001	0.000	0.001	0.001	0.000	0.000	0.000	0.002	0.001	0.000	0.000	0.000	0.000	0.000
Mg	0.000	0.000	0.000	0.000	0.000	0.000	0.000	0.000	0.001	0.000	0.000	0.000	0.000	0.000	0.000
Ca	0.002	0.002	0.002	0.002	0.002	0.000	0.001	0.001	0.002	0.000	0.002	0.002	0.002	0.002	0.002
Sr	0.000	0.002	0.002	0.001	0.000	0.000	0.002	0.003	0.000	0.001	0.001	0.001	0.000	0.000	0.000
Ba	0.000	0.000	0.000	0.000	0.001	0.000	0.000	0.000	0.000	0.000	0.001	0.000	0.000	0.000	0.000
Na	0.468	0.240	0.367	0.389	0.359	0.004	0.085	0.384	0.542	0.047	0.359	0.283	0.525	0.673	0.151
K	0.131	0.010	0.189	0.055	0.154	0.000	0.461	0.256	0.101	0.033	0.403	0.230	0.341	0.333	0.221
P	0.001	0.000	0.000	0.000	0.001	0.000	0.000	0.000	0.000	0.000	0.000	0.000	0.001	0.000	0.000
F	0.003	0.000	0.009	0.012	0.006	0.021	0.000	0.019	0.008	0.018	0.009	0.003	0.016	0.007	0.013
Cl	0.000	0.000	0.000	0.000	0.000	0.000	0.000	0.001	0.001	0.001	0.000	0.000	0.001	0.001	0.000
Sum	4.601	4.261	4.564	4.448	4.522	4.011	4.553	4.648	4.685	4.086	4.767	4.519	4.880	5.013	4.379

Quantitative Electron Microprobe Analyses

Rhyolite Dike Matrix: Circle Two cont.

	C2-Mat2-61	C2-Mat2-62	C2-Mat2-63	C2-Mat2-64	C2-Mat2-65	C2-Mat2-66	C2-Mat2-67	C2-Mat2-68	C2-Mat2-69	C2-Mat2-70	C2-Mat2-71	C2-Mat2-72	C2-Mat2-73	C2-Mat2-74	C2-Mat2-75
	Chemical Composition (Weight Percent)														
SiO_2	67.42	66.16	73.10	89.33	82.10	73.49	88.75	78.91	81.80	78.96	76.42	86.83	88.45	81.03	80.27
TiO_2	0.00	0.05	0.03	0.04	0.00	0.00	0.00	0.01	0.01	0.03	0.01	0.05	0.05	0.02	0.00
Al2O_3	19.58	19.82	14.98	5.76	9.47	15.47	6.60	11.79	11.24	11.82	13.85	7.66	6.75	9.40	11.69
Fe_2O_3	0.76	0.57	0.63	0.36	0.49	0.71	0.21	0.76	0.36	0.61	0.48	0.39	0.31	4.48	0.63
MnO	0.01	0.02	0.00	0.01	0.00	0.00	0.00	0.00	0.00	0.00	0.00	0.00	0.01	0.00	0.01
MgO	0.00	0.01	0.00	0.00	0.01	0.00	0.00	0.01	0.00	0.00	0.00	0.00	0.00	0.00	0.00
CaO	0.08	0.06	0.05	0.00	0.01	0.06	0.01	0.04	0.05	0.02	0.05	0.01	0.03	0.05	0.04
SrO	0.00	0.00	0.05	0.02	0.00	0.00	0.03	0.03	0.01	0.05	0.07	0.00	0.06	0.00	0.02
BaO	0.00	0.00	0.02	0.00	0.03	0.02	0.00	0.00	0.00	0.00	0.01	0.02	0.01	0.01	0.00
Na_2O	10.95	8.46	5.44	1.79	1.85	8.62	3.85	3.60	5.51	5.04	7.10	4.45	3.86	4.65	7.14
K_2O	1.18	4.76	5.68	2.55	5.88	1.59	0.43	4.72	0.96	3.44	1.97	0.55	0.41	0.35	0.13
P_2O_5	0.00	0.00	0.00	0.00	0.03	0.01	0.00	0.00	0.01	0.01	0.00	0.00	0.00	0.00	0.01
F	0.00	0.10	0.01	0.13	0.13	0.03	0.14	0.11	0.04	0.00	0.04	0.03	0.06	0.00	0.04
Cl	0.00	0.00	0.01	0.02	0.00	0.00	0.00	0.01	0.01	0.00	0.00	0.01	0.01	0.01	0.00
O=F	0.00	-0.04	0.00	-0.05	-0.05	-0.01	-0.06	-0.05	-0.02	0.00	-0.02	-0.01	-0.03	0.00	-0.02
O=Cl	0.00	0.00	0.00	0.00	0.00	0.00	0.00	0.00	0.00	0.00	0.00	0.00	0.00	0.00	0.00
Total	100.00	99.96	100.00	99.95	99.95	99.99	99.94	99.95	99.98	100.00	99.98	99.99	99.98	100.00	99.98
	Ions per 8 Oxygen (sum excludes F & Cl)														
Si	2.967	2.953	3.206	3.713	3.514	3.186	3.675	3.395	3.447	3.383	3.286	3.611	3.662	3.438	3.398
Ti	0.000	0.002	0.001	0.001	0.000	0.000	0.000	0.000	0.000	0.001	0.000	0.002	0.002	0.001	0.000
Al	1.016	1.042	0.774	0.282	0.477	0.790	0.322	0.598	0.558	0.597	0.702	0.376	0.329	0.470	0.583
Fe	0.025	0.019	0.021	0.011	0.016	0.023	0.007	0.025	0.011	0.020	0.015	0.012	0.010	0.143	0.020
Mn	0.000	0.001	0.000	0.000	0.000	0.000	0.000	0.000	0.000	0.000	0.000	0.000	0.000	0.000	0.001
Mg	0.000	0.001	0.000	0.000	0.001	0.000	0.000	0.000	0.000	0.000	0.000	0.000	0.000	0.000	0.000
Ca	0.004	0.003	0.002	0.000	0.001	0.003	0.000	0.002	0.002	0.001	0.002	0.001	0.001	0.002	0.002
Sr	0.000	0.000	0.001	0.000	0.000	0.000	0.001	0.001	0.000	0.001	0.002	0.000	0.001	0.000	0.001
Ba	0.000	0.000	0.000	0.000	0.001	0.000	0.000	0.000	0.000	0.000	0.000	0.000	0.000	0.000	0.000
Na	0.934	0.732	0.462	0.145	0.153	0.725	0.309	0.300	0.450	0.419	0.592	0.359	0.310	0.383	0.586
K	0.067	0.271	0.318	0.135	0.321	0.088	0.023	0.259	0.052	0.188	0.108	0.029	0.022	0.019	0.007
P	0.000	0.000	0.000	0.000	0.001	0.001	0.000	0.000	0.001	0.001	0.000	0.000	0.000	0.000	0.001
F	0.000	0.014	0.001	0.017	0.017	0.004	0.018	0.016	0.006	0.000	0.006	0.004	0.008	0.000	0.005
Cl	0.000	0.000	0.001	0.001	0.000	0.000	0.000	0.000	0.000	0.000	0.000	0.001	0.001	0.001	0.000
Sum	5.013	5.023	4.787	4.288	4.484	4.815	4.336	4.581	4.521	4.611	4.708	4.390	4.337	4.456	4.599

Quantitative Electron Microprobe Analyses

Rhyolite Dike Matrix: Circle Two cont.

	C2-Mat2-76	C2-Mat2-77	C2-Mat2-78	C2-Mat2-79	C2-Mat2-80	C2-Mat2-81	C2-Mat2-82	C2-Mat2-83	C2-Mat2-84	C2-Mat2-85	C2-Mat2-86	C2-Mat2-87	C2-Mat2-88	C2-Mat2-89	C2-Mat2-90
Chemical Composition (Weight Percent)															
SiO_2	71.23	74.48	75.81	67.83	70.16	81.40	72.45	76.34	86.44	68.22	79.85	78.29	74.50	92.51	67.43
TiO_2	0.04	0.00	0.02	0.02	0.00	0.00	0.01	0.00	0.03	0.02	0.02	0.04	0.00	0.04	0.00
$Al2O_3$	15.33	14.74	14.01	19.67	17.80	9.92	16.37	13.89	7.66	18.60	11.61	12.71	15.42	4.22	19.39
Fe_2O_3	0.82	0.34	0.54	0.52	0.27	0.30	0.24	0.42	0.30	0.92	0.21	0.46	0.43	0.14	0.37
MnO	0.00	0.00	0.00	0.00	0.00	0.02	0.00	0.00	0.01	0.01	0.00	0.00	0.02	0.00	0.01
MgO	0.00	0.00	0.00	0.00	0.00	0.01	0.00	0.00	0.00	0.00	0.00	0.01	0.00	0.00	0.01
CaO	0.02	0.04	0.06	0.09	0.08	0.02	0.06	0.05	0.03	0.06	0.05	0.03	0.08	0.02	0.04
SrO	0.01	0.03	0.01	0.06	0.00	0.07	0.01	0.06	0.05	0.00	0.05	0.09	0.00	0.05	0.04
BaO	0.02	0.03	0.01	0.00	0.01	0.02	0.03	0.02	0.01	0.00	0.00	0.04	0.00	0.00	0.00
Na_2O	2.26	6.39	6.70	11.48	9.94	2.58	8.98	7.71	3.62	8.12	5.16	5.66	8.76	2.85	9.76
K_2O	10.19	3.89	2.78	0.33	1.58	5.62	1.76	1.51	1.82	3.82	2.99	2.56	0.71	0.16	2.96
P_2O_5	0.00	0.00	0.00	0.00	0.00	0.03	0.00	0.00	0.03	0.05	0.05	0.00	0.04	0.00	0.00
F	0.08	0.00	0.06	0.00	0.17	0.00	0.09	0.00	0.00	0.17	0.00	0.11	0.04	0.00	0.00
Cl	0.00	0.06	0.00	0.00	0.00	0.00	0.02	0.00	0.00	0.00	0.00	0.00	0.00	0.00	0.00
O=F	-0.04	0.00	-0.03	0.00	-0.07	0.00	-0.04	0.00	0.00	-0.07	0.00	-0.05	-0.02	0.00	0.00
O=Cl	0.00	0.01	0.00	0.00	0.00	0.00	0.00	0.00	0.00	0.00	0.00	0.00	0.00	0.00	0.00
Total	99.96	100.01	99.97	100.00	99.93	100.00	99.97	100.00	100.00	99.93	100.00	99.95	99.98	100.00	100.00
Ions per 8 Oxygen (sum excludes F & Cl)															
Si	3.181	3.237	3.273	2.973	3.075	3.484	3.152	3.279	3.609	3.022	3.405	3.355	3.208	3.783	2.981
Ti	0.001	0.000	0.001	0.001	0.000	0.000	0.000	0.000	0.001	0.001	0.001	0.001	0.000	0.001	0.000
Al	0.807	0.755	0.713	1.016	0.919	0.500	0.839	0.703	0.377	0.971	0.584	0.642	0.783	0.203	1.010
Fe	0.028	0.011	0.018	0.017	0.009	0.010	0.008	0.014	0.009	0.031	0.007	0.015	0.014	0.004	0.012
Mn	0.000	0.000	0.000	0.000	0.000	0.001	0.000	0.000	0.000	0.000	0.000	0.000	0.001	0.000	0.000
Mg	0.000	0.000	0.000	0.000	0.000	0.001	0.000	0.000	0.000	0.000	0.000	0.001	0.000	0.000	0.001
Ca	0.001	0.002	0.003	0.004	0.004	0.001	0.003	0.002	0.002	0.003	0.002	0.001	0.004	0.001	0.002
Sr	0.000	0.001	0.000	0.001	0.000	0.002	0.000	0.002	0.001	0.000	0.001	0.002	0.000	0.001	0.001
Ba	0.000	0.001	0.000	0.000	0.000	0.000	0.001	0.000	0.000	0.000	0.000	0.001	0.000	0.000	0.000
Na	0.196	0.539	0.561	0.975	0.844	0.215	0.757	0.642	0.293	0.697	0.427	0.470	0.731	0.226	0.836
K	0.580	0.216	0.153	0.019	0.089	0.307	0.097	0.083	0.097	0.216	0.162	0.140	0.039	0.009	0.167
P	0.000	0.000	0.000	0.000	0.000	0.001	0.000	0.000	0.001	0.002	0.002	0.000	0.001	0.000	0.000
F	0.012	0.000	0.008	0.000	0.023	0.000	0.012	0.000	0.000	0.024	0.000	0.015	0.005	0.000	0.000
Cl	0.000	0.004	0.000	0.000	0.000	0.000	0.001	0.000	0.000	0.000	0.000	0.000	0.000	0.000	0.000
Sum	4.794	4.760	4.722	5.007	4.939	4.520	4.858	4.725	4.390	4.942	4.591	4.628	4.780	4.229	5.010

Quantitative Electron Microprobe Analyses

Rhyolite Dike Matrix: Circle Two cont.

	C2-Mat2-91	C2-Mat2-92	C2-Mat2-93	C2-Mat2-94	C2-Mat2-95	C2-Mat2-96	C2-Mat2-97	C2-Mat2-98	C2-Mat2-99	C2-Mat2-100
	Chemical Composition (Weight Percent)									
SiO_2	79.71	89.44	88.83	67.51	84.59	86.08	73.85	77.18	77.49	98.64
TiO_2	0.00	0.03	0.05	0.00	0.03	0.06	0.07	0.03	0.05	0.00
$Al2O_3$	11.46	5.69	6.33	18.43	8.65	8.23	12.74	12.68	13.26	0.73
Fe_2O_3	0.30	0.71	0.44	0.68	0.90	0.19	3.57	0.70	0.28	0.01
MnO	0.00	0.00	0.01	0.01	0.00	0.00	0.00	0.01	0.00	0.02
MgO	0.00	0.00	0.01	0.01	0.00	0.00	0.00	0.00	0.00	0.00
CaO	0.03	0.03	0.05	0.06	0.04	0.03	0.04	0.04	0.04	0.01
SrO	0.05	0.02	0.06	0.00	0.00	0.11	0.01	0.05	0.07	0.08
BaO	0.00	0.04	0.00	0.03	0.00	0.00	0.02	0.02	0.00	0.00
Na_2O	5.68	3.74	3.05	7.68	4.84	4.87	4.05	3.36	4.82	0.43
K_2O	2.68	0.16	1.11	5.51	0.88	0.21	5.63	5.90	3.88	0.06
P_2O_5	0.08	0.00	0.05	0.04	0.06	0.03	0.00	0.02	0.00	0.04
F	0.00	0.12	0.01	0.04	0.00	0.18	0.03	0.00	0.10	0.00
Cl	0.00	0.00	0.01	0.01	0.00	0.01	0.00	0.01	0.00	0.00
O=F	0.00	-0.05	0.00	-0.02	0.00	-0.07	-0.01	0.00	-0.04	0.00
O=Cl	0.00	0.00	0.00	0.00	0.00	0.00	0.00	0.00	0.00	0.00
Total	100.00	99.95	100.00	99.98	100.00	99.93	99.99	100.00	99.96	100.00
	Ions per 8 Oxygen (sum excludes F & Cl)									
Si	3.402	3.700	3.677	3.010	3.544	3.592	3.248	3.342	3.335	3.962
Ti	0.000	0.001	0.002	0.000	0.001	0.002	0.002	0.001	0.002	0.000
Al	0.576	0.278	0.309	0.968	0.427	0.405	0.661	0.647	0.673	0.034
Fe	0.010	0.022	0.014	0.023	0.028	0.006	0.118	0.023	0.009	0.000
Mn	0.000	0.000	0.000	0.000	0.000	0.000	0.000	0.000	0.000	0.001
Mg	0.000	0.000	0.000	0.001	0.000	0.000	0.000	0.000	0.000	0.000
Ca	0.002	0.002	0.002	0.003	0.002	0.001	0.002	0.002	0.002	0.000
Sr	0.001	0.000	0.002	0.000	0.000	0.003	0.000	0.001	0.002	0.002
Ba	0.000	0.001	0.000	0.001	0.000	0.000	0.000	0.000	0.000	0.000
Na	0.470	0.300	0.245	0.664	0.394	0.394	0.346	0.282	0.402	0.033
K	0.146	0.009	0.058	0.314	0.047	0.011	0.316	0.326	0.213	0.003
P	0.003	0.000	0.002	0.001	0.002	0.001	0.000	0.001	0.000	0.002
F	0.000	0.016	0.001	0.006	0.000	0.023	0.004	0.000	0.014	0.000
Cl	0.000	0.000	0.000	0.001	0.000	0.001	0.000	0.001	0.000	0.000
Sum	4.609	4.312	4.310	4.984	4.445	4.414	4.693	4.625	4.637	4.037

Quantitative Electron Microprobe Analyses

Rhyolite Dike Matrix: Circle Three (Analyzed using a 30 µm wide bean and taking 100 points on a 10 x 10 grid)

	C3-Mat3-1	C3-Mat3-2	C3-Mat3-3	C3-Mat3-4	C3-Mat3-5	C3-Mat3-6	C3-Mat3-7	C3-Mat3-8	C3-Mat3-9	C3-Mat3-10	C3-Mat3-11	C3-Mat3-12	C3-Mat3-13	C3-Mat3-14	C3-Mat3-15
	Chemical Composition (Weight Percent)														
SiO_2	63.52	74.37	79.21	73.36	78.81	92.24	69.88	83.16	84.58	75.65	83.85	68.89	78.99	94.71	72.06
TiO_2	0.00	0.02	0.02	0.00	0.01	0.02	0.00	0.00	0.04	0.03	0.00	0.00	0.03	0.02	0.00
$Al2O_3$	18.44	15.06	11.34	14.31	12.36	4.12	16.91	9.19	9.00	14.19	9.08	18.09	11.82	2.94	15.88
Fe_2O_3	3.36	0.45	0.47	0.67	0.35	0.25	0.61	0.20	0.27	0.62	0.29	0.47	0.45	0.15	0.40
MnO	0.01	0.00	0.00	0.03	0.03	0.00	0.00	0.03	0.01	0.00	0.00	0.01	0.00	0.01	0.00
MgO	0.00	0.00	0.00	0.00	0.02	0.00	0.00	0.01	0.01	0.00	0.01	0.00	0.01	0.01	0.00
CaO	0.02	0.04	0.02	0.02	0.03	0.01	0.06	0.02	0.04	0.04	0.04	0.03	0.05	0.01	0.04
SrO	0.01	0.00	0.03	0.00	0.00	0.07	0.02	0.02	0.07	0.00	0.02	0.00	0.04	0.03	0.00
BaO	0.04	0.00	0.03	0.01	0.06	0.00	0.04	0.00	0.02	0.02	0.00	0.01	0.01	0.02	0.00
Na_2O	4.55	7.20	2.71	3.77	6.06	1.11	6.43	3.44	4.48	7.14	5.59	8.29	5.26	1.16	6.89
K_2O	10.04	2.83	6.16	7.83	2.13	2.17	6.00	3.90	1.47	2.31	0.87	4.06	3.25	0.92	4.61
P_2O_5	0.02	0.00	0.00	0.00	0.03	0.00	0.00	0.00	0.00	0.01	0.02	0.05	0.00	0.00	0.03
F	0.00	0.00	0.00	0.00	0.10	0.00	0.04	0.00	0.00	0.00	0.21	0.09	0.08	0.00	0.07
Cl	0.00	0.02	0.00	0.00	0.00	0.01	0.00	0.01	0.00	0.00	0.00	0.00	0.00	0.03	0.01
O=F	0.00	0.00	0.00	0.00	-0.04	0.00	-0.02	0.00	0.00	0.00	-0.09	-0.04	-0.04	0.00	-0.03
O=Cl	0.00	0.01	0.00	0.00	0.00	0.00	0.00	0.00	0.00	0.00	0.00	0.00	0.00	0.01	0.00
Total	100.00	100.01	100.00	100.00	99.96	100.00	99.98	100.00	100.00	100.00	99.91	99.96	99.96	100.01	99.97
	Ions per 8 Oxygen (sum excludes F & Cl)														
Si	2.915	3.221	3.414	3.234	3.369	3.792	3.098	3.526	3.546	3.261	3.533	3.046	3.387	3.855	3.163
Ti	0.000	0.001	0.001	0.000	0.000	0.001	0.000	0.000	0.001	0.001	0.000	0.000	0.001	0.001	0.000
Al	0.997	0.769	0.576	0.744	0.623	0.200	0.884	0.459	0.445	0.721	0.451	0.943	0.598	0.141	0.821
Fe	0.116	0.015	0.015	0.022	0.011	0.008	0.021	0.007	0.009	0.020	0.009	0.016	0.014	0.005	0.013
Mn	0.000	0.000	0.000	0.001	0.001	0.000	0.000	0.001	0.001	0.000	0.000	0.000	0.000	0.000	0.000
Mg	0.000	0.000	0.000	0.000	0.001	0.000	0.000	0.001	0.001	0.000	0.001	0.000	0.001	0.001	0.000
Ca	0.001	0.002	0.001	0.001	0.002	0.001	0.003	0.001	0.002	0.002	0.002	0.002	0.003	0.001	0.002
Sr	0.000	0.000	0.001	0.000	0.000	0.002	0.001	0.000	0.002	0.000	0.001	0.000	0.001	0.001	0.000
Ba	0.001	0.000	0.001	0.000	0.001	0.000	0.001	0.000	0.000	0.000	0.000	0.000	0.000	0.000	0.000
Na	0.404	0.605	0.226	0.322	0.503	0.089	0.552	0.283	0.364	0.596	0.457	0.711	0.438	0.092	0.586
K	0.588	0.157	0.339	0.440	0.116	0.114	0.340	0.211	0.079	0.127	0.047	0.229	0.178	0.048	0.258
P	0.001	0.000	0.000	0.000	0.001	0.000	0.000	0.000	0.000	0.000	0.001	0.002	0.000	0.000	0.001
F	0.000	0.000	0.000	0.000	0.014	0.000	0.006	0.000	0.000	0.000	0.029	0.013	0.011	0.000	0.010
Cl	0.000	0.002	0.000	0.000	0.000	0.001	0.000	0.001	0.000	0.000	0.000	0.000	0.000	0.002	0.001
Sum	5.023	4.768	4.573	4.765	4.628	4.205	4.899	4.489	4.448	4.729	4.502	4.948	4.619	4.143	4.845

Quantitative Electron Microprobe Analyses

Rhyolite Dike Matrix: Circle Three cont.

	C3-Mat3-16	C3-Mat3-17	C3-Mat3-18	C3-Mat3-19	C3-Mat3-20	C3-Mat3-21	C3-Mat3-22	C3-Mat3-23	C3-Mat3-24	C3-Mat3-25	C3-Mat3-26	C3-Mat3-27	C3-Mat3-28	C3-Mat3-29	C3-Mat3-30
							Chemical Composition (Weight Percent)								
SiO_2	78.81	70.30	83.58	78.75	81.95	78.86	76.34	81.48	81.52	75.48	77.16	77.13	77.89	72.68	93.90
TiO_2	0.00	0.01	0.00	0.00	0.00	0.00	0.01	0.06	0.00	0.00	0.02	0.01	0.00	0.02	0.02
$Al2O_3$	12.35	16.49	9.70	12.12	10.74	12.45	13.26	10.56	10.18	13.97	12.42	13.14	12.11	15.32	3.46
Fe_2O_3	0.73	0.58	0.27	0.32	0.34	0.42	0.53	0.28	0.57	0.42	1.72	0.76	0.25	0.34	0.08
MnO	0.02	0.01	0.00	0.00	0.00	0.01	0.00	0.01	0.00	0.02	0.02	0.01	0.00	0.00	0.02
MgO	0.01	0.02	0.00	0.01	0.00	0.00	0.00	0.00	0.01	0.02	0.00	0.01	0.00	0.00	0.00
CaO	0.03	0.03	0.03	0.02	0.05	0.02	0.06	0.08	0.03	0.05	0.05	0.05	0.02	0.03	0.02
SrO	0.00	0.00	0.07	0.07	0.00	0.00	0.04	0.01	0.04	0.03	0.00	0.00	0.00	0.02	0.05
BaO	0.00	0.03	0.00	0.01	0.01	0.04	0.00	0.01	0.03	0.03	0.00	0.01	0.01	0.03	0.00
Na_2O	5.49	4.16	4.05	5.81	5.09	7.46	5.24	4.07	4.60	6.16	6.90	5.42	2.64	4.53	1.82
K_2O	2.44	8.35	2.28	2.78	1.63	0.68	4.51	3.42	2.91	3.68	1.69	3.40	7.07	6.93	0.56
P_2O_5	0.07	0.02	0.00	0.01	0.02	0.05	0.00	0.00	0.02	0.01	0.01	0.00	0.00	0.02	0.02
F	0.03	0.00	0.01	0.10	0.17	0.00	0.00	0.00	0.09	0.13	0.00	0.05	0.00	0.07	0.04
Cl	0.02	0.00	0.00	0.00	0.00	0.01	0.00	0.01	0.00	0.01	0.00	0.01	0.02	0.01	0.00
O=F	-0.01	0.00	0.00	-0.04	-0.07	0.00	0.00	0.00	-0.04	-0.06	0.00	-0.02	0.00	-0.03	-0.02
O=Cl	0.01	0.00	0.00	0.00	0.00	0.00	0.00	0.00	0.00	0.00	0.00	0.00	0.00	0.00	0.00
Total	99.99	100.00	100.00	99.96	99.93	100.00	100.00	100.00	99.96	99.95	100.00	99.98	100.00	99.97	99.98
							Ions per 8 Oxygen (sum excludes F & Cl)								
Si	3.366	3.126	3.518	3.376	3.468	3.356	3.305	3.462	3.470	3.275	3.317	3.322	3.377	3.201	3.829
Ti	0.000	0.000	0.000	0.000	0.000	0.000	0.001	0.002	0.000	0.000	0.001	0.000	0.000	0.001	0.001
Al	0.622	0.864	0.481	0.612	0.535	0.624	0.677	0.529	0.511	0.714	0.629	0.667	0.619	0.795	0.167
Fe	0.024	0.020	0.008	0.010	0.011	0.013	0.017	0.009	0.018	0.014	0.056	0.025	0.008	0.011	0.002
Mn	0.001	0.000	0.000	0.000	0.000	0.000	0.000	0.000	0.000	0.001	0.001	0.000	0.000	0.000	0.001
Mg	0.001	0.001	0.000	0.000	0.000	0.000	0.000	0.000	0.001	0.001	0.000	0.000	0.000	0.000	0.000
Ca	0.001	0.001	0.002	0.001	0.002	0.001	0.003	0.003	0.001	0.002	0.002	0.002	0.001	0.001	0.001
Sr	0.000	0.000	0.002	0.002	0.000	0.000	0.001	0.000	0.001	0.001	0.000	0.000	0.000	0.001	0.001
Ba	0.000	0.001	0.000	0.000	0.000	0.001	0.000	0.000	0.001	0.001	0.000	0.000	0.000	0.001	0.000
Na	0.455	0.359	0.330	0.483	0.417	0.615	0.440	0.336	0.380	0.518	0.575	0.453	0.222	0.387	0.144
K	0.133	0.474	0.123	0.152	0.088	0.037	0.249	0.185	0.158	0.204	0.093	0.187	0.391	0.389	0.029
P	0.002	0.001	0.000	0.001	0.001	0.002	0.000	0.000	0.001	0.001	0.000	0.000	0.000	0.001	0.001
F	0.004	0.000	0.001	0.014	0.023	0.000	0.000	0.000	0.013	0.018	0.000	0.007	0.000	0.010	0.006
Cl	0.002	0.000	0.000	0.000	0.000	0.001	0.000	0.001	0.000	0.001	0.000	0.001	0.001	0.001	0.000
Sum	4.604	4.847	4.464	4.637	4.522	4.649	4.692	4.527	4.540	4.730	4.674	4.656	4.617	4.788	4.175

Quantitative Electron Microprobe Analyses

Rhyolite Dike Matrix: Circle Three cont.

	C3-Mat3-31	C3-Mat3-32	C3-Mat3-33	C3-Mat3-34	C3-Mat3-35	C3-Mat3-36	C3-Mat3-37	C3-Mat3-38	C3-Mat3-39	C3-Mat3-40	C3-Mat3-41	C3-Mat3-42	C3-Mat3-43	C3-Mat3-44	C3-Mat3-45
							Chemical Composition (Weight Percent)								
SiO_2	85.01	91.05	88.60	86.17	89.95	83.18	80.02	74.26	87.14	81.07	85.46	78.29	69.54	68.25	76.70
TiO_2	0.00	0.05	0.02	0.03	0.00	0.00	0.01	0.02	0.01	0.00	0.00	0.02	0.00	0.00	0.00
$Al2O_3$	8.88	4.61	6.36	7.54	5.86	9.23	11.85	15.33	7.11	11.18	8.61	12.44	17.41	19.23	13.15
Fe_2O_3	0.43	0.38	0.15	0.27	0.16	0.30	0.25	0.37	0.17	0.37	0.19	0.61	0.60	0.38	0.44
MnO	0.00	0.00	0.02	0.00	0.01	0.00	0.01	0.00	0.01	0.01	0.00	0.01	0.01	0.00	0.00
MgO	0.00	0.00	0.00	0.00	0.00	0.01	0.00	0.00	0.00	0.00	0.00	0.00	0.01	0.00	0.00
CaO	0.05	0.03	0.00	0.01	0.02	0.03	0.03	0.07	0.05	0.05	0.03	0.05	0.06	0.05	0.03
SrO	0.04	0.00	0.05	0.03	0.06	0.08	0.05	0.02	0.06	0.02	0.03	0.00	0.00	0.00	0.00
BaO	0.02	0.00	0.04	0.02	0.01	0.04	0.01	0.00	0.00	0.02	0.03	0.00	0.03	0.00	0.03
Na_2O	4.72	1.20	2.60	2.52	2.87	3.88	5.62	9.52	1.57	5.89	5.26	3.72	7.13	10.87	4.07
K_2O	0.84	2.58	2.11	3.26	1.05	3.15	2.16	0.41	3.84	1.35	0.34	4.86	5.13	1.19	5.58
P_2O_5	0.00	0.05	0.05	0.00	0.00	0.00	0.00	0.00	0.02	0.02	0.02	0.00	0.02	0.02	0.00
F	0.00	0.05	0.00	0.13	0.00	0.10	0.00	0.00	0.00	0.00	0.02	0.00	0.06	0.00	0.00
Cl	0.00	0.00	0.00	0.01	0.00	0.02	0.00	0.00	0.02	0.02	0.01	0.01	0.01	0.00	0.01
O=F	0.00	-0.02	0.00	-0.05	0.00	-0.04	0.00	0.00	0.00	0.00	-0.01	0.00	-0.03	0.00	0.00
O=Cl	0.00	0.00	0.00	0.00	0.00	0.00	0.00	0.00	0.00	0.00	0.00	0.00	0.00	0.00	0.00
Total	100.00	99.98	100.00	99.95	100.00	99.96	100.00	100.00	100.00	100.00	99.99	100.00	99.98	100.00	100.00
							Ions per 8 Oxygen (sum excludes F & Cl)								
Si	3.553	3.762	3.679	3.621	3.710	3.526	3.402	3.200	3.647	3.432	3.566	3.366	3.078	2.995	3.323
Ti	0.000	0.002	0.001	0.001	0.000	0.000	0.000	0.001	0.000	0.000	0.000	0.001	0.000	0.000	0.000
Al	0.438	0.224	0.311	0.374	0.285	0.461	0.594	0.779	0.351	0.558	0.424	0.631	0.908	0.995	0.671
Fe	0.014	0.012	0.005	0.009	0.005	0.010	0.008	0.012	0.005	0.012	0.006	0.020	0.020	0.013	0.015
Mn	0.000	0.000	0.001	0.000	0.000	0.000	0.000	0.000	0.001	0.000	0.000	0.000	0.000	0.000	0.000
Mg	0.000	0.000	0.000	0.000	0.000	0.001	0.000	0.000	0.000	0.000	0.000	0.000	0.001	0.000	0.000
Ca	0.002	0.002	0.000	0.001	0.001	0.001	0.001	0.003	0.002	0.002	0.001	0.002	0.003	0.002	0.001
Sr	0.001	0.000	0.001	0.001	0.001	0.002	0.001	0.000	0.002	0.001	0.001	0.000	0.000	0.000	0.000
Ba	0.000	0.000	0.001	0.000	0.000	0.001	0.000	0.000	0.000	0.000	0.000	0.000	0.001	0.000	0.000
Na	0.382	0.096	0.210	0.205	0.230	0.319	0.464	0.795	0.128	0.484	0.426	0.310	0.612	0.925	0.342
K	0.045	0.136	0.112	0.175	0.055	0.171	0.117	0.023	0.205	0.073	0.018	0.266	0.290	0.067	0.308
P	0.000	0.002	0.002	0.000	0.000	0.000	0.000	0.000	0.001	0.001	0.001	0.000	0.001	0.001	0.000
F	0.000	0.007	0.000	0.017	0.000	0.013	0.000	0.000	0.000	0.000	0.003	0.000	0.009	0.000	0.000
Cl	0.000	0.000	0.000	0.001	0.000	0.001	0.000	0.000	0.001	0.001	0.001	0.001	0.001	0.000	0.001
Sum	4.435	4.235	4.321	4.386	4.288	4.490	4.587	4.813	4.341	4.562	4.442	4.596	4.912	4.996	4.660

Quantitative Electron Microprobe Analyses

Rhyolite Dike Matrix: Circle Three cont.

	C3-Mat3-46	C3-Mat3-47	C3-Mat3-48	C3-Mat3-49	C3-Mat3-50	C3-Mat3-51	C3-Mat3-52	C3-Mat3-53	C3-Mat3-54	C3-Mat3-55	C3-Mat3-56	C3-Mat3-57	C3-Mat3-58	C3-Mat3-59	C3-Mat3-60
Chemical Composition (Weight Percent)															
SiO_2	91.97	84.56	75.02	92.91	94.86	72.96	81.09	76.83	85.45	83.32	79.32	86.77	71.74	95.73	73.78
TiO_2	0.02	0.00	0.03	0.00	0.00	0.01	0.00	0.02	0.13	0.03	0.07	0.02	0.00	0.03	0.04
Al2O_3	4.40	8.57	13.88	3.98	2.70	15.29	11.12	12.36	5.37	9.13	10.82	7.45	16.16	2.26	15.64
Fe_2O_3	0.16	0.15	0.27	0.17	0.12	0.39	0.29	0.32	4.99	0.31	1.67	0.40	0.37	0.12	0.41
MnO	0.00	0.03	0.00	0.01	0.00	0.02	0.00	0.00	0.00	0.00	0.00	0.01	0.00	0.00	0.00
MgO	0.00	0.00	0.00	0.00	0.00	0.01	0.00	0.00	0.00	0.00	0.02	0.01	0.01	0.00	0.00
CaO	0.04	0.05	0.02	0.02	0.00	0.03	0.04	0.03	0.05	0.02	0.04	0.05	0.05	0.01	0.07
SrO	0.01	0.00	0.00	0.00	0.11	0.00	0.09	0.00	0.00	0.00	0.00	0.02	0.03	0.10	0.01
BaO	0.01	0.00	0.01	0.00	0.00	0.03	0.00	0.00	0.02	0.00	0.05	0.00	0.00	0.04	0.00
Na_2O	1.90	3.30	3.57	2.68	1.40	5.66	6.61	2.90	3.31	2.77	4.34	2.94	6.01	0.55	8.88
K_2O	1.29	3.31	7.08	0.07	0.67	5.55	0.75	7.42	0.50	4.26	3.64	2.31	5.55	0.98	0.97
P_2O_5	0.00	0.00	0.02	0.00	0.00	0.00	0.00	0.00	0.00	0.02	0.03	0.01	0.00	0.00	0.05
F	0.18	0.03	0.11	0.15	0.14	0.03	0.00	0.12	0.16	0.13	0.00	0.00	0.05	0.17	0.14
Cl	0.02	0.00	0.01	0.01	0.00	0.02	0.01	0.00	0.01	0.00	0.01	0.01	0.02	0.00	0.00
O=F	-0.08	-0.01	-0.04	-0.06	-0.06	-0.01	0.00	-0.05	-0.07	-0.05	0.00	0.00	-0.02	-0.07	-0.06
O=Cl	0.00	0.00	0.00	0.00	0.00	0.00	0.00	0.00	0.00	0.00	0.00	0.00	0.01	0.00	0.00
Total	99.93	99.99	99.96	99.94	99.94	99.99	100.00	99.95	99.93	99.95	100.00	100.00	99.98	99.93	99.94
Ions per 8 Oxygen (sum excludes F & Cl)															
Si	3.786	3.565	3.283	3.802	3.867	3.199	3.430	3.353	3.606	3.537	3.404	3.623	3.157	3.895	3.192
Ti	0.001	0.000	0.001	0.000	0.000	0.000	0.000	0.001	0.004	0.001	0.002	0.001	0.000	0.001	0.001
Al	0.213	0.426	0.716	0.192	0.130	0.790	0.554	0.636	0.267	0.457	0.547	0.366	0.838	0.109	0.797
Fe	0.005	0.005	0.009	0.005	0.004	0.013	0.009	0.011	0.159	0.010	0.054	0.013	0.012	0.004	0.013
Mn	0.000	0.001	0.000	0.000	0.000	0.001	0.000	0.000	0.000	0.000	0.000	0.000	0.000	0.000	0.000
Mg	0.000	0.000	0.000	0.000	0.000	0.001	0.000	0.000	0.000	0.000	0.001	0.001	0.000	0.000	0.000
Ca	0.002	0.002	0.001	0.001	0.000	0.001	0.002	0.001	0.002	0.001	0.002	0.002	0.002	0.000	0.003
Sr	0.000	0.000	0.000	0.000	0.003	0.000	0.002	0.000	0.000	0.000	0.000	0.000	0.001	0.002	0.000
Ba	0.000	0.000	0.000	0.000	0.000	0.001	0.000	0.000	0.000	0.000	0.001	0.000	0.000	0.001	0.000
Na	0.152	0.269	0.303	0.213	0.111	0.482	0.542	0.246	0.271	0.228	0.361	0.238	0.513	0.043	0.745
K	0.068	0.178	0.395	0.004	0.035	0.311	0.041	0.413	0.027	0.231	0.199	0.123	0.312	0.051	0.054
P	0.000	0.000	0.001	0.000	0.000	0.000	0.000	0.000	0.000	0.001	0.001	0.000	0.000	0.000	0.002
F	0.024	0.004	0.015	0.019	0.018	0.004	0.000	0.016	0.021	0.017	0.000	0.000	0.007	0.022	0.020
Cl	0.002	0.000	0.000	0.001	0.000	0.001	0.001	0.000	0.001	0.000	0.000	0.001	0.002	0.000	0.000
Sum	4.227	4.446	4.709	4.217	4.148	4.798	4.580	4.660	4.337	4.465	4.572	4.368	4.835	4.106	4.808

Quantitative Electron Microprobe Analyses

Rhyolite Dike Matrix: Circle Three cont.

	C3-Mat3-61	C3-Mat3-62	C3-Mat3-63	C3-Mat3-64	C3-Mat3-65	C3-Mat3-66	C3-Mat3-67	C3-Mat3-68	C3-Mat3-69	C3-Mat3-70	C3-Mat3-71	C3-Mat3-72	C3-Mat3-73	C3-Mat3-74	C3-Mat3-75
	Chemical Composition (Weight Percent)														
SiO_2	68.25	70.31	71.19	78.52	83.83	70.86	69.56	74.89	88.08	74.90	71.05	67.73	94.35	77.56	69.04
TiO_2	0.00	0.00	0.00	0.00	0.02	0.00	0.00	0.00	0.00	0.02	0.01	0.06	0.04	0.01	0.03
$Al2O_3$	18.80	18.30	16.37	12.31	9.27	17.38	17.46	13.17	6.41	14.63	16.17	15.41	3.26	12.60	17.62
Fe_2O_3	0.66	0.47	0.73	0.75	0.23	0.52	0.45	0.29	0.30	0.56	0.77	6.29	0.14	0.38	0.99
MnO	0.00	0.00	0.00	0.00	0.00	0.00	0.00	0.00	0.01	0.02	0.00	0.00	0.02	0.02	0.00
MgO	0.00	0.00	0.02	0.00	0.00	0.01	0.00	0.01	0.01	0.00	0.01	0.03	0.00	0.00	0.00
CaO	0.05	0.07	0.06	0.03	0.02	0.05	0.05	0.00	0.01	0.03	0.05	0.11	0.01	0.03	0.06
SrO	0.07	0.03	0.05	0.04	0.07	0.00	0.04	0.00	0.00	0.03	0.03	0.01	0.03	0.00	0.00
BaO	0.03	0.01	0.01	0.04	0.02	0.00	0.00	0.00	0.03	0.01	0.00	0.00	0.00	0.00	0.02
Na_2O	10.28	8.08	6.94	6.86	4.22	8.61	6.96	1.23	2.14	8.34	6.45	7.97	1.33	5.32	8.66
K_2O	1.85	2.71	4.55	1.42	2.17	2.56	5.46	10.35	2.78	1.46	5.36	2.28	0.72	4.00	3.58
P_2O_5	0.00	0.00	0.00	0.02	0.02	0.00	0.01	0.00	0.08	0.00	0.02	0.03	0.00	0.00	0.00
F	0.00	0.01	0.10	0.00	0.13	0.00	0.00	0.04	0.16	0.00	0.06	0.05	0.11	0.04	0.00
Cl	0.00	0.01	0.00	0.01	0.00	0.01	0.00	0.01	0.00	0.00	0.01	0.01	0.00	0.02	0.00
O=F	0.00	0.00	-0.04	0.00	-0.05	0.00	0.00	-0.02	-0.07	0.00	-0.03	-0.02	-0.05	-0.02	0.00
O=Cl	0.00	0.00	0.00	0.00	0.00	0.00	0.00	0.00	0.00	0.00	0.00	0.00	0.00	0.01	0.00
Total	100.00	100.00	99.96	100.00	99.95	100.00	100.00	99.98	99.93	100.00	99.98	99.98	99.95	99.99	100.00
	Ions per 8 Oxygen (sum excludes F & Cl)														
Si	3.004	3.071	3.134	3.354	3.535	3.096	3.077	3.308	3.677	3.232	3.136	3.023	3.845	3.345	3.049
Ti	0.000	0.000	0.000	0.000	0.001	0.000	0.000	0.000	0.000	0.001	0.000	0.002	0.001	0.000	0.001
Al	0.975	0.942	0.849	0.620	0.461	0.895	0.910	0.686	0.315	0.744	0.841	0.811	0.157	0.641	0.917
Fe	0.022	0.016	0.024	0.024	0.007	0.017	0.015	0.010	0.009	0.018	0.026	0.211	0.004	0.012	0.033
Mn	0.000	0.000	0.000	0.000	0.000	0.000	0.000	0.000	0.000	0.001	0.000	0.000	0.001	0.001	0.000
Mg	0.000	0.000	0.001	0.000	0.000	0.001	0.000	0.001	0.001	0.000	0.001	0.002	0.000	0.000	0.000
Ca	0.002	0.003	0.003	0.002	0.001	0.002	0.003	0.000	0.000	0.001	0.002	0.005	0.001	0.001	0.003
Sr	0.002	0.001	0.001	0.001	0.002	0.000	0.001	0.000	0.000	0.001	0.001	0.000	0.001	0.000	0.000
Ba	0.001	0.000	0.000	0.001	0.000	0.000	0.000	0.000	0.001	0.000	0.000	0.000	0.000	0.000	0.000
Na	0.878	0.685	0.593	0.568	0.345	0.729	0.597	0.105	0.173	0.698	0.552	0.690	0.105	0.444	0.742
K	0.104	0.151	0.255	0.077	0.117	0.143	0.308	0.583	0.148	0.080	0.302	0.130	0.037	0.220	0.201
P	0.000	0.000	0.000	0.001	0.001	0.000	0.001	0.000	0.003	0.000	0.001	0.001	0.000	0.000	0.000
F	0.000	0.001	0.015	0.000	0.017	0.000	0.000	0.006	0.021	0.000	0.009	0.007	0.014	0.006	0.000
Cl	0.000	0.001	0.000	0.001	0.000	0.001	0.000	0.001	0.000	0.000	0.001	0.001	0.000	0.002	0.000
Sum	4.988	4.869	4.860	4.647	4.469	4.883	4.912	4.692	4.327	4.775	4.861	4.876	4.151	4.665	4.946

Quantitative Electron Microprobe Analyses

Rhyolite Dike Matrix: Circle Three cont.

	C3-Mat3-76	C3-Mat3-77	C3-Mat3-78	C3-Mat3-79	C3-Mat3-80	C3-Mat3-81	C3-Mat3-82	C3-Mat3-83	C3-Mat3-84	C3-Mat3-85	C3-Mat3-86	C3-Mat3-87	C3-Mat3-88	C3-Mat3-89	C3-Mat3-90
							Chemical Composition (Weight Percent)								
SiO_2	87.78	68.25	88.16	95.31	83.00	96.74	83.38	76.46	89.68	91.82	67.52	79.02	67.41	95.22	80.12
TiO_2	0.01	0.02	0.02	0.01	0.00	0.08	0.00	0.00	0.00	0.00	0.00	0.04	0.03	0.04	0.00
$Al2O_3$	6.53	18.57	6.42	2.49	9.74	1.76	9.34	13.24	5.55	4.63	19.36	12.19	18.10	2.44	11.61
Fe_2O_3	0.25	0.50	0.20	0.19	0.37	0.20	0.29	0.52	0.74	0.14	0.48	0.39	1.43	0.21	0.41
MnO	0.01	0.00	0.00	0.00	0.00	0.02	0.00	0.00	0.00	0.02	0.01	0.00	0.00	0.01	0.01
MgO	0.00	0.00	0.00	0.00	0.00	0.00	0.00	0.01	0.00	0.01	0.00	0.00	0.01	0.00	0.00
CaO	0.03	0.03	0.00	0.03	0.05	0.01	0.04	0.03	0.03	0.02	0.07	0.04	0.06	0.01	0.04
SrO	0.08	0.00	0.00	0.13	0.06	0.03	0.00	0.00	0.04	0.07	0.00	0.00	0.00	0.08	0.02
BaO	0.02	0.00	0.00	0.00	0.00	0.00	0.01	0.00	0.00	0.02	0.00	0.02	0.01	0.00	0.00
Na_2O	2.60	8.95	1.73	0.79	4.90	1.09	4.03	6.15	3.07	3.04	10.80	5.68	6.88	1.44	7.06
K_2O	2.39	3.63	3.44	1.05	1.82	0.04	2.87	3.59	0.80	0.12	1.70	2.47	6.03	0.36	0.71
P_2O_5	0.03	0.00	0.00	0.00	0.00	0.00	0.02	0.00	0.04	0.00	0.03	0.00	0.03	0.00	0.00
F	0.26	0.04	0.02	0.00	0.05	0.03	0.00	0.00	0.03	0.10	0.01	0.13	0.00	0.20	0.00
Cl	0.01	0.01	0.01	0.00	0.00	0.00	0.01	0.00	0.00	0.00	0.00	0.02	0.00	0.00	0.01
O=F	-0.11	-0.02	-0.01	0.00	-0.02	-0.01	0.00	0.00	-0.01	-0.04	0.00	-0.06	0.00	-0.08	0.00
O=Cl	0.00	0.00	0.00	0.00	0.00	0.00	0.00	0.00	0.00	0.00	0.00	0.00	0.00	0.00	0.00
Total	99.89	99.98	99.99	100.00	99.98	99.99	100.00	100.00	99.99	99.96	100.00	99.95	100.00	99.92	100.00
							Ions per 8 Oxygen (sum excludes F & Cl)								
Si	3.673	3.019	3.678	3.875	3.503	3.908	3.521	3.303	3.706	3.768	2.976	3.381	3.011	3.878	3.399
Ti	0.001	0.001	0.001	0.000	0.000	0.003	0.000	0.000	0.000	0.000	0.000	0.001	0.001	0.001	0.000
Al	0.322	0.968	0.315	0.119	0.485	0.084	0.465	0.674	0.271	0.224	1.006	0.614	0.953	0.117	0.580
Fe	0.008	0.017	0.006	0.006	0.012	0.006	0.009	0.017	0.023	0.004	0.016	0.013	0.048	0.007	0.013
Mn	0.000	0.000	0.000	0.000	0.000	0.001	0.000	0.000	0.000	0.001	0.000	0.000	0.000	0.000	0.001
Mg	0.000	0.000	0.000	0.000	0.000	0.000	0.000	0.001	0.000	0.001	0.000	0.000	0.001	0.000	0.000
Ca	0.001	0.001	0.000	0.001	0.002	0.000	0.002	0.001	0.001	0.001	0.003	0.002	0.003	0.000	0.002
Sr	0.002	0.000	0.000	0.003	0.001	0.001	0.000	0.000	0.001	0.002	0.000	0.000	0.000	0.002	0.000
Ba	0.000	0.000	0.000	0.000	0.000	0.000	0.000	0.000	0.000	0.000	0.000	0.000	0.000	0.000	0.000
Na	0.211	0.768	0.140	0.062	0.401	0.085	0.330	0.515	0.246	0.242	0.923	0.471	0.596	0.113	0.581
K	0.128	0.205	0.183	0.055	0.098	0.002	0.154	0.198	0.042	0.006	0.096	0.135	0.344	0.019	0.039
P	0.001	0.000	0.000	0.000	0.000	0.000	0.001	0.000	0.002	0.000	0.001	0.000	0.001	0.000	0.000
F	0.034	0.006	0.003	0.000	0.007	0.004	0.000	0.000	0.004	0.013	0.001	0.018	0.000	0.025	0.000
Cl	0.001	0.001	0.000	0.000	0.000	0.000	0.000	0.000	0.000	0.000	0.000	0.001	0.000	0.000	0.001
Sum	4.347	4.978	4.323	4.121	4.502	4.089	4.483	4.708	4.292	4.249	5.022	4.617	4.956	4.138	4.615

Quantitative Electron Microprobe Analyses

Rhyolite Dike Matrix: Circle Three cont.

	C3-Mat3-91	C3-Mat3-92	C3-Mat3-93	C3-Mat3-94	C3-Mat3-95	C3-Mat3-96	C3-Mat3-97	C3-Mat3-98	C3-Mat3-99	C3-Mat3-100
	Chemical Composition (Weight Percent)									
SiO_2	73.13	89.80	92.90	68.82	70.07	65.59	65.23	76.31	82.81	88.92
TiO_2	0.00	0.00	0.05	0.00	0.04	0.02	0.02	0.00	0.02	0.00
Al2O_3	14.93	5.52	3.81	17.00	16.05	19.20	19.81	13.51	10.20	6.04
Fe_2O_3	0.53	0.26	0.41	0.72	0.35	0.76	0.86	0.59	0.30	0.26
MnO	0.02	0.00	0.00	0.00	0.00	0.00	0.00	0.00	0.00	0.02
MgO	0.00	0.00	0.01	0.02	0.00	0.01	0.04	0.00	0.02	0.00
CaO	0.03	0.02	0.01	0.05	0.03	0.04	0.05	0.05	0.00	0.02
SrO	0.10	0.06	0.05	0.03	0.00	0.01	0.03	0.05	0.02	0.11
BaO	0.00	0.01	0.00	0.00	0.00	0.02	0.03	0.03	0.00	0.00
Na_2O	5.15	1.95	1.72	4.89	3.65	5.78	6.60	6.24	5.51	2.72
K_2O	5.93	2.32	1.00	8.29	9.79	8.50	7.33	3.21	1.11	1.85
P_2O_5	0.02	0.02	0.04	0.02	0.00	0.03	0.00	0.00	0.00	0.01
F	0.16	0.00	0.00	0.15	0.00	0.02	0.00	0.01	0.00	0.03
Cl	0.00	0.02	0.01	0.00	0.01	0.01	0.01	0.00	0.00	0.00
O=F	-0.07	0.00	0.00	-0.06	0.00	-0.01	0.00	0.00	0.00	-0.01
O=Cl	0.00	0.00	0.00	0.00	0.00	0.00	0.00	0.00	0.00	0.00
Total	99.93	100.00	100.00	99.94	100.00	99.99	100.00	100.00	100.00	99.99
	Ions per 8 Oxygen (sum excludes F & Cl)									
Si	3.216	3.720	3.801	3.085	3.136	2.962	2.937	3.294	3.485	3.691
Ti	0.000	0.000	0.001	0.000	0.001	0.001	0.001	0.000	0.001	0.000
Al	0.774	0.270	0.184	0.898	0.846	1.022	1.051	0.687	0.506	0.296
Fe	0.018	0.008	0.013	0.024	0.012	0.026	0.029	0.019	0.009	0.008
Mn	0.001	0.000	0.000	0.000	0.000	0.000	0.000	0.000	0.000	0.001
Mg	0.000	0.000	0.001	0.001	0.000	0.001	0.002	0.000	0.001	0.000
Ca	0.001	0.001	0.001	0.003	0.001	0.002	0.003	0.002	0.000	0.001
Sr	0.003	0.002	0.001	0.001	0.000	0.000	0.001	0.001	0.001	0.003
Ba	0.000	0.000	0.000	0.000	0.000	0.000	0.001	0.000	0.000	0.000
Na	0.439	0.157	0.137	0.425	0.317	0.506	0.576	0.523	0.449	0.219
K	0.333	0.123	0.052	0.474	0.559	0.490	0.421	0.177	0.060	0.098
P	0.001	0.001	0.002	0.001	0.000	0.001	0.000	0.000	0.000	0.001
F	0.022	0.000	0.000	0.021	0.000	0.003	0.000	0.001	0.000	0.004
Cl	0.000	0.001	0.001	0.000	0.001	0.001	0.001	0.000	0.000	0.000
Sum	4.784	4.280	4.192	4.912	4.873	5.011	5.021	4.703	4.512	4.317

Quantitative Electron Microprobe Analyses
Matrix Averages

	Circle One		Circle Two		Circle Three		Average of 3 Grids	
	Avg	Std Dev	Avg	Std Dev	Avg	Std Dev	Avg	Std Dev
	Chemical Composition (Weight Percent)							
SiO_2	77.71	9.31	80.83	8.17	79.84	8.51	79.46	1.59
TiO_2	0.04	0.11	0.02	0.03	0.02	0.02	0.03	0.01
Al2O_3	12.09	4.90	10.77	4.82	11.36	4.89	11.41	0.66
Fe_2O_3	1.15	2.54	0.80	1.24	0.57	0.84	0.84	0.29
MnO	0.01	0.01	0.01	0.01	0.01	0.01	0.01	0.00
MgO	0.01	0.01	0.00	0.00	0.00	0.01	0.00	0.00
CaO	0.04	0.03	0.04	0.03	0.04	0.02	0.04	0.00
SrO	0.03	0.03	0.03	0.03	0.03	0.03	0.03	0.00
BaO	0.01	0.02	0.01	0.01	0.01	0.01	0.01	0.00
Na_2O	4.35	2.48	4.84	2.60	4.82	2.43	4.67	0.27
K_2O	4.49	2.73	2.57	2.10	3.25	2.45	3.44	0.97
P_2O_5	0.01	0.02	0.01	0.02	0.01	0.02	0.01	0.00
F	0.05	0.06	0.05	0.06	0.05	0.06	0.05	0.00
Cl	0.01	0.01	0.01	0.01	0.01	0.01	0.01	0.00
O=F	-0.02	0.03	-0.02	0.03	-0.02	0.03	-0.02	0.00
O=Cl	0.00	0.00	0.00	0.00	0.00	0.00	0.00	0.00
Total	99.98	0.03	99.98	0.03	99.98	0.03	99.98	0.00
	Ions per 8 Oxygen (sum excludes F & Cl)							
Si	3.346	0.291	3.433	0.257	3.405	0.266	3.395	0.044
Ti	0.001	0.004	0.001	0.001	0.000	0.001	0.001	0.000
Al	0.624	0.266	0.547	0.255	0.579	0.261	0.583	0.039
Fe	0.039	0.090	0.026	0.040	0.019	0.028	0.028	0.010
Mn	0.000	0.001	0.000	0.000	0.000	0.000	0.000	0.000
Mg	0.000	0.001	0.000	0.000	0.000	0.000	0.000	0.000
Ca	0.002	0.001	0.002	0.002	0.002	0.001	0.002	0.000
Sr	0.001	0.001	0.001	0.001	0.001	0.001	0.001	0.000
Ba	0.000	0.000	0.000	0.000	0.000	0.000	0.000	0.000
Na	0.369	0.215	0.404	0.223	0.403	0.209	0.392	0.020
K	0.251	0.157	0.142	0.117	0.180	0.140	0.191	0.055
P	0.000	0.001	0.000	0.001	0.000	0.001	0.000	0.000
F	0.007	0.009	0.007	0.009	0.007	0.008	0.007	0.000
Cl	0.001	0.001	0.000	0.001	0.000	0.001	0.000	0.000
Sum	4.634	0.266	4.556	0.253	4.590	0.259	4.593	0.039

APPENDIX B.

CRYSTAL SIZE DISTRIBUTION BULK DATA AND GRAPHS

Explanation of Data and Terms

The succeeding data and graphs are the raw data produced by the stereological program CSD Corrections 1.36. The 2-dimensional data section is the crystals sizes measured by ImageJ and CSD Corrections distributed them into bins. The 3-dimensional data section is the converted data (2-D to 3-D) used to produce the CSD graph. The Y-axis on the graph is the population density per volume per size bin and has units of mm^{-4} and the X-axis is the frequency abundance in each bin size of the major axis of the ellipsoids in millimeters. Below is a description of all of the terms as summarized by Higgins (2000).

2-D Data

Ellipse Major – The ellipses that were constructed around the crystal outlines to determine the major axis (the number represents the maximum size of the bin)

# of Crystals – The number of crystals in the corresponding to the Ellipse Major bin

Corr Factor – Correction factor is the ratio of the total tailing corrections to the original area number density. If the correction factor is greater than one then the calculated population density for that interval is negative and hence invalid.

3-D Data

Mid Interval – The midpoint of the size bin of the corrected long (major) axis of an ellipsoid when adjusting to 3-dimensions.

Pod Den – The natural logarithm of the population density.

Min PD and Max PD – The error limits of the population density. The error calculations do not take into account any error in the correction factors, and hence should be viewed as minimum errors.

Crystal Number - Numbers of crystals per unit volume in the in each size bin.

Vol % - Per cent volume in each interval.

Graph Data

Total Number – Number of crystals per unit volume.

Total Volume % - The sum of the volume %s in the 3-D column.

Regression Vol % - Extrapolated volume % calculated by using the trend line's slope and intercept.

Goodness of fit – Used to test the quality of fit. If it is over 0.1 then it is acceptable.

CSD Bulk Data and Graph of Alkali Feldspar (Slab) – Clustered Glomerocrysts

2-Dimension Data			3-Dimension Data					
Ellipse Major	# of Crystals	Corr Factor	Mid Interval	Pop Den	Min PD	Max PD	Crystal number	Vol %
10.00	1	0.00	26.71	-11.68	-Infinity	-10.99	3.12E-5	3.1
6.310	4	0.02	16.85	-9.39	-10.11	-8.98	0.0002	4.8
3.980	15	0.02	10.63	-7.15	-7.46	-6.92	0.0012	7.1
2.510	37	0.03	6.71	-5.34	-5.53	-5.19	0.0044	6.9
1.580	46	0.07	4.23	-4.24	-4.42	-4.1	0.0084	3.3
1.000	44	0.11	2.67	-3.41	-3.6	-3.25	0.0122	1.2
0.631	20	0.29	1.69	-3.5	-3.88	-3.23	0.0070	0.17
0.398	14	0.28	1.06	-2.92	-3.39	-2.61	0.0079	0.048
2.510	1	1.51	0.67	Over				
0.158	0							

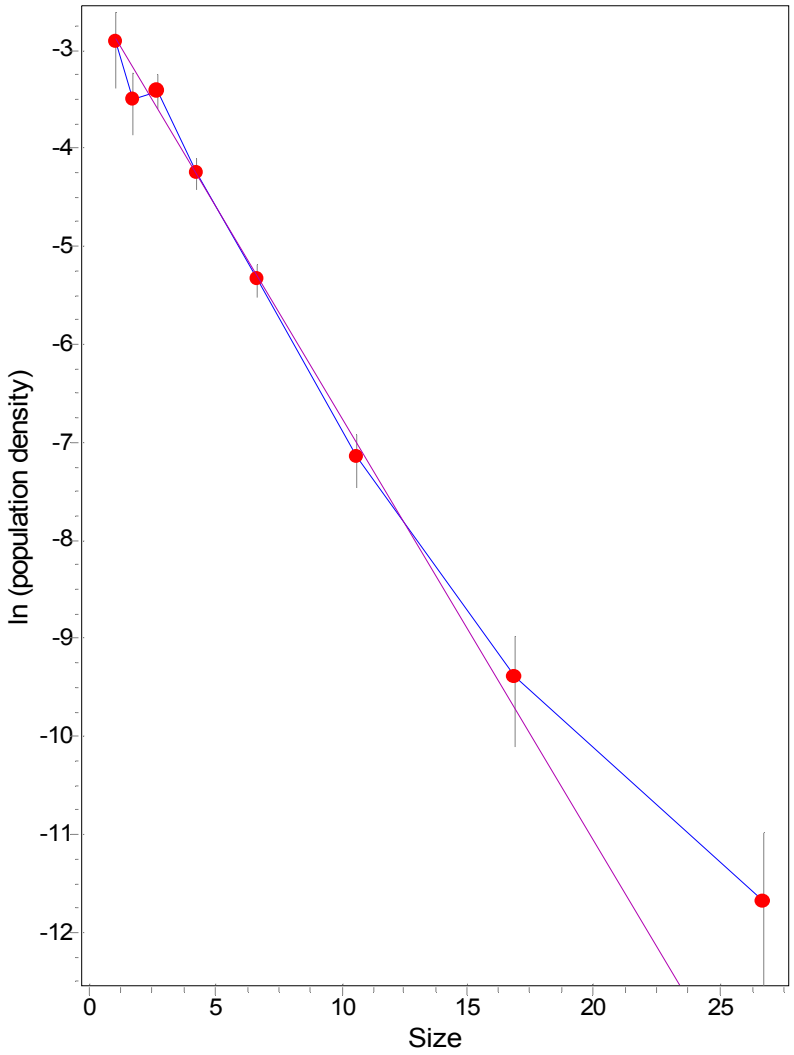

Graph Data (2nd column – 1 σ error)		
Total number	0.041	
Total volume (%)	26.2	9.2
Regress-intercept	-2.42	0.16
Regress-slope	-0.433	0.027
Regress-volume (%)	78.0	40.1
Goodness of fit	0.846	

CSD Bulk Data and Graph of Alkali Feldspar (Slab) – Deconstructed Glomerocrysts

2-Dimension Data			3-Dimension Data					
Ellipse Major	# of Crystals	Corr Factor	Mid Interval	Pop Den	Min PD	Max PD	Crystal number	Vol %
6.310	1	0.00	16.85	-10.77	-Infinity	-10.08	4.89E-5	1.2
3.980	11	0.01	10.63	-7.46	-7.82	-7.19	0.0008	5.2
2.510	37	0.02	6.71	-5.34	-5.53	-5.19	0.0044	6.9
1.580	94	0.03	4.23	-3.5	-3.61	-3.4	0.0177	6.9
1.000	114	0.07	2.67	-2.43	-2.53	-2.33	0.0326	3.2
0.631	72	0.17	1.69	-2.08	-2.23	-1.95	0.0291	0.72
0.398	38	0.32	1.06	-1.99	-2.26	-1.78	0.0201	0.12
2.510	8	0.48	0.67	-2.89	-4.03	-2.38	0.0051	0.0080
0.158	0							

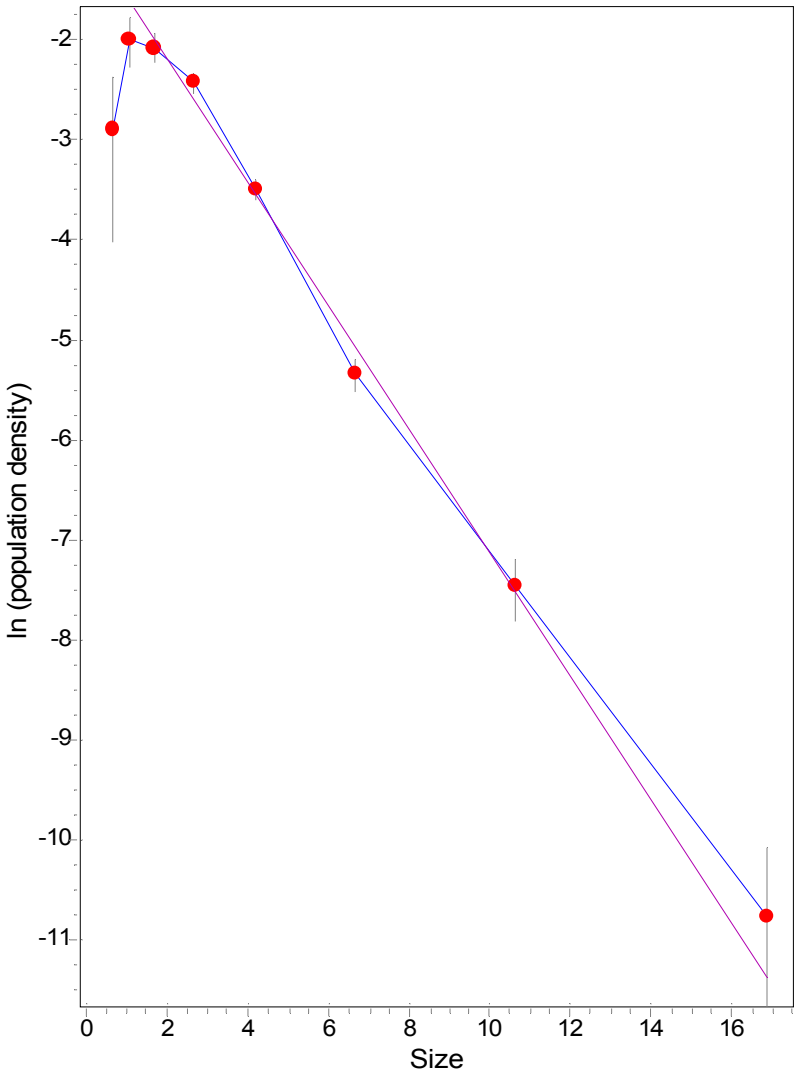

Graph Data (2nd column – 1 σ error)		
Total number	0.11	
Total volume (%)	24.3	5.2
Regress-intercept	-0.940	0.12
Regress-slope	-0.620	0.028
Regress-volume (%)	81.9	28.8
Goodness of fit	0.0684	

CSD Bulk Data and Graph of Alkali Feldspar (TS) – Clustered Glomerocrysts

2-Dimension Data			3-Dimension Data					
Ellipse Major	# of Crystals	Corr Factor	Mid Interval	Pop Den	Min PD	Max PD	Crystal number	Vol %
6.310	1	0.00	16.85	-10.78	-Infinity	-10.08	0.0000	1.2
3.980	16	0.00	10.63	-7.09	-7.38	-6.86	0.0012	7.6
2.510	38	0.03	6.71	-5.33	-5.51	-5.18	0.0045	7.0
1.580	55	0.06	4.23	-4.07	-4.22	-3.94	0.0100	3.9
1.000	31	0.18	2.67	-3.86	-4.1	-3.66	0.0078	0.76
0.631	27	0.18	1.69	-3.07	-3.34	-2.86	0.0108	0.26
0.398	26	0.18	1.06	-2.19	-2.46	-1.97	0.0165	0.10
2.510	15	0.22	0.67	-1.87	-2.27	-1.58	0.0143	0.022
0.158	1	1.77	0.42	Over				
0.100	0							

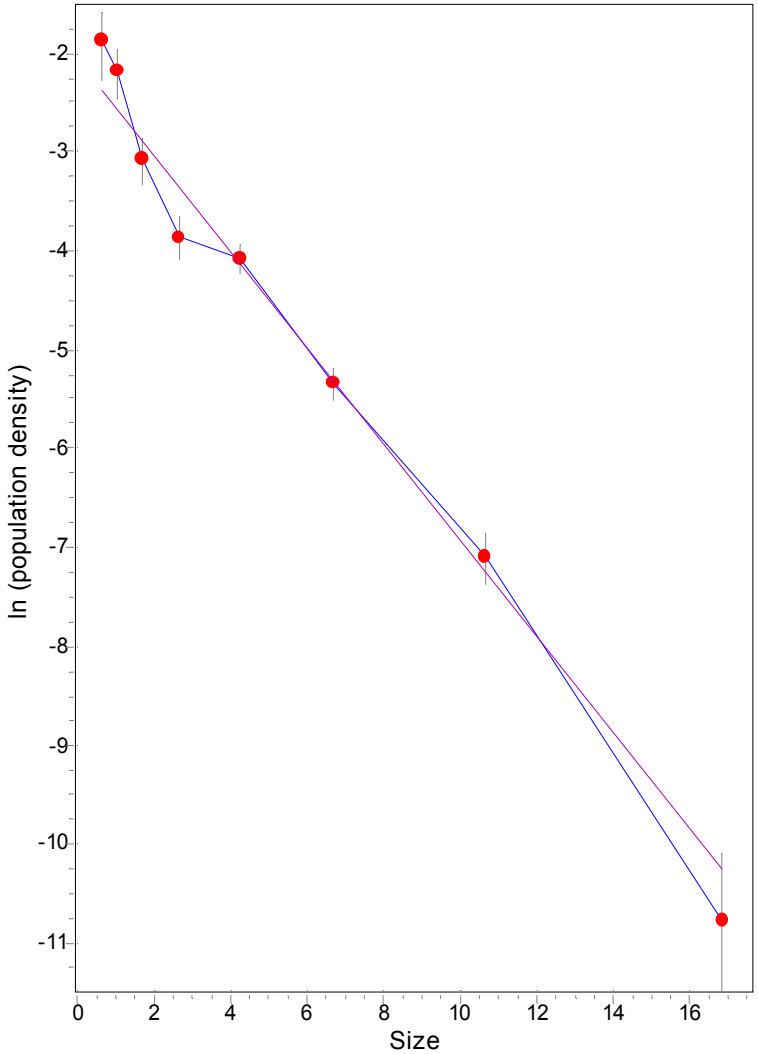

Graph Data (2nd column – 1 σ error)		
Total number	0.065	
Total volume (%)	20.8	5.1
Regress-intercept	-2.06	0.15
Regress-slope	-0.485	0.03
Regress-volume (%)	71.1	33.4
Goodness of fit	0.0902	

CSD Bulk Data and Graph of Alkali Feldspar (TS) – Deconstructed Glomerocrysts

2-Dimension Data			3-Dimension Data					
Ellipse Major	# of Crystals	Corr Factor	Mid Interval	Pop Den	Min PD	Max PD	Crystal number	Vol %
3.980	5	0.00	10.63	-8.25	-8.85	-7.88	0.0004	2.4
2.510	40	0.01	6.71	-5.26	-5.44	-5.11	0.0048	7.5
1.580	84	0.04	4.23	-3.63	-3.75	-3.52	0.0156	6.1
1.000	93	0.08	2.67	-2.65	-2.77	-2.54	0.0260	2.6
0.631	83	0.12	1.69	-1.89	-2.03	-1.77	0.0351	0.86
0.398	60	0.19	1.06	-1.38	-1.55	-1.23	0.0370	0.23
2.510	33	0.27	0.67	-1.16	-1.44	-0.95	0.0290	0.045
0.158	3	1.19	0.42	Over				
0.100	0							

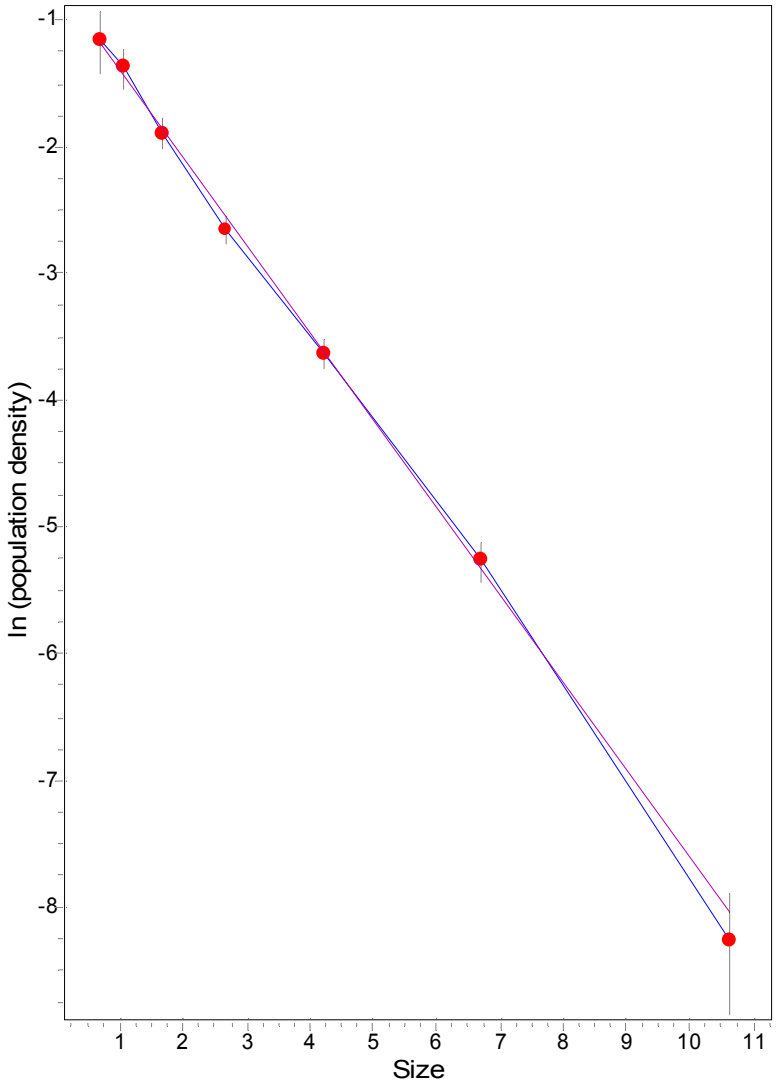

Graph Data (2nd column – 1 σ error)		
Total number	0.15	
Total volume (%)	19.6	3.4
Regress-intercept	-0.730	0.11
Regress-slope	-0.687	0.03
Regress-volume (%)	66.6	21.3
Goodness of fit	0.940	

CSD Bulk Data and Graph of Quartz (Slab) – Clustered Glomerocrysts

2-Dimension Data			3-Dimension Data					
Ellipse Major	# of Crystals	Corr Factor	Mid Interval	Pop Den	Min PD	Max PD	Crystal number	Vol %
3.160	3	0.00	5.25	-7.72	-8.59	-7.27	0.0004	1.3
2.150	11	0.03	3.58	-5.69	-6.07	-5.42	0.0023	2.1
1.470	33	0.05	2.44	-3.84	-4.04	-3.67	0.0101	3.0
1.000	71	0.07	1.66	-2.33	-2.46	-2.21	0.0311	2.9
0.681	39	0.29	1.13	-2.43	-2.69	-2.23	0.0191	0.56
0.464	29	0.46	0.77	-2.22	-2.64	-1.93	0.0160	0.15
0.316	5	0.86	0.53	-4.59	-Infinity	-3.14	0.0010	0.0030
0.215	0							

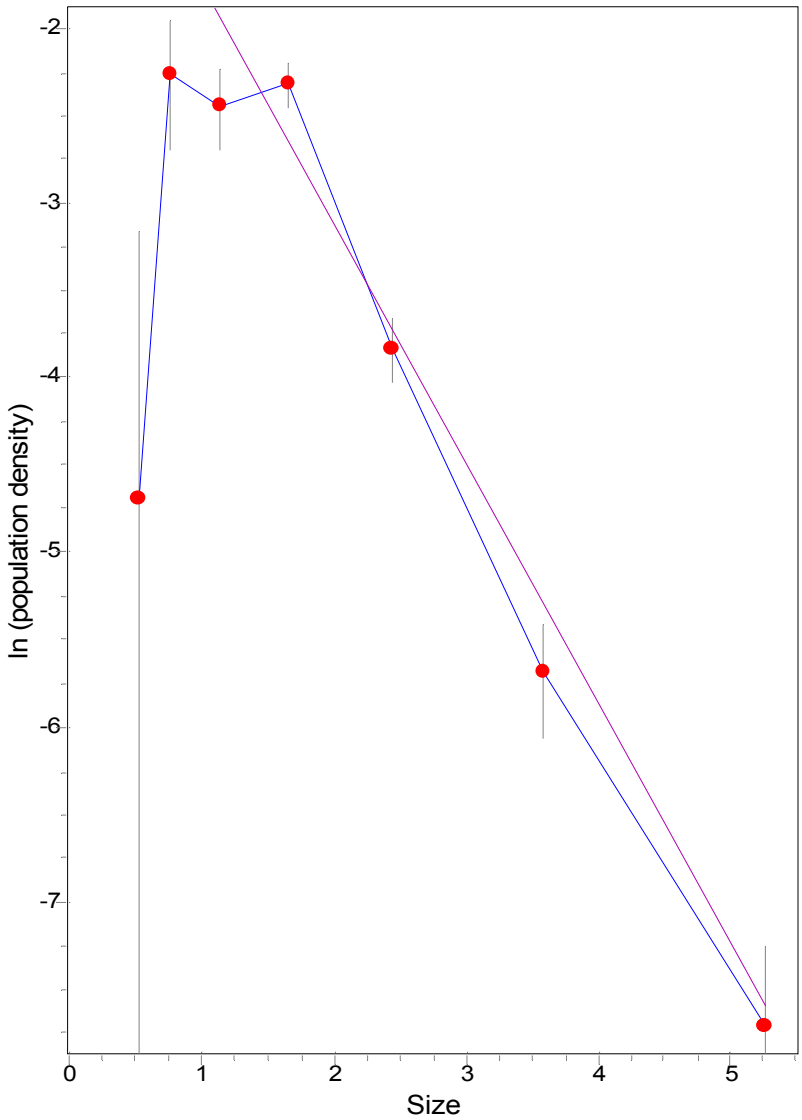

Graph Data (2nd column – 1 σ error)		
Total number	0.080	
Total volume (%)	10.0	2.5
Regress-intercept	-0.400	0.22
Regress-slope	-1.37	0.11
Regress-volume (%)	23.1	17.0
Goodness of fit	0.00256	

CSD Bulk Data and Graph of Quartz (Slab) – Deconstructed Glomerocrysts

2-Dimension Data			3-Dimension Data					
Ellipse Major	# of Crystals	Corr Factor	Mid Interval	Pop Den	Min PD	Max PD	Crystal number	Vol %
3.160	1	0.00	5.25	-8.81	-Infinity	-8.12	0.0002	0.44
2.150	4	0.03	3.58	-6.69	-7.42	-6.28	0.0009	0.79
1.470	40	0.01	2.44	-3.61	-3.78	-3.46	0.0127	3.7
1.000	86	0.06	1.66	-2.12	-2.25	-2.02	0.0381	3.5
0.681	49	0.28	1.13	-2.18	-2.4	-2	0.0246	0.72
0.464	33	0.5	0.77	-2.17	-2.59	-1.87	0.0169	0.16
0.316	7	0.66	0.53	-3.34	-Infinity	-2.6	0.0036	0.010
0.215	0							

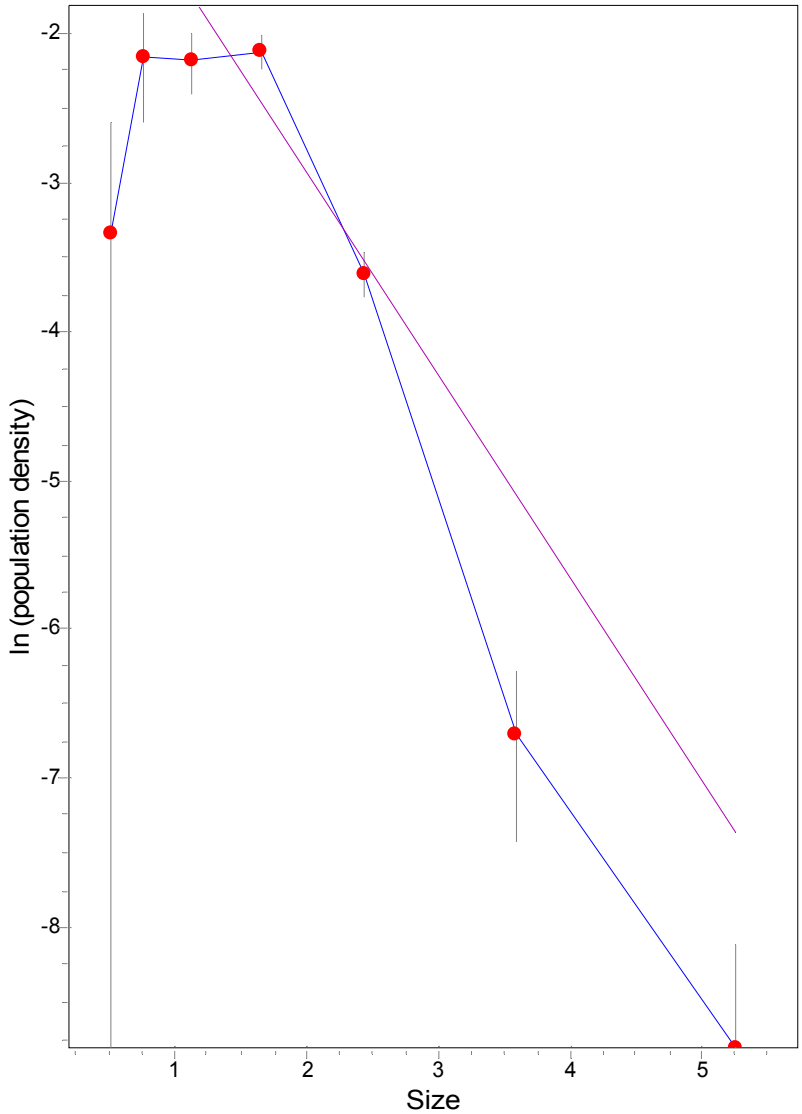

Graph Data (2nd column – 1 σ error)		
Total number	0.10	
Total volume (%)	9.37	2.06
Regress-intercept	-0.200	0.27
Regress-slope	-1.36	0.15
Regress-volume (%)	28.8	30.9
Goodness of fit	2.91E-5	

CSD Bulk Data and Graph of Quartz (Thin Section) – Clustered Glomerocrysts

2-Dimension Data			3-Dimension Data					
Ellipse Major	# of Crystals	Corr Factor	Mid Interval	Pop Den	Min PD	Max PD	Crystal number	Vol %
4.640	1	0.00	7.71	-9.6	-Infinity	-8.91	0.0001	0.93
3.160	0		5.25					
2.150	17	0.00	3.58	-5.24	-5.52	-5.02	0.0037	3.4
1.470	70	0.03	2.44	-3.08	-3.21	-2.97	0.0215	6.3
1.000	75	0.13	1.66	-2.35	-2.49	-2.23	0.0304	2.8
0.681	81	0.17	1.13	-1.55	-1.69	-1.43	0.0461	1.4
0.464	81	0.19	0.77	-0.81	-0.96	-0.69	0.0655	0.61
0.316	48	0.38	0.53	-0.84	-1.11	-0.63	0.0435	0.13
0.215	27	0.51	0.36	-0.89	-1.39	-0.55	0.0283	0.026
0.147	19	0.32	0.24	-0.14	-0.56	0.15	0.0406	0.011
0.100	3	1.18	0.17	Over				
0.07	0							

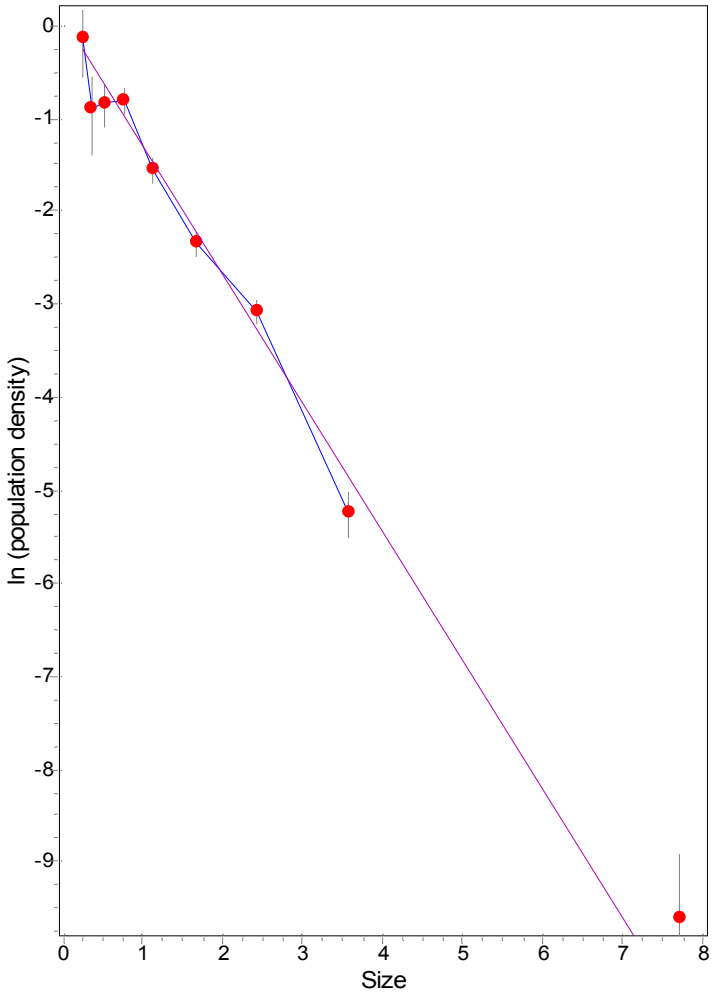

Graph Data (2nd column – 1 σ error)		
Total number	0.28	
Total volume (%)	15.5	3.2
Regress-intercept	0.0900	0.12
Regress-slope	-1.38	0.07
Regress-volume (%)	36.2	14.1
Goodness of fit	0.167	

CSD Bulk Data and Graph of Quartz (Thin Section) – Deconstructed Glomerocrysts

2-Dimension Data			3-Dimension Data					
Ellipse Major	# of Crystals	Corr Factor	Mid Interval	Pop Den	Min PD	Max PD	Crystal number	Vol %
1.470	47	0.00	2.44	-3.45	-3.61	-3.31	0.0149	4.4
1.000	108	0.05	1.66	-1.90	-2.01	-1.81	0.0475	4.4
0.681	166	0.10	1.13	-0.75	-0.84	-0.67	0.1020	3.0
0.464	176	0.16	0.77	0.01	-0.09	0.09	0.1490	1.4
0.316	115	0.30	0.53	0.16	0.02	0.29	0.1180	0.35
0.215	58	0.56	0.36	-0.22	-0.57	0.04	0.0554	0.051
0.147	25	0.61	0.24	-0.41	-1.12	0.00	0.0311	0.0090
0.100	5	0.54	0.17	-1.09	-4.53	-0.41	0.0107	0.0010
0.07	0							

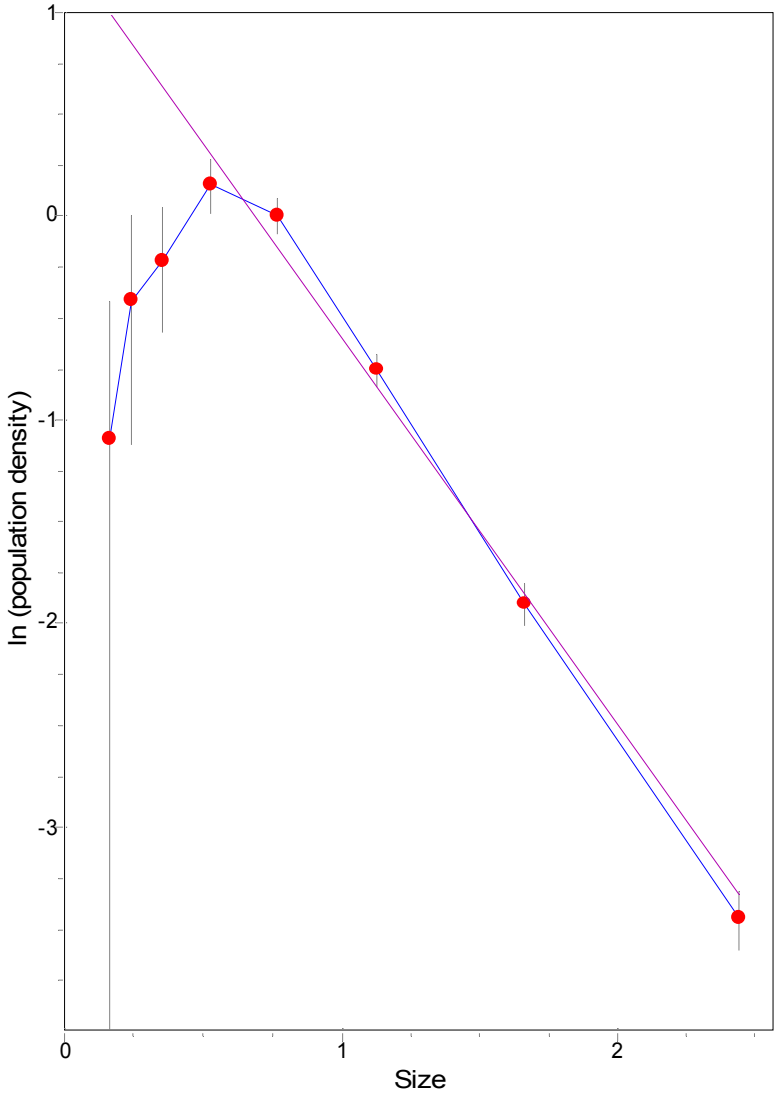

Graph Data (2nd column – 1 σ error)		
Total number	0.53	
Total volume (%)	13.6	1.5
Regress-intercept	1.32	0.11
Regress-slope	-1.91	0.08
Regress-volume (%)	34.3	11.2
Goodness of fit	0.00220	

VITA

Sean Patrick O'Donnell was born in Kankakee, Illinois on February 4, 1982, the son of Jim and Holly O'Donnell. After graduating from Kankakee High School in 2000, he enrolled at the University of Missouri - Rolla (UMR). He received the degree of Bachelor of Science from UMR in May of 2004. In August of 2004, he enrolled in the Graduate School at UMR. Taking a hiatus from his Master's thesis at UMR, in August of 2006 he attended the Graduate School at Washington University in St. Louis. He received his Masters of Science degree from Missouri University of Science and Technology (formerly UMR) in August of 2008.